QUARK MATTER FORMATION AND HEAVY ION COLLISIONS

A general review and status report

edited by

M. JACOB
CERN, Geneva, Switzerland

and

J. TRAN THANH VAN
Université de Paris-Sud, Orsay, France

With contributions by: M. FAESSLER, CERN; J. KAPUSTA, Los Alamos and CERN; L. McLERRAN, Univ. of Washington and Helsinki; J. RAFELSKI, Frankfurt; H. SATZ, Bielefeld; and W. WILLIS, CERN

NORTH-HOLLAND PUBLISHING COMPANY-AMSTERDAM

PHYSICS REPORTS (Review Section of Physics Letters) 88, No. 5 (1982) 321–413. NORTH-HOLLAND PUBLISHING COMPANY

QUARK MATTER FORMATION AND HEAVY ION COLLISIONS

A general review and status report

edited by:

M. JACOB

CERN, Geneva, Switzerland

and

J. TRAN THANH VAN*

Université de Paris-Sud, Orsay, France

Contents:

Single orders for this issue

PHYSICS REPORTS (Review Section of Physics Letters) 88, No. 5 (1982) 321–413.

Copies of this issue may be obtained at the price given below. All orders should be sent directly to the Publisher. Orders must be accompanied by check.

Single issue price Dfl. 48.00, postage included.

* Director of the Rencontres de Moriond.

Abstract

The reasons which lead one to expect that, at high enough density and (or) high enough temperature, a new form of matter – the quark-gluon plasma – should exist, are reviewed and discussed. It is shown that the relevant values of the density and temperature are likely to be met in head-on heavy ion collisions provided that the incident ion energy is in the range of 100 GeV per nucleon. The experimental observation of the expected signals is discussed. Recent information on $\alpha\alpha$ collisions at ISR energy is reviewed. Built out of separate contributions which can be read independently of one another, this review provides a global approach to the question of quark matter and its possible observation in heavy ion collisions.

Foreword

This Physics Reports issue brings together the texts of the review talks presented during a one-day session devoted to quark matter formation and heavy ion collisions, organized as part of the XVIII Rencontre de Moriond, held at Les Arcs, France, in March 1982. In view of the interest presently inspired by this still somewhat speculative but quite promising facet of high energy physics, which also appears as an interesting interface between nuclear and particle physics, it is deemed appropriate to publish this set of articles as a separate and specialized review. Such a document should be useful to trigger interest among particle and nuclear physicists alike about a new domain of physics where experimentation possibilities could soon develop. It should also be helpful in assessing the potential of such investigations, showing where a consensus prevails and where doubts remain.

In its own modest way this issue also bears witness to the fact that the Rencontres de Moriond have become an institution in particle physics. At first discussion meetings for French particle physicists, they have rapidly grown into a successful series of international topical meetings. Each rencontre offers the opportunity to discuss, in depth, recent findings and new ideas in a particular domain of high energy physics, and this in the pleasant and stimulating winter atmosphere of a mountain resort.

M. JACOB
Geneva, May 1982

PHYSICS REPORTS (Review Section of Physics Letters) 88, No. 5 (1982) 325–329. North-Holland Publishing Company

1. Introduction

M. JACOB
CERN, Geneva, Switzerland

Heavy ion collisions as discussed in this review lead us to a novel domain both in energy and matter density. Experimental information is at best limited to a few events observed in cosmic ray interactions or to ions probably too light to be of much relevance. We have indeed in mind centre-of-mass energies of the order of 10 GeV per nucleon or larger, and ions massive enough that head-on collisions could result in very large energy densities of the order of 1 GeV/fm^3, to be found over volumes which would greatly exceed in size that occupied by a single hadron. To obtain a nucleon–nucleon collision centre-of-mass energy of 20 GeV in a fixed target nucleus–nucleus collision we need an impinging ion with close to 200 GeV per nucleon. This is almost two orders of magnitude above what is presently considered as "high energy" in heavy ion collisions [1]. We are therefore led into an entirely new domain of investigation, where the composite nature of the nucleon in terms of quarks appears presently as far more important than the composite nature of the nucleus in terms of nucleons. It opens the possibility to reach both very high energy densities and very high quark densities over extended volumes. The great interest for such conditions originates from recent developments in quantum chromodynamics, QCD, which make it very plausible that, while colour confinement should prevail under standard circumstances, deconfinement should occur at sufficiently high density and (or) temperature [2]. Under such conditions, which could have been those of the very early Universe, less than 10^{-4} sec after the Big Bang, a new state of matter referred to as "quark matter" or as a "quark-gluon plasma" is likely to exist. In this state, quarks would still be sensitive to the (perturbative) part of their interactions through the gluon field, acting now as a long range force, but no longer to the (non-perturbative) string tension at larger distances (>1 fm) which parametrizes confinement under standard circumstances and results from the nature of the QCD vacuum. Reaching very high matter or energy densities over a relatively large volume (as compared to the hadron size) should alter the usual long range properties of the vacuum and could thus reveal hitherto unknown phenomena [3].

Assuming that this is the case, what are the parameters for such a transition? Could the necessary conditions be achieved in heavy ion collisions at the energies previously mentioned? How could one then observe the quark-gluon plasma which would be created this way, and which are the specific signals which could be recognizable against the background resulting from an expected huge multiplicity of secondaries? The purpose of this review is not so much to answer all these questions in a precise way than to set the stage for a wider discussion, trying to assess as far as possible at present the physics potential of heavy ion collisions at very high energies [4].

While the a priori most favorable case, uranium–uranium collisions in the energy range just considered would require an important and dedicated machine, the possibilities of using existing high energy proton machines at accelerating medium size ions are presently attracting some attention. This could be a way of performing some exploratory (and perhaps already decisive) work with a relatively limited effort. It is therefore deemed appropriate to review the pertinent physics questions in some detail, as attempted through this series of papers.

0 370-1573/82/0000–0000/$1.25

At present there seems to exist a rather general consensus that quarks are no longer subject to spatial confinement within small-size hadrons in any larger domain where the density and (or) the temperature would be high enough. This is more a consensus than a proof since the nature of confinement in QCD is not yet fully understood [5]. Nevertheless, the consensus goes further and one may quote values for the energy density and the temperature beyond which colour should no longer appear as confined. Both phenomenological models and lattice QCD calculations give converging values. The energy density should exceed values of the order of 0.4 GeV/fm^3. This is about the same as the energy density within a hadron (the standard confinement volume). It is, however, clearly in excess of the energy density inside a nucleus, which is of the order of 0.15 GeV/fm^3. At the same time, the temperature beyond which the quark matter phase should replace the standard hadronic phase of matter is expected to be of the order of 200 MeV. The general reasons for the occurrence of a deconfined phase under such conditions are discussed in some detail in ref. [2]. This phase should be viewed as a coalescence, or perhaps percolation, of hadrons into larger entities and not as an actual separation of free quarks. At an intuitive level one may say that when hadrons are squeezed together so that the overall energy density equals that inside each of them, the pressure of the vacuum separation between hadron bags disappears and hadrons merely coalesce into one single large bag within which quarks can freely move, interacting perturbatively. On the other hand, one may say that at high enough temperatures a configuration with a single flux tube extending between two separated coloured quarks, and thus imposing eventually confinement, is no longer strongly enough favoured in comparison to numerous higher energy configurations, in which the gluon field extends further and further out into space. This results in a decreasing force with increasing distance, which is no longer able to confine.

This review first considers the possible phase transition and the determination of the critical values of the energy density and temperature beyond which confinement should no longer hold. In order to illustrate the type of consensus achieved this is done following two quite different approaches. In the former and phenomenological one, presented by J. Rafelski, which constitutes section 2 of this report, one considers separately a hadron gas, as it is known to exist below the Hagedorn limiting temperature, and a quark-gluon plasma, which one expects to occur at high enough temperature. One then explores how the two different pictures may merge for parameter values which may be thus those of a phase transition. In the latter one, based on lattice gauge theory and presented by H. Satz in section 3 of this report, one studies the thermodynamics of a non-Abelian gluon field coupled to fermions, calculating the pertinent partition function on the lattice. The evaluation is carried out with the help of the presently very popular Monte Carlo techniques of lattice gauge theory. The occurrence of a phase transition is then most dramatically signalled by a singularity-like behaviour of the specific heat as a function of temperature. Going through sections 2 and 3 of this report, the reader will be able to assess the type of consensus which presently prevails, not only for the occurrence of a deconfined quark matter phase but also for the determination of the typical values of the parameters defining the transition.

The critical temperature corresponding to the phase transition depends on the quark density or on the chemical potential of the system. Relatively low for very high densities (neutron star regime or fragmentation region in heavy ion collisions) it would reach the quoted value of the order of 200 MeV, at low quark density (Early Universe of Central region in heavy ion collisions). This is discussed in section 2. In between the hadron phase and the quark-gluon plasma phase, there could also be an intermediate phase where chiral symmetry would still be spontaneously broken and thus with massive quarks. This is discussed in section 3 [6].

Having gained some confidence in the existence of a phase transition and having obtained somewhat reliable estimates for the relevant values of the key parameters, one may address the next essential

question which is, can such densities be reached in head-on heavy ion collisions, assuming centre-of-mass energies of several GeV per nucleon. Again there seems at present to exist a consensus that this is indeed the case. In the most favourable case of head-on U–U collisions (with an impact parameter of less than 1 fm, say) energy densities in excess of 1.5 GeV/fm^3 should be reached over an appreciable volume [7]. The high density value thus obtained should only slowly decrease with atomic number. Even with medium size ions one should thus be able to reach the energy densities previously associated with the phase transition to quark matter.

In this review we shall approach this new question again from two quite different points of view in order to illustrate once again the type of consensus which prevails. One line of approach, presented by J. Kapusta in section 4 of this report is based on hydrodynamical considerations. One obtains this way a rather dramatic though perhaps too "collective" picture of heavy ion collisions. While very large densities are expected to be reached, the vanishing mean free path of the hydrodynamical approximation is at odds with the relative permeability of nuclear matter to quarks, with a mean free path of the order of 0.5 fm. The other line of approach, followed here by L. McLerran in section 5, consists in getting a lower limit for the energy density reached through the collision, considering only the co-moving hadrons which are likely to be trapped in nuclear matter after having been formed. This appears presently as a more realistic point of view. Estimates for the energy density reached in the central region (negligible quark density) compare with those made for the fragmentation region (high quark density) [4].

While the reader will thus be able to realize the type of consensus which seems again to prevail with respect to the energy density attainable in heavy ion collisions, the question of thermalization may however appear as far less settled. Although it is possible that some type of equilibrium will be reached within the volume occupied by the quark-gluon plasma, it is however not yet taken for granted that a high density system will be large enough and long-lived enough for this to indeed occur. This is one of the questions still open, with optimistic as well as sceptic points of view to be found. Consensus seems to prevail that some thermalization should take place.

Granting the fact that a thermalized quark-gluon plasma is formed, then the next question concerns possible signals and their observation. This is already discussed in sections 2 and 5 but section 6, by W. Willis, faces this problem in detail.

There again there seems to be a consensus that the entire volume of the quark-gluon plasma will radiate a large number of photons (with a thermalized distribution at $T \approx 200$ MeV), while pions will be emitted mainly from the surface and at a lower temperature (160 MeV say). It would then follow that for a large enough blob of quark matter, most of the energy could be radiated by photons rather than by pions, as photons become relatively numerous while being more energetic. This is however an a priori extreme case and one should more generally expect very large fluctuations in the measured number of the γ/π ratio on an event to event basis. Since most of the photons are expected to be produced at relatively low p_t (thermalized emission), a clearer signal may actually be provided by low mass lepton pairs or by the overall energy fraction carried by neutrals. One may also notice that a large yield of large p_t photons could be produced in the pre-thermalization stage, when energetic quarks radiate as they are scattered at large angles. These photons are probably easier to detect, but they are part of an already known phenomenon and not very relevant while in search of quark-gluon matter in an equilibrium state.

If thermal equilibrium is achieved, chemical equilibrium may or may not be reached simultaneously. If this is the case one would expect a relatively large number of strange particles among the final fragments. Gluons could indeed more easily materialize into $s\bar{s}$ pairs in view of the high level of the u

and d quarks present within the blob of quark matter. Again very large fluctuations in the strange/non-strange ratio could be found on an event-to-event basis. Section 2 has an optimistic tilt towards this effect.

One may also anticipate some violent and spectacular effects. Indeed the expected multiplicity ranges in the thousands and an event may thus be considered to some extent as an experiment in itself. This has been emphasized by T.D. Lee, who points out the possibility of giant jets as the interior plasma erupts out of its hadronic shell [8]. There is also the possibility that the quark-gluon plasma may reflect some still unknown property of colour dynamics. It may be a "factory" producing new states which would be globally neutral with respect to colour but contain a larger number of quarks than the known hadrons. Such objects may be stable enough to be observed. If colour symmetry would be only approximate at large distance spectacular effects could result [9].

These questions, together with the experimental problems which they offer, are discussed in section 6.

The discussion of the expected collision conditions and of the resulting effects which they could generate, as they are presented in sections 5 and 6 respectively, assumes that heavy ion collisions produce in every case a large number of secondary particles (besides nuclear fragments) and that enough rescatterings take place among quarks and gluons to achieve some equilibrium. There is no reason that the first condition should not be fulfilled. One may indeed reasonably expect that the mean number of pion secondaries in an A–A collision should increase as A, that is proportionally to the number of possible independent nucleon–nucleon collisions, resulting in about 10^4 pions in a typical head-on U–U collision!

This is very different from multiplicities expected in a p–A collision, whatever the energy and the value of A may be. In this case the mean number of particles is not expected to be very much larger than that found in typical pp collisions, at most by about a factor 3.

Some evidence for very large multiplicities in cosmic ray heavy ion collisions is mentioned in section 5 but it is deemed appropriate to review here in some detail also the information obtained during a short run with α beams ($\sqrt{s_{NN}} = 31$ GeV) at the CERN ISR in 1980. Even though α's are probably too small to be very interesting probes in the present case of interest, they clearly show some encouraging features. This is the object of section 7, written by M. Faessler. Of particular interest are, on the one hand, the large pion yield observed in the central region, with a density exceeding by about 80% that measured in pp collisions at the same nucleon centre-of-mass energy and, on the other hand, the larger than 16 (A^2) factor by which one should multiply the large p_t yield in pp collisions in order to reproduce the one found in $\alpha\alpha$ collisions. The latter feature is probably related to the anomalous increase already found in pA collisions [10] and could be due to rescattering effects at the constituent level. While still relatively limited in $\alpha\alpha$ collisions, both features provide encouragement to look for more spectacular effects, as those expected for collisions among much heavier ions at a similar nucleon energy.

These different sections altogether review in some general way present prospects about heavy ion collisions as a probe for quark matter formation. Heavy ion collisions indeed provide the unique opportunity to reach high quark densities and thus to experiment with conditions hitherto not available in particle physics. While the specific dynamics of proton–nucleus interactions at very high energies is still poorly understood it may seem bold to investigate directly interactions among heavy nuclei which are certainly far more complex. The key purpose here is however not so much to study in detail the reaction mechanisms at work but rather to merely use the conditions reached, through the large energy release due to numerous nucleon–nucleon interactions and the multiple scattering of constituents within a relatively large interaction volume. One could reach densities and temperatures which may locally

modify the vacuum state and lead to the formation of quark matter. It is clear that such a prospect has many speculative elements and this may quell enthusiasm. The purpose of this report is to provide the reader with facts and ideas so that he can judge for himself the potential interest of such research. While this report is built as a whole, each section can be read independently of the others. The proceedings of the Bielefeld Workshop [4] could provide the dedicated reader with further information on all the physics issues discussed here.

References

[1] For a review of present results on high energy heavy ion collisions see 5th High Energy Heavy Ion Study (1981) LBL-12652, ed. L.S. Schroeder.
[2] E.V. Shuryak, Quantum Chromodynamics and the Theory of Superdense Matter, Phys. Reports 61, No. 2 (1980);
A.M. Polyakov, Phys. Lett. 72B (1978) 477;
L. Susskind, Phys. Rev. D 20 (1979) 2610;
D.J. Gross, R.D. Pisanski and L.G. Yaffe, Rev. Mod. Phys. 53 (1981) 43.
[3] T.D. Lee, Is the Physical Vacuum a Medium, CU-TP-170 (1981).
[4] For further information one should consult the Proceedings of the Bielefeld Workshop on Quark Matter Formation and Heavy Ion Collisions, Bielefeld, Germany (1982), eds. H. Satz and M. Jacob (World Scientific, Singapore).
[5] M. Bander, Theories of Quark Confinement, Phys. Reports 78, No. 3 (1981).
[6] As discussed at different places in this review it is possible that two different phase transitions actually occur, the second one corresponding to the spontaneous breakdown of chiral symmetry, quarks and antiquarks still binding in mesons acting as Goldstone bosons while all other hadrons would have "melted" into quark matter. The restauration of chiral symmetry would almost certainly occur at a larger temperature than that quoted for deconfinement (see section 3).
[7] R. Anishetty et al., Phys. Rev. D 22 (1980) 2793;
L. McLerran, Proc. Blacksburg Conf., 1981 (Plenum Press, 1982).
[8] T.D. Lee, Relativistic Heavy Ion Collisions and Future Physics, Festschrift for Feza Gürsey, to be published.
[9] R. Slansky, T. Goldman and G.L. Shaw, Phys. Rev. Lett. 47 (1981) 887.
[10] D. Antreasyan et al., Phys. Rev. Lett. 36 (1976) 1110; 40 (1978) 917;
J.W. Cronin et al., Phys. Rev. D 11 (1979) 3105.

PHYSICS REPORTS (Review Section of Physics Letters) 88, No. 5 (1982) 331–347. North-Holland Publishing Company

2. Formation and Observation of the Quark-Gluon Plasma*

J. RAFELSKI

Institut für Theoretische Physik der Universität, Frankfurt, Germany

2.1. Overview

What purpose could we follow when arguing for the study of high energy nuclear collisions [1]? It would appear that the complexity of such collisions, involving several hundreds of valence quarks, must cover up all the interesting feature of fundamental interactions. I would like to argue in this report that much in the nature and properties of strong interactions can be studied by creating in the laboratory a new state of matter – the quark-gluon plasma [2]. Unlike hadron–hadron collisions we anticipate that, in an important fraction of nucleus–nucleus collisions, each participating quark will scatter many times before joining into an asymptotic hadronic state. The associated simplification of the involved physics arises because we can use in such a case the well established methods of statistical physics in order to connect the microscopic world with effects and properties visible to experimentalists' eyes. Alone the presumption of an approximate thermochemical equilibrium frees us from the dependence on details of quark wavefunctions in a small hadronic bag consisting of only few quarks.

There are several stages in this new and exciting field of high energy physics. The first one concerns the willingness to accept the fact that available energy is equipartitioned among accessible degrees of freedom. This means that there exists a domain in space, in which, in a proper Lorentz form, the energy of the longitudinal motion has been largely transformed to transverse degrees of freedom. We call this region "fireball". The physical variables characterising a fireball are: energy density, baryon number density and volume. The basic question concerns the internal structure of the fireball – it can consist either of individual hadrons or, instead, of quarks and gluons in a new physical phase: they look deconfined as they move freely over the volume of the fireball. It appears that the phase transition from the hadronic gas phase to the quark-gluon plasma is mainly controlled by the energy density of the fireball. Several estimates [2], lead to 0.6–1 GeV/fm^3 for the critical energy density, to be compared with a value of 0.16 GeV/fm^3 inside individual hadrons. Many theoretical questions about strong interactions will be settled if the parameters and nature of the phase transition are determined. We turn to these problems further below.

The second stage of the developments in this field concerns the interaction of the experimentalists with the plasma. It is quite difficult to insert a thermometer and to measure baryon density at $T = 150$ MeV and threefold or even higher nuclear compressions. We must either use only electromagnetically interacting particles [3] (photons, lepton pairs) in order to get them out of the plasma or study the heavy flavour abundance generated in the collision [4]. To obtain a better impression of what is meant imagine that strange quarks are very abundant in the plasma (and indeed they are!). Then, since a (sss)-state is bound and stable in the hot perturbative QCD-vacuum, it would be the most abundant

* In part supported by Deutsche Forschungsgemeinschaft.

0 370-1573/82/0000–0000/$4.25

baryon to emerge from the plasma. I doubt that such an "Omegaisation" of nuclear matter could leave any doubts about the occurrence of a phase transition. Other exotic hadrons [5] such as e.g. csq, $c\bar{s}$ etc. would also support this conclusion. But even the enhancement of the more accessible abundances of $\bar{\Lambda}$ may already be sufficient for our purposes.

But there is more to meet the eyes. Restoration of the perturbative QCD vacuum may be followed at higher and higher energy densities by restoration of chiral symmetry, as shown qualitatively in fig. 2.1, then by SU(2) symmetry (and finally by SU(5) symmetry!). If the fact that we can trace back the evolution of the universe [6] in the laboratory does not excite one's fantasy, one may then remember that the plasma state is the only place known (after the universe was created) where one can "burn" baryon number, thus releasing the energy from the Big Bang stored in matter. Perhaps sufficiently extreme conditions that are here necessary are "created" inside quasars, thus leading to the enormous energies radiated by these stellar objects.

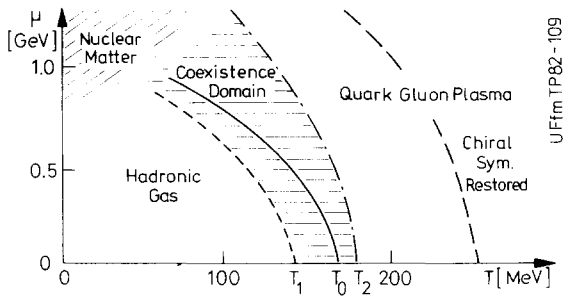

Fig. 2.1. Phase diagram of hadronic matter in the μ-T plane.

Coming back to earth we begin by recalling that in a statistical description of matter the unhandy microscopical variables: energy, baryon number etc. are replaced by thermodynamical quantities; the temperature T is a measure of energy per degree of freedom, the baryon chemical potential μ controls the mean baryon density: Statistical quantities such as entropy (measure of the number of accessible states), pressure, heat capacity etc. will be also functions of T and μ, to be determined. The theoretical techniques required for the description of both and quite different phases: the hadronic gas and the quark gluon plasma, must allow for the formation of numerous hadronic resonances on the one side [7], which then dissolve at sufficiently high spatial density in a state consisting of the fundamental constituents. At this point we must appreciate the importance and help provided by high temperature. To obtain high particle density we may, instead of compressing matter (which as it turns out is quite difficult), heat it up; many pions are easily generated, leading to the occurrence of a transition at moderate (even vanishing) baryon density [8].

2.2. Thermodynamics of interacting hadrons

The main hypothesis which allows one to simplify the situation is to postulate the resonance dominance of hadron–hadron interactions [7] – in this case the hadronic gas phase is practically a superposition of an infinity of different hadronic gases and all information about the interaction is hidden in the mass spectrum $\tau(m^2, b)$, which describes the number of hadrons of baryon number b in a mass interval dm^2 [9].

We survey in the following the developments discussed in refs. [8, 9]. We assume that the mass

spectrum $\tau(m^2, b)$ is already known. The grand microcanonical level density is then given by an invariant phase space integral. The extreme richness of the spectrum $\tau(m^2, b) \sim \exp(m/T_0)$ enables us to neglect Fermi and Bose statistics above $T \approx 50$ MeV and to treat all particles as "Boltzmannions". We find:

$$\sigma(p, V_{ex}, b) = \delta^4(p)\,\delta_K(b) + \sum_{N=1}^{\infty} \frac{1}{N!}\,\delta^4\Big(p - \sum_{i=1}^{N} p_i\Big) \sum_{\{b_i\}} \delta_K\Big(b - \sum_{i=1}^{N} b_i\Big) \prod_{i=1}^{N} \frac{2\Delta_\mu p_i^\mu}{(2\pi)^3}\,\tau(p_i^2, b_i)\,\mathrm{d}^4 p_i\,. \tag{1}$$

In this expression the first term corresponds to the vacuum state. The Nth term is the sum over all possible partitions of the total baryon number and of the total momentum p among N Boltzmannions, each having an internal number of quantum states given by $\tau(p_i^2, b_i)$. These Boltzmannions are hadronic resonances of baryon number b_1 $(-\infty < b_i < \infty)$. Every resonance can move freely in the remaining volume Δ left over from the external volume V_{ex}, after subtracting the proper volume V_c associated with all the hadrons:

$$\Delta^\mu := V_{ex}^\mu - \sum_{i=1}^{N} V_{c,i}^\mu\,; \tag{2}$$

V^μ is a covariant generalisation of V_i. In the rest frame, we have $V_\mu = (V, 0)$.

In the generalisation (1) of the popular phase space formula, three essential features of hadronic interactions are now explicitly included:

(a) The dense set of hadronic resonances dominating particle scattering via $\tau(m_i^2, b_i)$.

(b) The proper natural volumes of hadronic resonances. This is done via Δ^μ.

(c) The conservation of baryon number and the clustering of hadrons into lumps of matter with $|b| > 1$.

The thermodynamic properties of the hot hadronic gas follow from the study of the grand partition function $Z(\beta, V\lambda)$, as obtained from the level density $\sigma(p, V, b)$, namely:

$$Z(\beta, V, \lambda) = \sum_{b=-\infty}^{\infty} \lambda^b \int \mathrm{e}^{-\beta\cdot p}\sigma(p, V, b)\,\mathrm{d}^4 p\,. \tag{3}$$

A covariant generalisation of thermodynamics, with an inverse temperature four vector β_μ has been used here. In the rest frame of the relativistic baryon chemical potential μ, we have:

$$\lambda = \exp(\mu/T)\,. \tag{4}$$

This is introduced in order to conserve baryon number in the statistical ensemble. All quantities of physical interest can then be derived as usual, differentiating $\ln Z$ with respect to its variables.

Eqs. (1–3) leave us with the task of finding the mass spectrum τ. Experimental knowledge of τ is limited to low excitations and/or to low baryon number. Following Hagedorn, we introduce here a theoretical model: "the statistical bootstrap", in order to obtain a mass spectrum consistent with direct (and indirect) experimental evidence. The qualitative arguments leading to an integral equation for $\tau(m^2, b)$ are the following: when V_{ex} in eq. (1) is just the proper volume V_c of a hadronic cluster, then σ in eq. (1), up to a normalization factor, is essentially the mass spectrum τ. Indeed, how could we distinguish between a composite system [as described by eq. (1)] compressed to the natural volume of a hadronic cluster and an "elementary" cluster having the same quantum numbers? We thus demand

$$\sigma(p, V, b)|_{V=V_c} \simeq H\tau(p^2, b) \tag{5}$$

where the "bootstrap constant" H is to be determined below. It is not simply sufficient to insert eq. (5) into eq. (1) to obtain the bootstrap equation for τ. More involved arguments are indeed necessary [8, 9] in order to obtain a "bootstrap equation" for the mass spectrum such as:

$$H\tau(p^2, b) = Hz_b\,\delta_0(p^2 - M_b^2) + \sum_{N=2}^{\infty} \frac{1}{N!} \int \delta^4\Big(p - \sum_{i=1}^{N} p_i\Big) \sum_{\{b_i\}} \delta_K\Big(b - \sum_{i=1}^{N} b_i\Big) \prod_{i=1}^{N} H\tau(p_i^2, b_i)\, \mathrm{d}^4 p_i\,. \tag{6}$$

The first term is the lowest one-particle contribution to the mass spectrum, z_b is its statistical weight $(2I + 1)(2J + 1)$. The index "0" restricts the δ function to the positive root only. Only terms with $b = 0$, ± 1, corresponding to the lowest energy $q\bar{q}$ (pions) and qqq (nucleons) states contribute in the first term of eq. (6). All excitations are contained in the second term since an arbitrary quark constant can be achieved by combining $[(q\bar{q})^n(qqq)^m]$. Heavy flavours are ignored at this point but can easily be introduced. However they do not essentially influence the behaviour of τ. In the course of deriving the bootstrap equation (6) it turns out that the cluster volume V_c grows proportional to the invariant cluster mass [9]

$$V_c(p^2) = \sqrt{p^2}/(4B)\,. \tag{7}$$

The proportionality constant has been called $4B$ in order to establish a close relationship with the quark bag model [10]. The value of B can be derived from different considerations involving the true and perturbative QCD states. While the original MIT-bag fit gives $V^{1/4} = 145\,\mathrm{MeV}$, the most generally accepted value today is perhaps

$$B^{1/4} = 190\,\mathrm{MeV} \qquad \text{or} \qquad B = 170\,\mathrm{MeV/fm^3}\,. \tag{8}$$

The bootstrap constant H and the bag constant B are the only seemingly free parameters in this approach. As just pointed out, B is determined from other considerations, while H turns out to be inversely proportional to B. Hence, if one wishes to believe the last detail of the statistical bootstrap approach, there remains no free parameter in this approach. What this means for the transition from gas to plasma will be now shown.

Instead of solving eq. (6), which will lead us to the exponential mass spectrum [7],

$$\tau(m^2, b) \sim \exp(m/T_0) \tag{9}$$

we wish to concentrate here on the double integral (Laplace) transform of eq. (6) which will be all we need to establish the physical properties of the hadronic gas phase. Introducing the transforms of the one particle term, eq. (6)

$$\varphi(\beta, \lambda) := \sum_{b=-\infty}^{\infty} \lambda^b H z_b\,\delta_0(p^2 - M_b^2)\,\mathrm{e}^{-\beta\cdot p}\,\mathrm{d}^4 p \tag{10}$$

with pions and nucleons only

$$\varphi(\beta,\lambda)=2\pi HT\left[3mK_1\left(\frac{m_\pi}{T}\right)+4\left(\lambda+\frac{1}{\lambda}\right)m_N K_1\left(\frac{m_N}{T}\right)\right], \tag{11}$$

and of the mass spectrum:

$$\phi(\beta,\lambda):=\sum_{b=-\infty}^{\infty}\lambda^b\int H\tau(p^2,b)\,e^{-\beta\cdot p}\,d^4p. \tag{12}$$

We find for the entire eq. (6) the simple relation

$$\phi(\beta,\lambda)=\varphi(\beta,\lambda)+\exp[\phi(\beta,\lambda)]-\phi(\beta,\lambda)-1. \tag{13}$$

To study the behaviour of $\phi(\beta,\lambda)$ we make use of the apparent implicit dependence:

$$\phi(\beta,\lambda)=G(\varphi(\beta,\lambda)) \tag{14a}$$

with function G being defined by eq. (13)

$$\varphi=2G+1-\exp[G]. \tag{14b}$$

This function $G(\varphi)$ is shown in fig. 2.2. As is apparent there there is a maximal value φ_0

$$\varphi_0=\ln(4/e)=0.3863\ldots, \tag{14c}$$

beyond which the function G has no real solutions. Recalling the physical meaning of G, eqs. (14a, 12), we conclude that eq. (14c) establishes a boundary in the λ (i.e. μ), T plane beyond which the hadronic gas phase cannot exist. This boundary is implicitly given by the relation (11):

$$\ln(4/e)=2\pi HT_{cr}[3m_\pi K_1(m_\pi/T_{cr})+8\cosh(\mu_{cr}/T_{cr})\,m_N K_1(m_N/T_{cr})] \tag{15}$$

shown in fig. 2.3. The region denoted "Hadronic Gas Phase" is that described by our current approach.

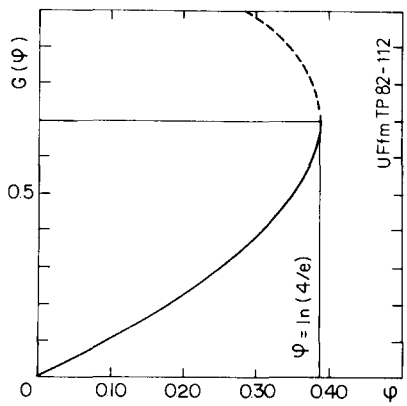

Fig. 2.2. Bootstrap function $G(\varphi)$ – the dashed line represents the unphysical branch.

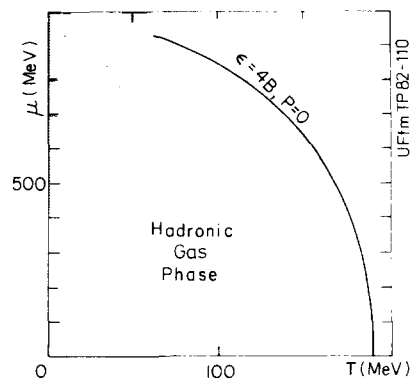

Fig. 2.3. Boundary to the "hadronic gas phase" in the bootstrap model. In the shaded region quantum statistics cannot be neglected.

With our choice of parameters we find that

$$T_{cr}(\mu_{cr} = 0) = T_0 \sim 160\text{–}170\,\text{MeV}\,. \tag{16}$$

Note that $\mu = 0$ implies zero baryon number for the plasma state. For $\mu_0 = \mu_{cr}$ ($T_{cr} = 0$) the solution of eq. (15) is simply $\mu_{cr} \sim m_N$ since no quantum statistics effects have been included. Thus the dashed region in fig. 2.2 "nuclear matter" is excluded from our considerations. As we shall shortly see, the boundary of the hadronic gas phase is also characterized by a constant energy density $\varepsilon = 4B$.

Given the function $G(\varphi) = \phi(\beta, \lambda)$ we can in principle study the form of the hadronic mass spectrum. As it turns out we can obtain the partition function directly from ϕ: The formal similarity between eq. (3) and eq. (12) can be exploited to derive a relation between their integral transforms [1] (from here on: $\beta = \sqrt{\beta_\mu \beta^\mu}$);

$$\ln Z(\beta, V_{ex}, \lambda) = -\frac{2\Delta(V_{ex})}{H\ (2\pi)^3} \frac{\partial}{\partial\beta} \phi(\beta, \lambda) \tag{17}$$

which can also be written in a form which makes the different physical inputs more explicit:

$$\ln Z(\beta, V_{ex}, \lambda) = \frac{\Delta(V_{ex})}{V_{ex}} \cdot \frac{\partial G(\varphi)}{\partial\varphi} \cdot Z_1(\beta, \lambda, V)\,. \tag{18}$$

In the absence of a finite hadronic volume and with interactions described by the first two terms, we would simply have an ideal Boltzmann gas, described by the one-particle partition function Z_1:

$$Z_1 = Z_{q\bar{q}} + 2\cosh(\mu/T)\, Z_{qqq} \tag{19}$$

where

$$Z_{q\bar{q}}/Z_{qqq} \approx (2I + 1)(2S + 1)\frac{VT^3}{2\pi^2}\left(\frac{m_{\pi/N}}{T}\right)^2 K_2\left(\frac{m_{\pi/N}}{T}\right). \tag{20}$$

Let us now briefly discuss the rôle of the available volume: as we have explicitly assumed, all hadrons have an internal energy density $4B$ (actually at finite pressure there is a small correction, see ref. [4a] for details). Hence the total energy of the fireball E_F can be written as

$$E_F \equiv \varepsilon V_{ex} = 4B(V_{ex} - \Delta) \tag{21}$$

where $V_{ex} - \Delta$ is the volume occupied by hadrons. We thus find

$$\Delta = V_{ex} - E_F/4B = V_{ex}(1 - \varepsilon/(4B)) \tag{22}$$

when working out the relevant physical consequences we must always remember that the fireball is an isolated physical system, for which a statistical approach has been followed in view of the internal disorder (high number of available states) rather than because of a coupling to a heat bath.

The remainder of the discussion of the hadronic gas is a simple application of the rules of statistical

thermodynamics. By investigating the meaning of the thermodynamic averages it turns out that the apparent (β, λ) dependence of the available volume Δ in eq. (18) must be disregarded when differentiating $\ln Z$ with respect to β and λ. As eq. (1) shows explicitly, the density of states for extended particles in V_{ex} is the same as that for point particles in Δ. Therefore

$$\ln Z(\beta, V_{ex}, \lambda) \equiv \ln Z_{pt}(\beta, \Delta, \lambda) . \tag{23}$$

We thus first calculate the *point* particle energy, baryon number densities, pressure, and entropy density

$$\varepsilon_{pt} = -\frac{1}{\Delta}\frac{\partial}{\partial\beta} \ln Z_{pt} = \frac{2}{H(2\pi)^3}\frac{\partial^2}{\partial\beta^2}\phi(\beta, \lambda) \tag{24}$$

$$\nu_{pt} = \frac{1}{\Delta}\lambda\frac{\partial}{\partial\lambda} \ln Z_{pt} = -\frac{2}{H(2\pi)^3}\lambda\frac{\partial^2}{\partial\lambda\,\partial\beta}\phi(\beta, \lambda) \tag{25}$$

$$P_{pt} = \frac{T}{\Delta} \ln Z_{pt} = -\frac{2T}{H(2\pi)^3}\frac{\partial}{\partial\beta}\phi(\beta, \lambda) \tag{26}$$

$$s_{pt} = \frac{1}{\Delta}\frac{\partial}{\partial T}(T \ln Z_{pt}) = \frac{P_{pt}}{T} + \frac{\varepsilon_{pt} - \mu\nu_{pt}}{T} . \tag{27}$$

From this, we easily find the energy density, as

$$\varepsilon = \frac{\langle E\rangle}{V_{ex}} = -\frac{1}{V_{ex}}\frac{\partial}{\partial\beta} \ln Z(\beta, V_{ex}, \lambda) = \frac{\Delta}{V_{ex}} \cdot \varepsilon_{pt} . \tag{28}$$

Inserting eq. (22) into eq. (28) and solving for ε, we find:

$$\varepsilon(\beta, \lambda) = \frac{\varepsilon_{pt}(\beta, \lambda)}{1 + \varepsilon_{pt}(\beta, \lambda)/4B} , \tag{29}$$

and hence another form for eq. (22):

$$V_{ex} = \Delta \cdot (1 + \varepsilon_{pt}(\beta, \lambda)/4B) \tag{30}$$

and similarly for the baryon density, pressure and entropy density

$$\nu = \frac{\nu_{pt}}{1 + \varepsilon_{pt}/4B} \tag{31}$$

$$p = \frac{P_{pt}}{1 + \varepsilon_{pt}/4B} \tag{32}$$

$$s = \frac{s_{pt}}{1 + \varepsilon_{pt}/4B} . \tag{33}$$

We now have a complete set of equations of state for observable quantities as functions of the

chemical potential μ, the temperature T and the external volume V_{ex}. While these equations are semi-analytic, one has to evaluate the different quantities numerically due to the implicit definition of $\phi(\beta, \lambda)$ that determines $\ln Z$. However, when β, λ approach the critical curve, fig. 2.3, we easily find from the singularity of ϕ that ε_{pt} diverges and therefore

$$\begin{aligned} \varepsilon &\to 4B \\ p &\to 0 \\ \Delta &\to 0\,. \end{aligned} \tag{34}$$

These limits indicate that at the critical line, matter has lumped into one large cluster with the energy density $4B$. No free volume is left, and, since only one cluster is present, the pressure has vanished. However, the baryon density varies along the critical curve; it falls with increasing temperature. This is easily understood: as temperature is increased, more mesons are produced that take up some of the available space. Therefore hadronic matter can saturate at lower baryon density. We further note here that in order to properly understand the approach to the phase boundary, one has to incorporate and understand the properties of the hadronic world beyond the critical curve. We turn now to the study of the perturbative quark-gluon plasma phase.

2.3. QCD and the quark-gluon plasma

We begin with a summary of the relevant postulates and results that characterize the current understanding of strong interactions in quantum chromodynamics (QCD). The most important postulate is that the proper vacuum state in QCD is not the (trivial) perturbative state that we (naively) imagine to exist everywhere and which is hardly changed when the interactions are turned off/on. In QCD the true vacuum state is believed to have a complicated structure which originates in the glue (pure gauge field) sector of the theory. The perturbative vacuum is an excited state with an energy density B above the true vacuum. It is to be found inside hadrons where perturbative quanta of the theory, in particular quarks, can therefore exist. The occurrence of the true vacuum state is intimately connected to the glue–glue interaction; gluons also carry the colour charge that is responsible for the quark–quark interaction. In the above discussion, the confinement of quarks is a natural feature of the hypothetical structure of the true vacuum.

Another feature of the true vacuum is that it exercises a pressure on the surface of the region of the perturbative vacuum to which quarks are confined. Indeed, this is just the idea of the original MIT bag model [10]. The Fermi pressure of almost massless light quarks is in equilibrium with the vacuum pressure B. When many quarks are combined to form a giant quark bag, then their properties inside can be obtained using the standard methods of many-body theory [2]. In particular, this also allows one to include the effect of internal excitation through a finite temperature and through a change in the chemical composition.

A further effect which must be taken into consideration is the quark–quark interaction. We shall use here the first order contribution in the QCD running coupling constant $\alpha_s(q^2) = g^2/4\pi$. However, as $\alpha_s(q^2)$ increases when the average momentum exchanged between quarks decreases, this approach will have only a limited validity at relatively low densities and/or temperatures. The collective screening effects in the plasma are of comparable order of magnitude and should reduce the importance of the perturbative contribution.

As u and d quarks are almost massless inside a bag, they can be produced in pairs and at moderate temperatures many $q\bar{q}$ pairs will be present. In particular also $s\bar{s}$ pairs will be produced and we will return to this point below. Furthermore, real gluons can be present when $T \neq 0$ and will be included here in our considerations.

As it was outlined in the previous section, a complete description of the thermodynamical behaviour of a many-particle system can be derived from the grand partition function Z. For the case of the quark-gluon plasma in the perturbative vacuum, one finds an analytic expression to first order in α neglecting quark masses. We obtain for the quark Fermi gas [2b]

$$\ln Z_q(\beta, \lambda) = \frac{gV}{6\pi^2}\beta^{-3}\left[\left(1-\frac{2\alpha_s}{\pi}\right)\left(\frac{1}{4}\ln^4 \lambda_q + \frac{\pi^2}{2}\ln^2 \lambda_q\right) + \left(1-\frac{50}{21}\frac{\alpha_s}{\pi}\right)\frac{7\pi^4}{60}\right] \tag{35}$$

where $g = (2s+1)(2I+1)N = 12$ counts the number of the components in the quark gas, and λ_q is the fugacity related to quark number. Since each quark has baryon number $\frac{1}{3}$, we find

$$\lambda_q^3 = \lambda = e^{\mu/T} \tag{36}$$

where λ, as previously, allows one to have conservation of baryon number. Consequently

$$3\mu_q = \mu\,. \tag{37}$$

The glue contribution is [2]

$$\ln Z_g(\beta, \lambda) = V\frac{8\pi^2}{45}\beta^{-3}\left(1-\frac{15\alpha_s}{4\pi}\right). \tag{38}$$

We notice two relevant differences with the photon gas: (i) the occurrence of a factor eight associated with the number of gluons; (ii) the glue–glue interaction since gluons carry the colour charge.

Finally, let us introduce the true vacuum term as

$$\ln Z_{vac} = -\beta B V. \tag{39}$$

This leads to the required positive energy density B within the volume occupied by the coloured quarks and gluons and to a negative pressure on the surface of this region. At this stage, this term is entirely phenomenological as discussed above. The equations of state for the quark-gluon plasma are easily obtained by differentiating

$$\ln Z = \ln Z_q + \ln Z_g + \ln Z_{vac} \tag{40}$$

with respect to β, λ and V. The energy density, baryon number density, pressure and entropy density are respectively, written in terms of μ and T

$$\varepsilon = \frac{6}{\pi^2}\left[\left(1-\frac{2\alpha_s}{\pi}\right)\left(\frac{1}{4}\left(\frac{\mu}{3}\right)^4 + \frac{1}{2}\left(\frac{\mu}{3}\right)^2(\pi T)^2\right) + \left(1-\frac{50}{21}\frac{\alpha_s}{\pi}\right)\frac{7}{60}(\pi T)^4\right] + \frac{8}{15\pi^2}(\pi T)^4\left(1-\frac{15}{4}\frac{\alpha_s}{\pi}\right) + B \tag{41}$$

$$\nu = \frac{2}{3\pi^2}\left[\left(1-\frac{2\alpha_s}{\pi}\right)\left(\left(\frac{\mu}{3}\right)^3+\frac{\mu}{3}(\pi T)^2\right)\right] \tag{42}$$

$$p = \frac{1}{3}(\varepsilon - 4B) \tag{43}$$

$$s = \frac{2}{\pi}\left(1-\frac{2\alpha_s}{\pi}\right)\left(\frac{\mu}{3}\right)^2(\mu T)+\frac{14}{15\pi}\left(1-\frac{50}{21}\frac{\alpha_s}{\pi}\right)(\pi T)^3+\frac{32}{45\pi}\left(1-\frac{15}{4}\frac{\alpha_s}{\pi}\right)(\pi T)^3 . \tag{44}$$

In eqs. (41, 44) the second T^4 (respt. T^3) term originates from the gluonic degrees of freedom. In eq. (43) we have right away used the relativistic relation between the quark and gluon energy density and pressure

$$p_q = \tfrac{1}{3}\varepsilon_q , \qquad p_g = \tfrac{1}{3}\varepsilon_g \tag{45}$$

in order to derive this simple form of the equation of state.

This simple equation of state of the quark-gluon plasma is slightly modified when finite quark masses are considered, or when the QCD coupling constant α_s is dependent on the dimensional parameter Λ. From eq. (43) it follows that when the pressure vanishes, the energy density is $4B$, independently of the values of μ and T which fix the line $P = 0$. We recall that this has been precisely the kind of behaviour found for the hadronic gas. This coincidence of the physical observables strongly suggests that, in an exact calculation, both lines $P = 0$ should coincide; we will return to this point again below. For $P > 0$ we have $\varepsilon > 4B$ – we recall that in the hadronic gas we always had $\varepsilon \leq 4B$. Thus, in this domain of the μ–T plane, we have a quark-gluon plasma exposed to an external force.

In order to obtain an idea of the form of the ($P = 0$) critical curve in the μ–T plane as obtained for the quark-gluon plasma, we rewrite eq. (43) for $P = 0$:

$$B = \frac{(1-2\alpha_s/\pi)}{162\pi^2}[\mu^2+(3\pi T)^2]^2-\frac{T^4\pi^2}{45}\left[\left(1-\frac{5\alpha_s}{3\pi}\right)\cdot 12-\left(1-\frac{15\alpha_s}{4\pi}\right)\cdot 8\right]. \tag{46}$$

Here, the last term is the glue pressure contribution. We find that the greatest lower bound on temperature T_q, at $\mu = 0$ is about ($\alpha_s = \frac{1}{2}$)

$$T_q \approx 0.83\, B^{1/2} \sim 160\ \text{MeV} \approx T_0 . \tag{47}$$

This result shows the expected order of magnitude. The most remarkable point is, that it leads, for $B^{1/4} = 190$ MeV, to almost exactly the same value as that found in the hadronic gas study presented in the previous section.

Let us further note here that for $T \ll \mu$ the baryon chemical potential tends to

$$\mu_B = 3\mu_q \Rightarrow 3B^{1/4}\left[\frac{2\pi^2}{(1-2\alpha_s/\pi)}\right]^{1/4} = 1320\ \text{MeV} \quad [\alpha_s = \tfrac{1}{2},\ B^{1/4} = 190\ \text{MeV}] . \tag{48}$$

Concluding this discussion of the $P = 0$ line for the quark-gluon plasma, let us note that the choice $\alpha_s \sim \frac{1}{2}$ is motivated by fits of the charmonium and upsilonium spectra as well as by the analysis of deep inelastic scattering. In both these cases spacelike domains of momentum transfer are explored. The

much smaller value of $\alpha_s \sim 0.2$ is found in timelike regions of momentum transfer, in $e^+e^- \to$ hadrons experiments. In the quark-gluon plasma, as described up to first order in perturbation theory, positive and negative momentum transfers occur: the perturbative corrections to the radiative T^4 contribution is dominated by timelike momentum transfers, while the correction to the μ^4 term originates from spacelike quark–quark scattering. Finally we consider the energy density at $\mu = 0$. Restructuring some factors again, we find the simple result:

$$\varepsilon = B + \frac{\pi^2}{30} T^4 \left[2_s \cdot 8_c \cdot \left(1 - \frac{15}{4} \frac{\alpha_s}{\pi} \right) + 2_I \cdot 2_s \cdot 2_c \frac{7}{4} \left(1 - \frac{50}{21} \frac{\alpha_s}{\pi} \right) \right]. \tag{49}$$

We note that for both quarks and gluons the interaction conspires to *reduce* the effective number of degrees of freedom which are accessible. At $\alpha_s = 0$ we find a handy relation

$$\varepsilon_q + \varepsilon_g = (T/160\,\text{MeV})^4 [\text{GeV/fm}^3]\,. \tag{50}$$

At $\alpha_s = \frac{1}{2}$ we are seemingly left with only ~50% of the degrees of freedom, and the temperature "unit" in the above formula drops to 135 MeV.

I have so far neglected to include heavy flavours into the description. For charm, with a mass of about 1500 MeV, the thermodynamic abundance is sufficiently low that we can ignore its influence on the properties of the plasma. Also, even the equilibrium abundance is quite small. Evaluating the phase-space integrals that the ratio of charm to light antiflavour (either $\bar{u}$ or $\bar{d}$) gives

$$c/\bar{q} = \bar{c}/\bar{q} = \exp\{-(m_c - \mu/3)/T\}(m_c/T)^{3/2} \tfrac{1}{2}\sqrt{\pi/2}\,. \tag{51}$$

Taking as a numerical example $m_c = 1500$ MeV, $T = 200$ MeV, $\mu = 0$, one finds with $c/\bar{q} = 7 \times 10^{-3}$ a small, but still quite significant abundance. However, the approach to chemical equilibrium (see below) is to be studied to establish if the chemical equilibrium assumption is justified. We note that the energy fraction carried by intrinsic charm in the plasma would be ~0.2% in the above example.

Clearly, we must turn our attention to strangeness – with a current quark mass of about 180 MeV, we are actually above threshhold and indeed one finds that there is a quite appreciable s-abundance (see again next part). An explicit calculation [4b] has shown that chemical equilibrium will be reached during the short time interval of a heavy ion reaction. The motion of the particles being already semirelativistic, an increase by about 15% of the number of available degrees of freedom (eq. (49)) is due to $s\bar{s}$ production. The appearance of strangeness is a very important qualitative factor and we shall return to its discussion in section 2.5.

2.4. Phase transition from the hadronic gas to the quark-gluon plasma

We have shown that two inherently different descriptions lead to the prediction of a qualitatively similar region where a transition between both phases of hadronic matter can occur. From our results we cannot deduce the order of the phase transition. However, the physics arguments which went into these theoretical approaches require that this is a first order phase transition.

Consider the p–V diagram shown in fig. 2.4. Here we distinguish three domains – the hadonic gas region is simply a Boltzmann gas where the pressure increases with reduction of the volume. However,

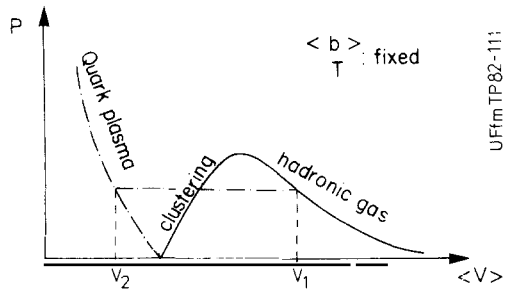

Fig. 2.4. p–V diagram for the gas-plasma first order transition.

when internal excitation becomes important, the individual hadrons begin to cluster, reducing the increase in the Boltzmann pressure since smaller number of particles exercises smaller pressure. In the proper description we would have to describe this situation by allowing a coexistence of hadrons with the plasma – this becomes necessary when the clustering overwhelms the compressive effects and the pressure falls to zero as V reaches the proper volume of hadronic matter. At this point the pressure rises again very quickly, since we now compress the hadronic constituents. By performing the Maxwell construction as indicated in fig. 2.4 between volumes V_1 and V_2 we can find the most likely way taken by the compressed hadronic gas in a nuclear collision. In our approach it seems to be a first order transition. We should remember, that on the way out, during the expansion of the plasma state, the entropy generated in the plasma (e.g. by s-production, shocks etc.) may require that the isolated plasma state must expand to vanishing pressure $P = 0$ before it can disintegrate into individual hadrons. In an extreme situation this disintegration may be quite a slow process with successive fragmentations!

It is interesting to follow the path taken by an isolated quark-gluon plasma fireball in the μ–T plane, or equivalently in the ν–T plane. Several cases are depicted in fig. 2.5. After the Big Bang, with expansion of the universe, the cooling shown by the dashed line occurs in a universe in which most of the energy is in the form of radiation – hence we have for the chemical potential $\mu \ll T$. Similarly the baryon density ν is quite small. In normal stellar collapse leading to cold neutron stars we follow the dashed-dotted line parallel to the μ- resp. ν-axis. The compression is accompanied by little heating. In nuclear collision shown by the full line, the entire μ–T and ν–T plane can be explored by varying the parameters of the colliding nuclei. It is important to appreciate that the arrows show the time evolution, i.e. path of increasing entropy for the hadronic fireball at fixed total energy and baryon number.

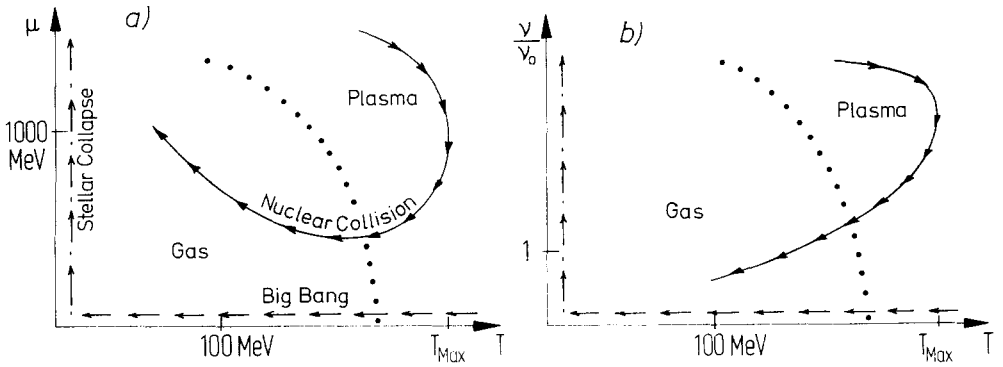

Fig. 2.5. Paths taken in the (a) μ–T plane and (b) ν–T plane by different physical events.

In the expansion period during which the temperature decreases, there is an associated decrease of the chemical potential and of the density in the plasma phase while in the hadronic *gas* phase the chemical potential can increase while the baryon density decreases. As it is evident from fig. 2.5, one expects that the transition *from gas to plasma* takes place at higher baryon density and lower temperature than the transition *from plasma to gas.* Obviously the larger volume fireball at higher temperature contains more entropy at fixed total energy and baryon number. The initial heating of the fireball at almost constant baryon density is done at the expense of a significant reduction in the baryon chemical potential. This conversion of chemical energy to thermal excitation stops at some T_{Max} the value of which depends on the available internal fireball energy. The qualitative curves are typical representatives obtained from the equations of sections 2.2 and 2.3 for fixed E, b. Finally, the question arises: how does the hadronic gas enter into the plasma state? As we follow the full line backwards, μ (resp. ν) increases with decreasing T and we stay in the plasma phase until quite low temperatures. This suggests that in order to get into the plasma at moderate temperatures and baryon densities (say: $T = 150$ MeV, $\nu \sim 3\nu_0 \leftrightarrow \mu \sim 800$ MeV) we must blow off (perhaps in a manner similar to supernovae explosions) some cold surface matter – or otherwise generate by internal nonequilibirum processes *sufficient amounts of entropy.* It is for that reason that we have avoided to indicate the gas → plasma transition in fig. 2.5, as it must be a highly nonequilibrium transition to which values μ, T cannot perhaps be assigned at all: On the other hand, the expansion of the plasma seems to be an adiabatic process, although here also some significant amounts of entropy are produced.

As a last related comment we turn to the question: is the transition "hadronic gas → quark-gluon plasma" in principle a phase transition or is it only a change in the nature of hadronic matter which is not associated with any kind of singularity in the partition function in the limit of infinite volume. In the spirit of the theoretical approaches taken here one needs a first order transition. However, this cannot be considered as final – since contrary evidence can be found arguing that, in any finite volume, only a finite number of *incompressible* hadrons can be studied. Here it turns out that one must very carefully study the meaning of the thermodynamical limits before a conclusion can be reached; even worse is the observation that for compressible individual hadrons we might find a second order phase transition. From this remark we learn how sensitive this theory is to even the slightest improvement. I would like to conclude that it is experiment which should teach us this important aspect of strong interactions.

2.5. Strangeness in the plasma

In order to observe the properties of the quark-gluon plasma we must design a thermometer, or an isolated degree of freedom weakly coupled to hadronic matter. Nature has provided several such thermometers: leptons, direct photons and quarks of heavy flavours. We would like to point here to a particular phenomenon perhaps quite uniquely characteristic of quark matter. First we note that, at a given temperature, the quark-gluon plasma will contain an equal number of strange (s) quarks and antistrange ($\bar{s}$) quarks. They are present during a hadronic collision time much too short to allow for weak interaction conversion of light flavours to strangeness. Assuming chemical equilibrium in the quark plasma, we find the density of the strange quarks to be (two spins and three colour):

$$\frac{s}{V} = \frac{\bar{s}}{V} = 6 \int \frac{\mathrm{d}^3 p}{(2\pi)^3} \exp\{-\sqrt{p^2 + m_s^2}/T\} = 3 \frac{T m_s^2}{\pi^2} K_2\left(\frac{m_s}{T}\right) \tag{52}$$

(neglecting, for the time being, perturbative corrections). As the mass of the strange quarks, m_s, in the perturbative vacuum is believed to be of the order of 150–280 MeV, the assumption of equilibrium for $m_s/T \sim 2$ may indeed be correct. In eq. (52) the Boltzmann distribution can be used, as the density of strangeness is relatively low. Similarly, there is a certain light antiquark density ($\bar{q}$ stands for either $\bar{u}$ or $\bar{d}$):

$$\frac{\bar{q}}{V} \cong 6 \int \frac{d^3p}{(2\pi)^3} \exp\{-|p|/T - \mu_q/T\} = \exp\{-\mu_q/T\} \cdot T^3 \frac{6}{\pi^2} \tag{53}$$

where the quark chemical potential is $\mu_q = \mu/3$. This exponent suppresses the $q\bar{q}$ pair production, since only for energies higher than μ_q, there is a large number of empty states available for quarks.

What I now intend to show is that there are many more $\bar{s}$ quarks than antiquarks of each light flavour. Indeed:

$$\frac{\bar{s}}{\bar{q}} = \frac{1}{2}\left(\frac{m_s}{T}\right)^2 K_2\left(\frac{m_s}{T}\right) e^{\mu/3T}. \tag{54}$$

The function $x^2 K^2(x)$ varies between 1.3 and for $x = m_s/T$ between 1.5 and 2. Thus, we almost always have more $\bar{s}$ than $\bar{q}$ quarks and, in many cases of interest, $\bar{s}/\bar{q} \sim 5$. As $\mu \to 0$ there are about as many $\bar{u}$ and $\bar{q}$ quarks as there are $\bar{s}$ quarks. This is shown quantitatively in fig. 2.6. Another important aspect is the total strangeness abundance since for $T = 200$ MeV, $m_s = 150$ MeV, chemical equilibrium predicts it at about twice the normal baryon density: $s/b = 0.4$; hence there are as many strange and antistrange quarks as there are baryons in the hadronic gas, or even much more, if we are in the "radiation" i.e. baryon number depleted region.

The crucial question which arises is whether there is enough time to create $s\bar{s}$ pairs in nuclear collisions. To answer it one has to compute [4b] (say in lowest order in perturbative QCD) the two contributing invariant reaction rates (per unit time and per unit volume)

$$\begin{aligned} &A_{q\bar{q}} : q\bar{q} \to s\bar{s} \\ &A_{gg} : gg \to s\bar{s} \,. \end{aligned} \tag{55}$$

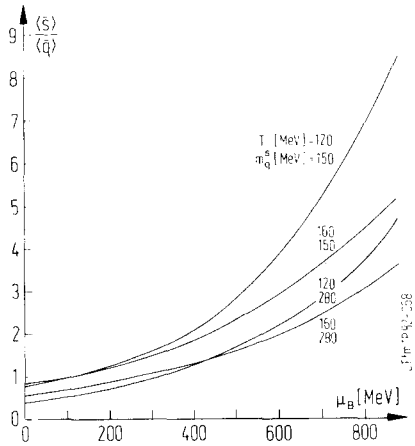

Fig. 2.6. Abundance of strange (= antistrange) quarks relative to light quark as a function of μ for several choices of T (= 120, 160 MeV) and strange quark mass (m_q^s = 150, 280 MeV).

The contributing diagrams are shown in figs. 2.7 a and b, respectively. These rates are dominated by the glue–glue reaction and at $T = 200$ MeV, $m_s = 150$ MeV, $\alpha_s = 0.6$ one finds $A_{gg} \approx 16/\text{fm}^4$. This is quite a large rate, indicating that the typical relaxation time

$$\tau = n(\infty)/A \tag{56}$$

($n(\infty)$ is the density at infinite time) will be about 10^{-23} sec. In fig. 2.8 the strangeness population evolution is shown as a function of time at fixed $\mu = 900$ MeV. During the minimal anticipated lifetime of the plasma we thus find that the strange quark abundance saturates at its chemical equilibrium point.

One can study how much more total strangeness is found in the quark-gluon plasma as compared to the hadronic gas phase. While the total yields are up to 5–7 times higher (again depending on some parameters) it is more appropriate to concentrate attention on those reaction channels which will be particularly strongly populated when the quark plasma dissociates into hadrons. Here in particular, it appears that the presence of quite rare multistrange hadrons will be enhanced, first because of the relative high phase space density of strangeness in the plasma, and second because of the attractive ss-QCD interaction in the $\bar{3}_c$ state and $\bar{s}s$ in the 1_c state. Hence one should search for an increase of the abundances of particles like Ξ, $\bar{\Xi}$, Ω, $\bar{\Omega}$, ϕ and perhaps for highly strange pieces of baryonic matter, rather than in the K-channels. However, it appears that already a large value for the $\bar{\Lambda}/\Lambda$ ratio would be a significant signal. Not to be forgotten are secondary effects, e.g. those due to $s\bar{s}$ annihilation into γ (and infrared glue) in the plasma. Different experiments will be sensitive to different energy ranges.

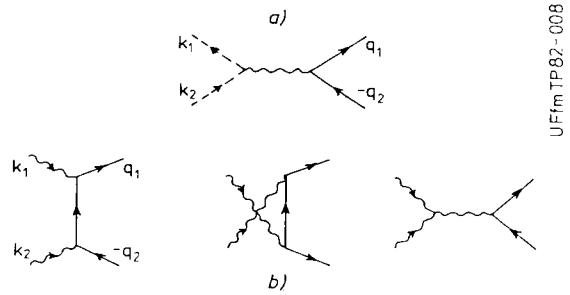

Fig. 2.7. First order diagrams for $s\bar{s}$ production reactions; (a) $q\bar{q} \to s\bar{s}$, (b) $gg \to s\bar{s}$.

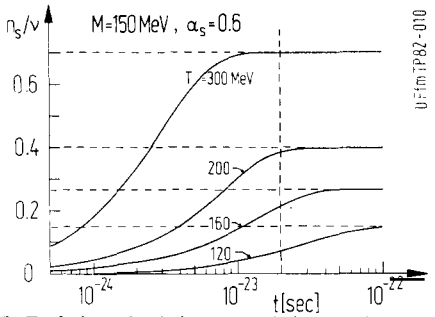

Fig. 2.8. Evolution of relative s population per baryon number as function of time in the plasma. For $T \geq 160$ MeV chemical saturation is noticeable in about 2×10^{-23} sec, the anticipated minimal plasma livetime.

2.6. Summary and outlook

Our aim has been to obtain a description of highly excited hadronic matter. By postulating a kinetic and chemical equilibrium we have been able to develop a thermodynamic description valid for high temperatures and different chemical compositions. Along this line we have found two physically different domains; firstly a hadronic gas phase, in which individual hadrons can exist as separate entities, but are sometimes combined into larger hadronic clusters; and secondly, a domain in which individual hadrons dissolve into one large cluster consisting of hadronic constituents – the quark-gluon plasma.

In order to obtain a theoretical description of both phases we have used some "common" knowledge and a plausible interpretation of the currently available experimental facts. In particular, in the case of

the hadronic gas, we have completely abandoned a more conventional Lagrangian approach in favour of a semiphenomenological statistical bootstrap model of hadronic matter that incorporates those properties of hadronic interaction which are, in our opinion, most important.

In particular, the attractive interactions are included through the rich, exponentially growing hadronic mass spectrum $\tau(m^2, b)$ while the introduction of a finite volume for each hadron is responsible for an effective short-range repulsion. We have neglected quantum statistics in the hadronic gas phase since a quantitative study reveals that this is allowed above $T \approx 50$ MeV. But we allow particle production, which introduces a quantum physical aspect into the otherwise "classical" theory of Boltzmann particles.

Our considerations lead us to an equation of state for hadronic matter which reflects what we have included in our considerations. It is the *quantitative* nature of this approach that allows a detailed comparison with experiment. It is important to observe that the predicted temperatures and mean transverse momenta of particles agree with the experimental results available at $E_{k,lab}/A = 2$ GeV [BEVELAC–] and at 100 GeV [ISR–] as much as a comparison is permitted.

The internal theoretical consistency of this description of the gas phase leads, in a straightforward fashion, to the postulate of a first order phase transition to a quark-gluon plasma. This second phase is treated by a quite different method; in addition to the standard Lagrangian quantum field theory of ("weakly") interacting particles at finite temperature and density, we also introduce the phenomenological vacuum pressure and energy density B. This term is required in a consistent theory of hadronic structure. It turns out that $B^{1/4} \sim 190$ MeV is just, to within 20%, the temperature of the quark phase before its dissociation into hadrons. This is similar to the maximal hadronic temperature $T_0 \simeq 160$ MeV.

Perhaps the most interesting aspect of our work is the realization that the transition to quark matter will occur at very much lower baryon density for highly excited hadronic matter than for matter in its ground state ($T = 0$). Using the currently accepted value for B, we find that at $\nu \sim 2$–$3\nu_0$, $T = 150$ MeV, a quark phase may indeed already be formed. The detailed study of the different aspects of this phase transition must still be carried out. However, initial results look very encouraging, since the required baryon density and temperatures are well within the range of fixed target, heavy nucleon collisions with 100 GeV per nucleon. We look forward to such a heavy ion facility which should provide us with the required experimental information.

References

[1] Proceedings of the Workshop on Future Relativistic Heavy Ion Experiments, eds. R. Stock and R. Bock, GSI 81-6, Orange Report 1981.

[2] An incomplete list of quark-gluon plasma papers includes:
(a) B.A. Freedman and L.D. McLerran, Phys. Rev. D16 (1977) 1169;
(b) S.A. Chin, Phys. Lett. 78B (1978) 552;
(c) P.D. Morley and M.B. Kislinger, Phys. Reports 51 (1979) 63;
(d) J.I. Kapusta, Nucl. Phys. B148 (1979) 461;
(e) O.K. Kalashnikov and V.V. Klimov, Phys. Lett. 88B (1979) 328;
(f) E.V. Shuryak, Phys. Lett. 81B (1979) 65 and Phys. Reports 61 (1980) 71;
(g) J. Rafelski and R. Hagedorn, From Hadron Gas to Quark Matter II, in: Thermodynamics of Quarks and Hadrons, ed. H. Satz (North-Holland, Amsterdam, 1981).

[3] (a) G. Domokos and J.I. Goldman, Phys. Rev. D23 (1981) 203;
(b) K. Kajantie and H.I. Miettinen, Temperature Measurements of Quark-Gluon Plasma Formed in High Energy Nucleus-Nucleus Collisions, Helsinki Preprint HU-TFT-81-7 (1981);
(c) K. Kajantie and H.I. Miettinen, Muon Pair Production in Very High Energy Nucleus-Nucleus Collisions, Helinski Preprint HU-TFT 82-16 (1982).

[4] (a) J. Rafelski, Extreme States of Nuclear Matter, in ref. [1] p. 282; Universität Frankfurt Preprint UFTP 52/1981;
(b) J. Rafelski and B. Müller, Phys. Rev. Lett. 48 (1982) 1066;
(c) P. Koch, J. Rafelski and W. Greiner, Equilibrium Chemistry of Strange Particles in Hot Nuclear Matter, Universität Frankfurt Preprint UFTP 77/1982.
[5] J. Rafelski, Hot Hadronic Matter, in: New Flavours and Hadron Spectroscopy, ed. J. Tran Thanh Van (Editions Frontières, 1981) p. 619.
[6] J. Ellis, Phenomenology of Unified Gauge Theories, CERN-preprint TH 3174.
[7] These ideas originate in Hagedorn's statistical Bootstrap theory, see:
R. Hagedorn, Suppl. Nuovo Cimento 3 (1964) 147; Nuovo Cimento 6 (1968) 311;
R. Hagedorn, How to Deal with Relativistic Heavy Ion Collisions, in ref. [1] p. 236.
[8] R. Hagedorn and J. Rafelski, Phys. Lett. 97B (1980) 136.
[9] The extension of Statistical Bootstrap to finite baryon number and volume has been introduced in:
R. Hagedorn, I. Montvay and J. Rafelski, Lecture at Erice Workshop 'Hadronic Matter at Extreme Energy Density', ed. N. Cabibbo (Plenum Press, NY, 1980) p. 49.
[10] K. Johnson, Acta Phys. Polon. B6 (1975) 865;
T. de Grand, R.L. Jaffe, K. Johnson and J. Kiskis, Phys. Rev. D12 (1975) 2060.

PHYSICS REPORTS (Review Section of Physics Letters) 88, No. 5 (1982) 349–364. North-Holland Publishing Company

3. Critical Behaviour in Finite Temperature QCD

Helmut SATZ

Fakultät für Physik, Universität Bielefeld, Germany

3.1. Introduction

Quarks and gluons appear confined as long as we consider hadrons in the physical vacuum: any constituent can then travel a spatial distance of not more than 10^{-13} cm before it reaches confinement constraints

In sufficiently dense matter, we expect this situation to change. Colourless hadronic matter should then undergo a phase transition to colour conducting quark matter. With sufficient overlap, the constituents can no longer be associated to a given hadron and can move over macroscopic distances without ever leaving an overall confinement environment.

The idea of a phase transition from hadronic to quark matter is as old [1] as the quark structure of hadrons. Since then, a great variety of phenomenological approaches to the two-phase nature of strongly interacting matter have been pursued [2]. They all have in common two phases as input. The advent of quantum chromodynamics (QCD) gave rise to the hope that both the two-phase character and the transition might be obtained from one basic theory [3]. Exciting recent developments in lattice QCD at finite temperature seem to indicate that such a hope is justified [4–14]; these developments will be the subject of my survey.

Quantum chromodynamics specifies the basic interaction of quarks and gluons; from this we are to obtain the description of strongly interacting matter in its different states. Not surprisingly, the first attempts concentrated on limiting behaviour.

Asymptotic freedom makes interactions at very short distances (or high momenta) arbitrarily weak, so that a perturbation expansion in powers of the effective coupling may be expected to converge in the limit of high temperature or density [15]. Sufficiently hot and/or dense matter should therefore become a gas of non-interacting quarks and gluons.

In the confinement region, at lower temperatures and densities, strongly interacting matter should exhibit hadronic behaviour. One has here considered on the lattice an expansion in terms of the inverse coupling (strong coupling expansion [3]) or used in the continuum semiclassical solutions to the field equations (instanton gas [16]). The resulting description indeed provided many aspects of hadron phenomenology, as given e.g. by dual string or bag models.

Strong and weak coupling approaches have evidently specified regions of applicability and thus basically give one-phase descriptions. Nevertheless, they already provide hints for a phase transition near the boundary of their regions of validity. In the perturbative treatment of the quark-gluon gas, the pressure (in first order) becomes negative at some temperature value, and this has been interpreted as the onset of confinement [15]. In the strong coupling expansion, there are indications for a phase transition due to Debye screening of colour charges [3]. The suppression of large scale instantons leads to similar conclusions [16]. It is clear, however, that these limiting approaches cannot give us the unified "whole-range" description we would like to obtain from a basic theory.

0 370-1573/82/0000–0000/$4.00

The Monte Carlo evaluation of finite temperature QCD on the lattice now provides us with such a unified picture. The evaluation method itself was devised for and first applied to the study of the confinement problem [17]. Its application to finite temperature statistical mechanics is, however, quite straight-forward – perhaps it is even more natural here, where the real physical temperature plays the role of the Euclidean time in the confinement problem. In either case, the lattice acts as scaffolding during the evaluation: both discreteness and finiteness are to be removed at the end, to give us continuum theory results.

3.2. Two-phase phenomenology

In order to introduce some of the questions and concepts of critical strong interaction physics, we shall in this part briefly consider simple phenomenological models for the two "limiting" phases.

For the statistical mechanics of hadronic matter, we consider an ideal gas of ground state hadrons and all their resonance excitations. The partition function of such a resonance gas is

$$\ln Z_{\mathrm{H}}(\beta, V) = \frac{V}{(2\pi)^3} \int_0^\infty \mathrm{d}m\, \tau(m) \int \mathrm{d}^3k\, \exp\{-\beta\sqrt{k^2+m^2}\}, \tag{2.1}$$

for a system with zero chemical potential and, for simplicity, with Boltzmann statistics; $\beta^{-1} = T$ is the temperature, V the spatial volume. From hadron dynamics (dual string [18], bag [19] models), the resonance spectrum $\tau(m)$ is known to have the form

$$\begin{aligned} &\tau(m) = d\,\delta(m - m_0) + c\,\theta(m - 2m_0) m^{-a}\, \mathrm{e}^{bm}, \\ &a, b, c, d = \text{const.}, \end{aligned} \tag{2.2}$$

as first proposed by Hagedorn [20]. The first term in eq. (2.2) corresponds to a d-fold degenerate ground state; for $c = 0$, we would thus simply obtain an ideal gas of ground state hadrons. While a depends on the details of the model used [2], b is related quite generally to the string tension σ ($b^2 = 3\sigma/4\pi$ in four dimensions) or equivalently to the Regge slope.

From eqs. (2.1) and (2.2) we obtain for the energy density of the resonance gas

$$\varepsilon_{\mathrm{H}}(\beta) = \lim_{V\to\infty} \frac{-1}{V} \left(\frac{\partial \ln Z_{\mathrm{H}}}{\partial \beta}\right)_V \tag{2.3}$$

$$\simeq \varepsilon_0(\beta) + \frac{c}{(2\pi\beta)^{3/2}} \int_{2m_0}^\infty \mathrm{d}m\, m^{-a+5/2}\, \mathrm{e}^{-m(\beta-b)} \tag{2.4}$$

with $\varepsilon_0(\beta)$ denoting the energy density of an ideal gas of ground state hadrons m_0. The corresponding specific heat becomes

$$c_{\mathrm{H}}(\beta) = c_0(\beta) + \beta\left\{\tfrac{3}{2}(\varepsilon_{\mathrm{H}} - \varepsilon_0) + \frac{c}{(2\pi\beta)^{3/2}} \int_{2m_0}^\infty \mathrm{d}m\, m^{-a+7/2}\, \mathrm{e}^{-m(\beta-b)}\right\}; \tag{2.5}$$

again the first term describes the ideal ground state gas.

It is well-known [22] and from eqs. (2.3, 2.4) also immediately evident that the spectral form (2.2) leads to critical behaviour. Depending on the exact value of a, from some derivative of the partition function on we will have divergent expressions at and/or above the critical temperature $T_c = b^{-1}$.

To illustrate what happens, we choose $a = 4$, $c = d = 1$. The specific heat of the resonance gas then diverges at $T_c = b^{-1}$, while the energy density remains finite there. Both are not defined for $T > T_c$. We have thus reached the end of hadron physics when $T = T_c$; without further information, we cannot say what lies beyond T_c.

The statistical mechanics of an ideal gas of massless quarks and gluons is obtained from the partition function

$$\ln Z_p(\beta, V) = \frac{V\beta}{(2\pi)^3} \int d^3k \left[g_B \ln\left\{\frac{1}{1 - e^{-\beta|k|}}\right\} + g_F \ln\left\{\frac{1}{1 + e^{-\beta|k|}}\right\}\right]. \tag{2.6}$$

Here g_B and g_F denote the bosonic and fermionic degrees of freedom, respectively; for colour SU(3) and two quark flavours, we have (with spins and antifermions)

$$g_B = 8 \times 2 = 16\,, \qquad g_F = 3 \times 2 \times 2 \times 2 = 24\,.$$

This leads to the Stefan–Boltzmann form of the energy density

$$\varepsilon^P_{SB}/T^4 = [(8\pi^2/15) + (7\pi^2/10)] \simeq 12.2 \tag{2.7}$$

with the first term corresponding to the gluon and the second to the quark component of the gas.

In fig. 3.1, we compare the energy density of hadronic matter, eq. (2.4), with that of an ideal gas of quarks and gluons, eq. (2.7). We expect that with increasing temperature, the constituent degrees of freedom, "frozen" in the hadronic state, will "thaw" to make ε attain its plasma value. We hope that QCD will give us a unified description of this development, including the phase transition(s) separating the two limiting states. In the next parts we shall find these expectations at least in part fulfilled.

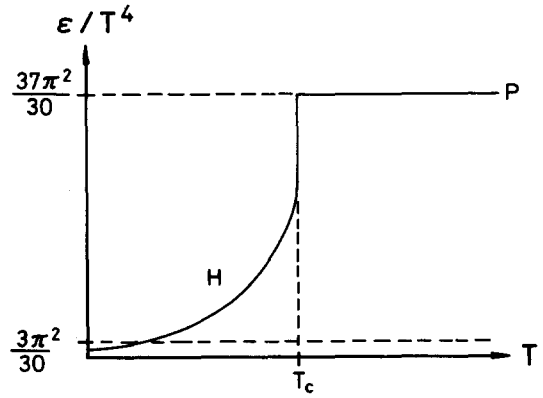

Fig. 3.1. Energy density of hadronic matter (H) and of an ideal quark-gluon plasma (P).

3.3. Yang–Mills thermodynamics on the lattice

We shall follow the historical development of QCD thermodynamics and treat first the case of pure Yang–Mills theory. This restriction to finite temperature gluon matter allows us to introduce both formalism and evaluation method for a simpler system already exhibiting many of the essential features of the full theory; also at present the precision of the evaluation is definitely higher in this simplified case. Since calculations based on colour SU(2) [3–6, 12] and those using SU(3) [8, 10] do lead to essentially the same results, it is moreover possible to reduce computer times by considering the smaller colour group. – The extension to full QCD with fermions will be presented in section 3.4.

The partition function for a quantum system described in terms of fields $A(x)$ by a Hamiltonian $H(A)$ is defined as

$$Z = \mathrm{Tr}\, \mathrm{e}^{-\beta H}, \tag{3.1}$$

where $T = \beta^{-1}$ is again the physical temperature. The conventional lattice formalism is obtained from this in three steps: (1) reformulation of Z as path integral; (2) introduction of the lattice; (3) change of "variables" from gauge field to gauge group. Let us look at this procedure in a little more detail.

The Lagrange density of gluon QCD is given by

$$\mathscr{L} = -\tfrac{1}{4} F^a_{\mu\nu} F^{\mu\nu}_a \tag{3.2}$$

with

$$F^a_{\mu\nu} = \partial_\mu A^a_\nu - \partial_\nu A^a_\mu - g f^a_{bc} A^b_\mu A^c_\nu \,. \tag{3.3}$$

Here the f^{abc} are the structure functions of the relevant underlying gauge group, whose generators λ_i satisfy $[\lambda_a, \lambda_b] = \mathrm{i} f^c_{ab} \lambda_c$; for SU(2), the colour indices a, b, c each run from one to two, for SU(3) from one to three. If we set the structure functions equal to zero, we recover the photon gas structure: it is the non-Abelian nature which gives us the gluon–gluon interaction. The partition function Z can now be written [23] in the form of a path integral

$$Z(\beta, V) = \int [\mathrm{d}A] \exp\Big\{ \int_0^\beta \mathrm{d}\tau \int_V \mathrm{d}^3 x \, \mathscr{L}[A(x, \tau)] \Big\} \tag{3.4}$$

using the Euclidean Lagrange density, $\mathscr{L}$, with $\mathrm{i}t = \tau$, and with periodicity in τ, $A(x, 0) = A(x, \beta)$. The three-dimensional integral of the Hamiltonian form ($H \sim \int \mathrm{d}^3 x \, \mathscr{H}(x)$) thus becomes an asymmetric four-dimensional one, with the "special" dimension measuring the temperature.

In the next step, we replace the Euclidean $x - \tau$ continuum by a finite lattice [24], with N_σ sites and spacing a_σ in the spatial part, N_β sites and spacing a_β in the temperature direction. To assure the required periodicity in τ, we chose a lattice closed on itself: $1 \triangleq 1 + N_\beta$. For economy in the later calculations, we work with lattices which are symmetric and also periodic in the space part, although neither property would be necessary. – The integrals in the exponent of eq. (3.4) now become sums, and we have $V = (N_\sigma a_\sigma)^3$, $\beta = N_\beta a_\beta$. The thermodynamic limit requires $N_\sigma \to \infty$ at fixed a_σ; the continuum limit is obtained by a_σ, $a_\beta \to 0$ with fixed $N_\beta a_\beta$, which forces also $N_\beta \to \infty$. The success of the approach rests on the (lucky) facts that already rather small lattices ($N_\sigma \sim 5$–10, $N_\beta \sim 3$–5) seem to be asymptotic,

and such that scale changes (changes in lattice spacings) can be connected to changes in the coupling strength g by the renormalization group relation, indicating continuum behaviour.

In the last step [24], we replace the gauge field "variable" $A_\mu((x_i + x_j)/2)$ associated to the link between two adjacent sites i and j by the gauge group element

$$U_{ij} = \exp\{-\mathrm{i}(x_i - x_j)^\mu A_\mu((x_i + x_j)/2)\}, \tag{3.5}$$

where $A_\mu(x) = \lambda_a A^a_\mu(x)$. With this transformation, the partition function becomes

$$Z(\beta, V) = \int \prod_{\{\text{links}\}} \mathrm{d}U_{ij} \exp\{-S(U)\}, \tag{3.6}$$

where the SU(N) lattice action is given by

$$S(U) = \frac{2N}{g^2}\left\{\frac{a_\beta}{a_\sigma}\sum_{\{\mathrm{P}_\sigma\}}\left[1 - \frac{1}{N}\mathrm{Re\ Tr}\, U_{ij}U_{jk}U_{kl}U_{li}\right] + \frac{a_\sigma}{a_\beta}\sum_{\{\mathrm{P}_\beta\}}\left[1 - \frac{1}{N}\mathrm{Re\ Tr}\, U_{ij}U_{jk}U_{kl}U_{li}\right]\right\}. \tag{3.7}$$

Here the sum $\{\mathrm{P}_\sigma\}$ runs over all purely spacelike lattice plaquettes ($ijkl$), while $\{\mathrm{P}_\beta\}$ runs over all those with two spacelike and two "temperature-like" links. – If we insert eq. (3.5) in eqs. (3.6, 3.7) and expand for small lattice spacings ($|x_i - x_j| \to 0$), then we recover in leading order the starting form (3.4).

From eqs. (3.6, 3.7), the energy density

$$\varepsilon \equiv (-1/V)(\partial \ln Z/\partial\beta)_V = -(N_\sigma^3 N_\beta a_\sigma^3)^{-1}(\partial \ln Z/\partial a_\beta)_{a_\sigma} \tag{3.8}$$

is found to be [6, 25]

$$\varepsilon \simeq 2N(N_\sigma^3 N_\beta a_\sigma^3 a_\beta g^2)^{-1}\left\{\left\langle\frac{a_\beta}{a_\sigma}\sum_{\{\mathrm{P}_\sigma\}}\left[1 - \frac{1}{N}\mathrm{Re\ Tr}\, UUUU\right]\right\rangle - \left\langle\frac{a_\sigma}{a_\beta}\sum_{\{\mathrm{P}_\beta\}}\left[1 - \frac{1}{N}\mathrm{Re\ Tr}\, UUUU\right]\right\rangle\right\} \tag{3.9}$$

with $\langle\,\rangle$ denoting the usual thermodynamic average

$$\langle X\rangle \equiv \left\{\int \prod \mathrm{d}U\, \mathrm{e}^{-S(U)}\, X(U)\right\} \Big/ \left\{\int \prod \mathrm{d}U\, \mathrm{e}^{-S(U)}\right\}. \tag{3.10}$$

Eq. (3.9) is our starting point for the Monte Carlo evaluation of gluon thermodynamics.

The evaluation is now carried out as follows [26]. The computer simulates an $N_\sigma^3 \times N_\beta$ lattice; for convenience we choose $a_\sigma = a_\beta = a$. Starting from a given ordered (all $U = 1$, "cold start") or disordered (all U random, "hot start") initial configuration, successively each link is assigned a new element U', chosen randomly with the weight $\exp\{-S(U)\}$. One traverse of this procedure through the entire lattice is called one iteration. In general, it is found that five hundred or so iterations provide reasonable first indications about the behaviour of the energy density (3.9), but for some precision one should have more. The results to be shown here are obtained for colour SU(2), with typically around three thousand iterations, after which we observe quite stable behaviour; we have moreover reproduced our results also with the finite subgroup approximation to SU(2) [27]. Our work was done with $N_\sigma = 7$,

9, 10 for $N_\beta = 2, 3, 4, 5$; apart from expected finite lattice size effects [9] there was no striking N_σ dependence of ε, suggesting that in general the thermodynamic limit is reached. To give at least some intuitive grounds for this, note that a $10^3 \times 3$ lattice has about 12 000 link degrees of freedom.

As a result of the Monte Carlo evaluation, we obtain for a lattice of given size (N_σ, N_β) the energy density ε as function of g. In the continuum limit, g and the lattice spacing a are for colour SU(N) related through

$$a\Lambda_L = (11Ng^2/48\pi^2)^{-51/121} \exp\{-24\pi^2/11Ng^2\}; \tag{3.11}$$

this relation is found by requiring a dimensional parameter Λ_L to remain constant under scale changes accompanied by corresponding changes in coupling strength. Hence once we are in the region of validity of the continuum limit, eq. (3.11) gives us the connection between g and a. Since $(N_\beta a)^{-1}$ is the temperature in units of Λ_L, we than have the desired continuum form of $\varepsilon(\beta)$.

In fig. 3.2, we show the resulting energy density ε as function of the temperature T. We first note that

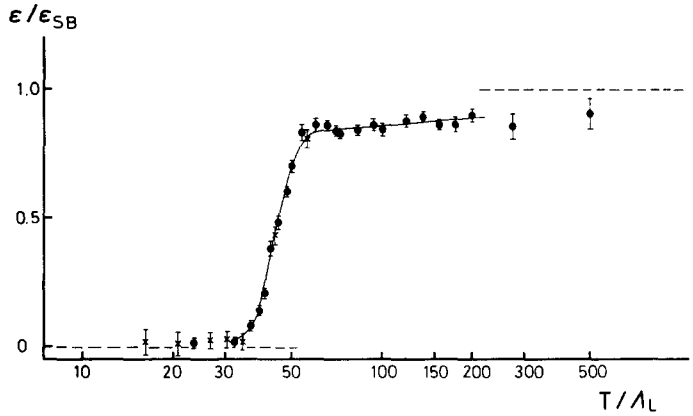

Fig. 3.2. Energy density of the SU(2) Yang-Mills system, compared to the ideal gas value ε_{SB}, as function of temperature T. The curve is a fit.

at high temperatures ($T/\Lambda_L \gtrsim 100$), the results of the Monte Carlo evaluation agree quite well with the anticipated Stefan–Boltzmann form

$$\varepsilon/T^4 = \pi^2/5\,. \tag{3.12}$$

Let us now go to lower T. At about $T = 50\Lambda_L$, ε drops sharply. The derivative of ε gives us the specific heat, shown in fig. 3.3. At $T \simeq 43\Lambda_L$, it has a singularity-like peak, which signals the transition from bound to free gluons. With Λ_L taken in physical units [28], this gives us $T_c \simeq 200$ MeV. How do we know that it is the deconfinement transition which occurs here? There are two separate pieces of evidence. We shall see shortly that below T_c the SU(2) Yang–Mills system follows the behaviour of hadronic matter [6], as given in part 3.2. Alternatively, one can study the behaviour of a static $q\bar{q}$ pair immersed in a gluon system of temperature T [4, 5, 8]; the free energy F of an isolated quark then serves to define the thermal Wilson loop $\langle L \rangle = \exp\{-\beta F\}$ as order parameter. It is found that $\langle L \rangle$ is essentially zero below and non-zero above T_c. Since $\langle L \rangle = 0$ corresponds to an infinite free energy of an isolated colour source, we have confinement below T_c.

Coming now, as promised, to the temperature region just below T_c, we show in fig. 3.4 the difference

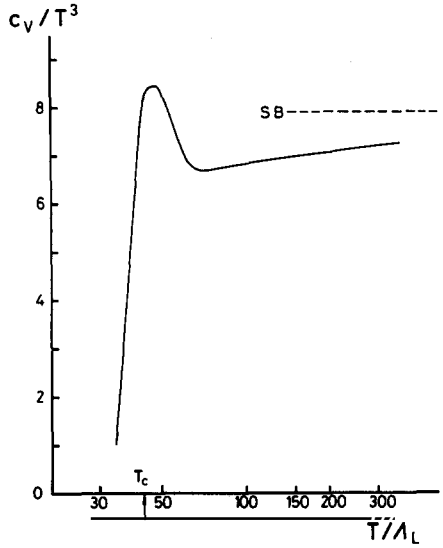

Fig. 3.3. The specific heat of the SU(2) Yang–Mills system as function of temperature T, obtained by differentiating the fit of fig. 3.2.

between energy density and pressure,

$$\Delta \equiv (\varepsilon - 3P)/T^4 \tag{3.13}$$

as taken from the Monte Carlo evaluation, compared to the corresponding hadronic gas form Δ_H from section 3.2; both are given as functions of $x = (T_c/T) - 1$. This comparison, if it leads to agreement on functional behaviour, also allows us to determine the mass m_G of the glueball, as lowest gluonium state. We see from fig. 3.4 that $m_G \simeq 4.5 T_c \simeq 190 \Lambda_L$ provides quite good agreement with the Monte Carlo

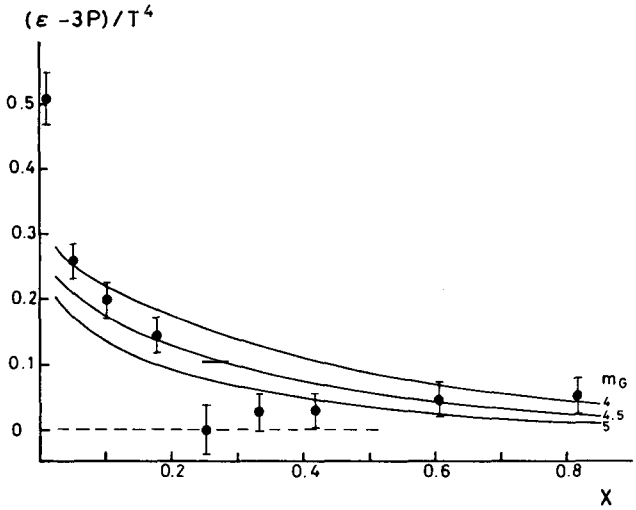

Fig. 3.4. Interaction measure $\Delta \equiv (\varepsilon - 3P)/T^4$ as function of $X = T_c/T - 1$, compared to the resonance gas prediction with glueball mass $m_G = 4$, 4.5 and 5 T_c.

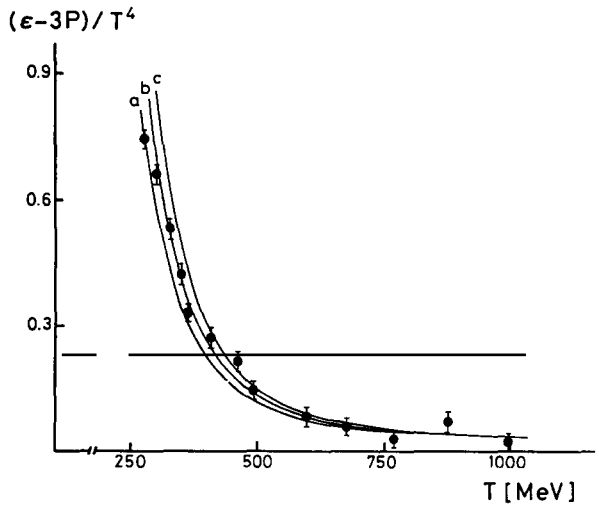

Fig. 3.5. Interaction measure $\Delta \equiv (\varepsilon - 3P)/T^4$ as function of temperature, compared to the leading order perturbative form with bag correction $B^{1/4} = 180$ (a), 190 (b) and 200 (c) MeV.

data. Moreover, this value of m_G (with physical parameters about 850–1000 MeV) is in reasonable accord with other lattice QCD determinations [34].

Finally let us have a look at how the Yang–Mills system behaves just above deconfinement [12]. While we expect perturbative behaviour at very high temperature, it seems likely that the form just above T_c is still non-perturbative. If we parametrize the contributions of the physical vacuum bubbles still present in the plasma close to T_c in terms of a bag description, we have in the case of colour SU(2) for the pressure

$$P = \frac{\pi^2}{15} T^4 \left[1 - \frac{5\alpha_s}{2\pi}\right] - B \tag{3.14}$$

and

$$\varepsilon = 3P + \tfrac{11}{18}\alpha_s^2 T^4 + 4B \tag{3.15}$$

for the energy density. Here B denotes the bag pressure and $\alpha_s = 3\pi/(11 \ln 4T/\Lambda)$ is the running coupling constant, with Λ as scale parameter. In fig. 3.5 we see that $B^{1/4} \simeq 190$ MeV and $\Lambda \simeq 100$ MeV yield a very good description of the functional form of $\Delta \equiv (\varepsilon - 3P)/T^4$. This implies a basically non-perturbative approach towards asymptotic freedom at least up to $T \sim 2T_c$. The role of higher order perturbation corrections is presently still unclear [29].

All lattice results presented here were obtained with the Wilson form (3.7) of the action, which provides the correct continuum limit. There are, however, other lattice actions which also do this, and we may therefore ask if deconfinement, both qualitatively and quantitatively, is independent of the choice of action. It was recently shown that this is indeed the case [30].

In closing this part, we note that also the extension to the SU(3) system has now been carried out [8, 10]; it requires greater computational efforts, because there are eight group parameters instead of three. The behaviour observed is, however, in good agreement with that of the SU(2) system. In particular, we note that at high temperature the energy density now approaches [10]

$$\varepsilon/T^4 \simeq 8\pi^2/15\,, \tag{3.16}$$

instead of eq. (3.12) in the SU(2) case. Both times we thus find the number of degrees of freedom of a system of massless, non-interacting gluons for the corresponding colour group. The deconfinement transition in the SU(3) case occurs at $T_c/\Lambda_L \simeq 75$–83, which with the string tension relation [28] gives $T_c \simeq 150$–170 MeV, also in accord with the SU(2) value.

In conclusion: we have seen that Monte Carlo techniques applied to lattice QCD allow us to evaluate gluon thermodynamics over the whole temperature range. The resulting behaviour shows the expected two-phase nature: at low temperatures, we have a hadronic resonance gas of gluonium states; heating brings us to a deconfinement transition and beyond that to an ideal gluon gas.

3.4. QCD thermodynamics with quarks

We now want to extend the considerations of part 3.3 to include quarks and antiquarks. We shall see that this brings in a basically new feature – the question of chiral symmetry restoration at high temperature. The lattice formulation encounters as a result the problem of species doubling [24, 31],

and in addition the Monte Carlo evaluation becomes considerably more complex. Nevertheless, first results both on the full QCD energy density [13] and on chiral symmetry restoration [13, 14] have now appeared; we shall here consider the former, returning to chiral symmetry in section 3.5.

The QCD Lagrangian density for massless quarks of one flavour only can be written

$$\mathscr{L}(\psi, A) = -\tfrac{1}{4}F^a_{\mu\nu}F^{\mu\nu}_a + \bar{\psi}_\alpha(\mathrm{i}\not{\partial} - g\not{A}_a\lambda^a)_{\alpha\beta}\,\psi_{\alpha\beta}\,. \tag{4.1}$$

Here, μ, ν denote tensor, α, β spinor and a, b, c colour indices. The finite temperature Euclidean action becomes

$$S_\beta(\psi, A) = -\int_V \mathrm{d}^3x \int_0^\beta \mathrm{d}\tau\, \mathscr{L}(\psi, A) \tag{4.2}$$

with periodic (antiperiodic) boundary conditions in the temperature integration of the boson (fermion) fields. The full action thus is a sum

$$S_\beta(\psi, A) = S^{\mathrm{G}}_\beta(A) + S^{\mathrm{F}}_\beta(\psi, A) \tag{4.3}$$

of the pure Yang–Mills part S^{G} and the quark-gluon part S^{F}. The Yang–Mills system was treated in section 3.3; we shall concentrate here on S^{F}.

Fermion theories on the lattice generally lead to species doubling [31], unless one is willing to accept chiral symmetry breaking [24]. We shall here use Wilson's form [24], in which chiral symmetry is recovered only in the continuum limit. We consider again an asymmetric lattice, with N_σ spatial and N_β temporal sites.

On this lattice, the action S^{F} on the quark-gluon sector is written [13, 25]

$$\begin{aligned} S^{\mathrm{F}} = \sum_n \Big\{ & \bar{\psi}_n\psi_n - \frac{k_{\mathrm{F}}(g^2)}{8}\frac{4a_\sigma}{3a_\beta + a_\sigma}\left[\bar{\psi}_n(1-\gamma_0)U_{n,n+\hat{0}}\psi_{n+\hat{0}} + \bar{\psi}_n(1+\gamma_0)U^+_{n-\hat{0},n}\psi_{n-\hat{0}}\right] \\ & - \frac{k_{\mathrm{F}}(g^2)}{8}\frac{4a_\beta}{3a_\beta + a_\sigma}\sum_{\mu=1}^{3}\left[\bar{\psi}_n(1-\gamma_\mu)\,U_{n,n+\hat{\mu}}\psi_{n+\hat{\mu}} + \bar{\psi}_n(1+\gamma_\mu)U^+_{n-\hat{\mu},n}\psi_{n-0}\right]\Big\} \end{aligned} \tag{4.4}$$

where we have suppressed all but symbolic lattice indices. The second term in eq. (4.4) refers to that part of the lattice summation in which the gauge group elements U_{nm} are associated with timelike lattice links n, m; in the third, the links are spacelike. The fermionic coupling $K(g^2) = k^2_{\mathrm{F}}(g^2)/8$ is the usual "hopping" parameter [24, 32].

In terms of S^{F} and S^{G}, the Euclidean form of the QCD partition function on the lattice is now given by

$$Z = \int \prod_{\text{links}} \mathrm{d}U \prod_{\text{sites}} \mathrm{d}\psi\, \mathrm{d}\bar{\psi}\, \exp\{-S^{\mathrm{G}}(U) - S^{\mathrm{F}}(U, \psi, \bar{\psi})\} \tag{4.5}$$

with the $\mathrm{d}U$ integration to be carried out for all links, the $\mathrm{d}\psi\,\mathrm{d}\bar{\psi}$ integrations for all sites of the lattice. Since the fermion action S^{F} has the form

$$S^{\mathrm{F}} = \bar{\psi}(1 - KM)\psi\,, \tag{4.6}$$

$$M_\mu = (1-\gamma_\mu)U_{nm}\delta_{n,m-\hat{\mu}} + (1+\gamma_\mu)U^+_{mn}\delta_{n,m+\hat{\mu}}\,, \tag{4.7}$$

the integration over the anti-commuting spinor fields can be carried out [33] to give an effective boson form

$$Z = \int \prod_{\text{links}} \mathrm{d}U \exp\{-S^{\mathrm{G}}(U)\} \det(1-KM)\,. \tag{4.8}$$

The Euclidean energy density ε is obtained from Z; it also becomes the sum $\varepsilon = \varepsilon^{\mathrm{G}} + \varepsilon^{\mathrm{F}}$ of the pure gluon part (eq. (3.9)) and the quark-gluon part [25]

$$\varepsilon^{\mathrm{F}} \equiv -\xi^2 (N_\sigma^3 N_\beta a_\sigma^4 Z)^{-1} \int \prod_{\text{links}} \mathrm{d}U \exp\{-S^{\mathrm{G}}(U)\} \det Q$$
$$* \left\{ \frac{3K(g^2)}{4} \mathrm{Tr}(M_0 Q^{-1}) - \frac{K(g^2)}{4} \sum_{\mu=1}^{3} \mathrm{Tr}(M_\mu Q^{-1}) \right\} \tag{4.9}$$

with $Q \equiv 1 - KM(U)$.

The computational problem beyond what is encountered in the pure Yang–Mills case lies in the evaluation of det Q and of Q^{-1}. We shall here use the expansion of these quantities in powers of the fermionic coupling K ("hopping parameter expansion" [32]), and retain in both cases only the leading term. By calculating an ideal gas of massless fermions in the same approximation, we shall then get some idea of how valid this procedure may be.

For det Q the leading term is

$$\det Q = \det(1-KM) \simeq 1 \tag{4.10}$$

("quenched approximation" [34]), while in the expansion

$$Q^{-1} = [1-KM]^{-1} = \sum_{l=0}^{\infty} K^l [M(U)]^l\,, \tag{4.11}$$

because of gauge invariance, the first contribution to $\mathrm{Tr}(Q^{-1}M)$ arises for the shortest non-vanishing closed loop obtained from $M(U) \sim U$. For $N_\beta = 2$ and 3, this is a thermal loop, i.e., one closed in the temperature direction; hence in that case, the first term is $l = N_\beta - 1$. For $N_\beta \geq 4$, these loops are not the only ones; but the non-thermal loops lead to negligibly small contributions, so that we obtain on an isotropic lattice

$$\varepsilon^{\mathrm{F}} a^4 \simeq \tfrac{3}{4} [K(g^2)]^{N_\beta} 2^{N_\beta+2} \langle L \rangle \tag{4.12}$$

with $\langle L \rangle$ for the expectation value of the thermal Wilson loop, and a for the lattice spacing.

To test the convergence of the hopping parameter expansion, we compare [13] in table 3.1 the resulting energy density of an ideal gas of massless quarks with the exact form [9] for such a system, both calculated on lattices of the same size. For low N_β values, the approximation given by just the leading term is found to be quite reasonable, with less than 10% errors for $N_\beta = 2$ and 3. This leads us to expect that also for QCD we can obtain an indicative estimate by retaining that term only. This

Table 3.1
Ratio R of the leading term of the hopping parameter expansion for the energy density of an ideal gas of massless fermions to the exact energy density on an infinite spatial lattice, at several N_β values.

N_β	2	3	4	5
R	1.086	0.944	0.764	0.557

expectation is supported by preliminary results for SU(2) fermions [35]: the energy density obtained by including all terms up to $l = 20$ in eq. (4.11) differs only by 10% from the leading term.

We now return to eq. (4.12) for the quark-gluon energy density of SU(N) QCD. The fermion coupling $K(g^2)$ for massless quarks has been evaluated numerically both at large [36] and at small [37] g^2. The thermal Wilson loop $\langle L \rangle$ can be calculated by the usual finite temperature Monte Carlo techniques.

With the connection between g^2, the lattice spacing a and the lattice scale Λ_L, as given by the renormalization group relation [38] (3.11) we can then from eq. (4.12) obtain ε^F as function of the temperature $T = \beta^{-1} = (N_\beta a)^{-1}$.

Comparing the leading term of the hopping parameter expansion for ε^F with that of an ideal gas of massless fermions, ε^F_{SB}, we have from eq. (4.12)

$$\varepsilon^F/\varepsilon^F_{SB} = [8K(g^2)]^{N_\beta}\langle L \rangle/N \tag{4.13}$$

with $K = 1/8$, $\langle L \rangle = N$ for the ideal gas analog of the SU(N) case.

For the SU(3) case, which is obviously the physically most interesting one, we display in table 3.2, for $N_\beta = 3$ and 4, the values of $\langle L \rangle$ from ref. [10], together with the coupling $K(g^2)$, which is taken from the u, d form of ref. [36], and the resulting energy density ratio $\varepsilon^F/\varepsilon^F_{SB}$. We note that the energy density

Table 3.2
Hopping parameter K, thermal Wilson loop $\langle L \rangle$ and ratio $\varepsilon^F/\varepsilon^F_{SB}$ for SU(3).

N_β	T/Λ_L	$8K$	$\langle L \rangle$	$\varepsilon^F/\varepsilon^F_{SB}$
3	80	1.536	0.31	0.374
	84	1.512	0.63	0.726
	89	1.496	0.73	0.815
	95	1.472	0.88	0.935
	100	1.456	0.96	0.988
	110	1.416–1.448	1.04	1.01 ± 0.03
	120	1.384–1.440	1.08	1.02 ± 0.07
	130	1.360–1.440	1.13	1.04 ± 0.10
	140	1.328–1.432	1.17	1.03 ± 0.12
4	76	1.456	0.29	0.434
	84	1.416–1.448	0.60	0.84 ± 0.04
	90	1.384–1.440	0.64	0.85 ± 0.07
	100	1.328–1.432	0.73	0.89 ± 0.13

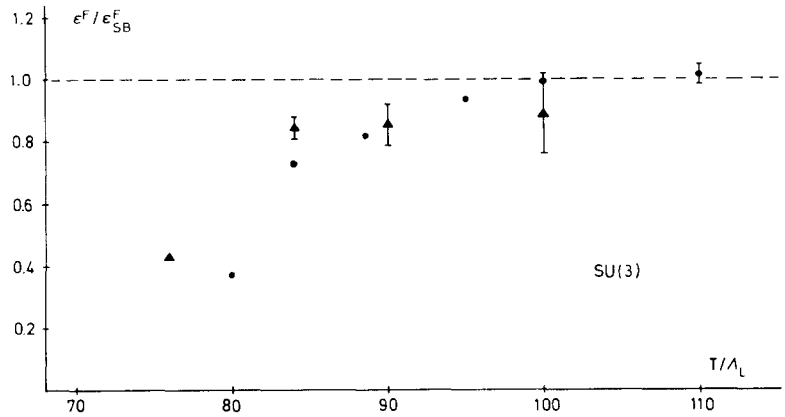

Fig. 3.6. Fermionic energy density of the SU(3) system, compared to the ideal gas value ε^F_{SB}, as function of the temperature. Circles correspond to $N_\beta = 3$, triangles to $N_\beta = 4$.

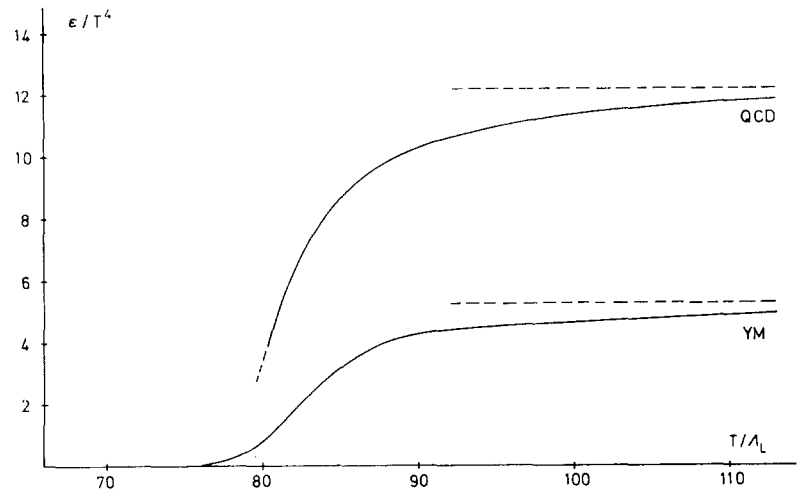

Fig. 3.7. Comparison of the energy density of full QCD with that of the SU(3) Yang–Mills theory, as obtained from a fit to fig. 3.6 and from ref. [10].

very quickly approaches its asymptotic value – and not because K and $\langle L \rangle$ separately do so, but rather because these quantities, for each N_β, together provide an almost asymptotic energy density. In fig. 3.6 we display the temperature behaviour of the combined $N_\beta = 3$ and 4 results. We note a sharp drop around $T \sim 80\Lambda_L$ ($\sim 0.4\sigma^{1/2}$), which presumably corresponds to the onset of confinement.

In fig. 3.7 we show the overall energy density ε/T^4, obtained by combining our above results for ε^F with the pure Yang–Mills results of part 3.3. We conclude that full quantum chromodynamics with fermions indeed appears to lead to the deconfinement behaviour observed in the study of Yang–Mills systems alone. In particular, we note that at temperatures $T \gtrsim 2T_c$ essentially all constituent degrees of freedom have been "thawed".

3.5. Deconfinement and chiral symmetry restoration

Quantum chromodynamics, for massless quarks a priori free of dimensional scales, contains the intrinsic potential for the spontaneous generation of two scales: one for the confinement force coupling

quarks to form hadrons, and one for the chiral force binding the collective excitations to Goldstone bosons [39]. These two lead in thermodynamics to two possible phase transitions, characterized by two critical temperatures, T_c and T_{ch}. Above T_c, the density is high enough to render confinement unimportant: hadrons dissolve into quarks and gluons. Above T_{ch}, chiral symmetry is restored, so that quarks must be massless. For T below both T_c and T_{ch}, we have a gas of massive hadrons; for T above both T_c and T_{ch}, we have a plasma of massless quarks and gluons. Conceptually simplest would be $T_c = T_{ch}$; the possibility $T_c > T_{ch}$ appears rather unlikely [40]. On the other hand, $T_c < T_{ch}$ would correspond to a regime of unbound massive "constituent" quarks [40], as they appear in the additive quark model for hadron–hadron and hadron–lepton interactions [41]. The question of deconfinement vs. chiral symmetry restoration thus confronts us with one of the most intriguing aspects of quark-gluon thermodynamics.

The fermionic action of Wilson [24] used in the last section avoids species doubling at the cost of chiral invariance. Even an ideal gas of massless quarks in this formulation is not chirally invariant [42], since the expectation value $\langle\bar{\psi}\psi\rangle$ is always different from zero. It has therefore been suggested [42] to use the difference between this "Stefan–Boltzmann" value and the corresponding QCD value for Wilson fermions as the physically meaningful order parameter: it would vanish when the behaviour of a non-interacting system of massless fermions is reached.

In fig. 3.8 we show this order parameter as calculated for colour SU(3), in leading power of the hopping parameter expansion [13]. It is non-zero up to $T_{ch} \simeq 100\Lambda_L$, and vanishes for higher temperatures. This suggests chiral symmetry restoration slightly above deconfinement, with

$$T_{ch}/T_c \simeq 1.3\,. \tag{5.1}$$

It remains open at present to what extent this will be modified by the inclusion of virtual quark loops, or if there are any significant finite lattice effects.

Using for the SU(2) case a chirally invariant action with the resulting species doubling, it was found in ref. [14] that chiral symmetry restoration occurs at

$$T_{ch} = (0.55 \pm 0.07)\sqrt{\sigma}; \tag{5.2}$$

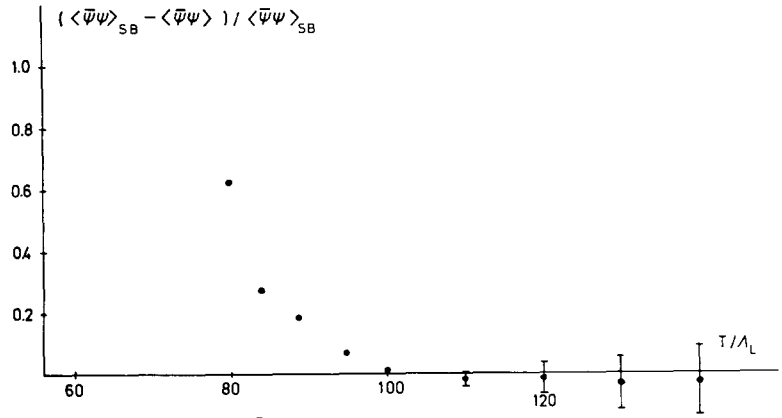

Fig. 3.8. The chiral order parameter $[(\langle\bar{\psi}\psi\rangle_{SB} - \langle\bar{\psi}\psi\rangle)/\langle\bar{\psi}\psi\rangle_{SB}]$, where $\langle\bar{\psi}\psi\rangle_{SB}$ measures the chiral symmetry breaking of an ideal gas of massless Wilson fermions on a finite lattice.

here also virtual quark loops are neglected. Since in this determination only $\langle\bar{\psi}\psi\rangle$ is studied, it does not provide any information about T_c. To obtain T_{ch}/T_c, one therefore has to rely on some other T_c determination. With the rather low value of ref. [5], it is found that [14]

$$T_{ch}/T_c = 1.6 \pm 0.2 . \tag{5.3}$$

Using the largest T_c obtained [6], we have instead

$$T_{ch}/T_c = 1.0 \pm 0.1 \tag{5.4}$$

so that the question of whether or not $T_c = T_{ch}$ appears to remain open.

3.6. Phase transition parameters

In the lattice evaluation of QCD thermodynamics, we have calculated all physical quantities in terms of the dimensional lattice scale Λ_L. To convert Λ_L into physical units, we just have to measure one of these physical observables. String tension considerations give for Yang–Mills systems

$$\Lambda_L = \begin{cases} (1.1 \pm 0.2) \times 10^2 \sqrt{\sigma} = (4.4 \pm 0.8)\,\text{MeV} & [43] \\ (1.3 \pm 0.2) \times 10^{-2} \sqrt{\sigma} = (5.2 \pm 0.8) & [44] \end{cases} \tag{6.1}$$

in case of colour SU(2) and

$$\Lambda_L = (5.0 \pm 1.5) \times 10^{-3} \sqrt{\sigma} = (2.0 \pm 0.6)\,\text{MeV} \qquad [45] \tag{6.2}$$

for colour SU(3). The deconfinement temperature is found to be

$$T_c = (38\,[4]\text{–}43\,[6])\Lambda_L \tag{6.3}$$

for SU(2) and

$$T_c = (75\,[8]\text{–}83\,[10])\Lambda_L \tag{6.4}$$

for SU(3). Taking the average of eq. (6.1), we have

$$T_c = \begin{cases} [(170\text{–}210) \pm 30]\,\text{MeV} & \text{SU(2)} \\ [(150\text{–}170) \pm 50]\,\text{MeV} & \text{SU(3)} \end{cases} \tag{6.5}$$

and thus little or no dependence of T_c on the colour group. This Yang–Mills value of the deconfinement temperature remains unaffected by the introduction of quarks in the scheme of section 3.4. The temperature for chiral symmetry restoration is accordingly given by relation (5.1).

From eq. (6.5) and the form of fig. 3.7, we can now estimate the energy density values at the two transition points. For the SU(3) Yang–Mills case, we obtain

$$\varepsilon(T_c) \simeq 200\text{–}300\,\text{MeV/fm}^3 , \tag{6.6}$$

where we have assumed that the turn-over in ε occurs at about half the Stefan–Boltzmann value. This range, corresponding roughly to hadronic energy density, seems physically quite reasonable. It is not known at present if and how much it would be increased by the introduction of quarks; a shift proportional to that of the Stefan–Boltzmann limit would double the value of eq. (6.6). This suggests twice standard nuclear density ($n_0 = 150\,\mathrm{MeV/fm^3}$) as lower and four times nuclear density as upper bound for the deconfinement transition. Present estimates for the energy density expected in ultrarelativistic heavy ion collisions [46] thus put deconfinement within reach.

Chiral symmetry restoration, even if it occurs at only slightly higher temperatures, seems to be considerably more difficult to attain. Just a small increase beyond T_c brings us to the top of the Stefan–Boltzmann "shelf", where the energy density is above $4\,\mathrm{GeV/fm^3}$.

3.7. Conclusions

Our basic conclusion is certainly that the lattice formulation of quantum chromodynamics appears to be an extremely fruitful approach to the thermodynamics of strongly interacting matter. It is so far the only way to describe within one theory the whole temperature range from hadronic matter to the quark-gluon plasma. It leads to deconfinement and provides first hints on chiral symmetry restoration.

We are still at the beginning. It is not really clear if $T_c \neq T_{ch}$, finite size scaling near the phase transitions has not been studied at all for $T \neq 0$, and the lattice thermodynamics of systems with non-zero baryon number has not been touched. Nevertheless, there seems to emerge today from QCD something already suggested by percolation methods [47], instanton considerations [48] and mean field calculations [49]: a three state picture of strongly interacting matter.

Acknowledgement

It is a pleasure to thank J. Engles, P. Hasenfratz, F. Karsch, L. McLerran, I. Montvay and B. Petersson for stimulating discussions.

References

[1] Ya.B. Zeldovich, JETP 37 (1959) 569;
Ya.B. Zeldovich, L.B. Okun and S.B. Pikelner, Usp. Fiz. Nauk. 87 (1965) 113;
D. Ivanenko and D.E. Kurdgelaidze, Astrofizika 1 (1965) 479;
F. Pacini, Nature 209 (1966) 389;
Ya.B. Zeldovich and I.D. Novikov, Relativistic Astrophysics (in Russian), (Izdat. Nauka, Moscow, 1967; Engl. translation: U. of Chicago Press, 1971);
D. Ivanenko and D.E. Kurdgelaidze, Nuovo Cim. Lett. 2 (1969) 13;
N. Itoh, Progr. Theoret. Phys. 44 (1970) 291.
[2] For references, see H. Satz, in: Proc. 5th High Energy Heavy Ion Study (Berkeley, California, 1981); see also section 2.
[3] A.M. Polyakov, Phys. Lett. 72B (1978) 477;
L. Susskind, Phys. Rev. D20 (1979) 2610.
[4] L.D. McLerran and B. Svetitsky, Phys. Lett. 98B (1981) 195;
L.D. McLerran and B. Svetitsky, Phys. Rev. D24 (1981) 450.
[5] J. Kuti, J. Polónyi and K. Szlachányi, Phys. Lett. 98B (1981) 199.
[6] J. Engles, F. Karsch, I. Montvay and H. Satz, Phys. Lett. 101B (1981) 89;
J. Engels, F. Karsch, I. Montvay and H. Satz, Phys. Lett. 102B (1981) 332;
J. Engels, F. Karsch, I. Montvay and H. Satz, Nucl. Phys. in press, BI-TP 81/29.

[7] A. Billoire, G. Lazarides and Q. Shafi, Phys. Lett. 103B (1981) 450.
[8] K. Kajantie, C. Montonen and E. Pietarinen, Z. Phys. C9 (1981) 253.
[9] J. Engels, F. Karsch and H. Satz, Nucl. Phys. B205 [FS 5] (1982) 239.
[10] I. Montvay and E. Pietarinen, Phys. Lett. 110B (1982) 148;
I. Montvay and E. Pietarinen, Thermodynamical Properties of the Gluon Matter, Helsinki Preprint, HU-TFT-82-8, 1982.
[11] F. Karsch, Nucl. Phys. B205 [FS 5] (1982) 285.
[12] H. Satz, Phys. Lett. in press, BI-TP 82/05.
[13] J. Engels, F. Karsch and H. Satz, Phys. Lett. in press, BI-TP 82/08.
[14] J. Kogut, M. Stone, H. Wyld, J. Shigemitsu, S. Shenker and D. Sinclair, The scales of chiral symmetry breaking in QCD, Illinois Preprint ILL-TH-82-5, March 1982.
[15] J.I. Kapusta, Nucl. Phys. B148 (1979) 461;
O.K. Khalashnikov and V.V. Klimov, Phys. Lett. 88B (1979) 328.
[16] E.V. Shuryak, Phys. Reports 61 (1980) 71;
D.J. Gross, R.D. Pisarski and L.G. Yaffe, Rev. Mod. Phys. 53 (1981) 43.
[17] M. Creutz, Phys. Rev. D21 (1980) 2308.
[18] See e.g., M. Jacob (ed.), Dual Theory (North-Holland Publ. Co., Amsterdam, 1974).
[19] A. Chodos, R.L. Yaffe, K. Johnson and V. Weisskopf, Phys. Rev. D9 (1974) 3471.
[20] R. Hagedorn, Nuovo Cim. Suppl. 3 (1965) 147.
[21] K. Huang and S. Weinberg, Phys. Rev. Lett. 25 (1970) 855;
H. Satz, Phys. Rev. D20 (1979) 582.
[22] N. Cabbibo and G. Parisi, Phys. Lett. 59B (1975) 67.
[23] C. Bernard, Phys. Rev. D9 (1974) 3312.
[24] K. Wilson, Phys. Rev. D10 (1974) 2445; in: New Phenomena in Subnuclear Physics (Erice 1975), ed. A. Zichichi (Plenum Press, New York, 1977).
[25] We neglect here and in the remainder the fact that on an asymmetric lattice g a priori depends on two variables, a_β and a_σ; the resulting changes are, however, quite small. For a correct treatment, see the last paper of ref. [6].
[26] The method is that developed for the confinement problem by M. Creutz, loc. cit. [17].
[27] D. Petcher and H.D. Weingarten, Phys. Rev. D22 (1980) 2465.
[28] M. Creutz, Phys. Rev. Lett. 45 (1980) 313;
G. Bhanot and C. Rebbi, Nucl. Phys. B180 [FS 2] (1981) 469.
[29] C.-G. Källmann and C. Montonen, What lattice calculations can tell us about the gluon gas, Helsinki Preprint 1982.
[30] R.V. Gavai, The deconfinement transition in SU(2) lattice gauge theories, Bielefeld Preprint BI-TP 82/11.
[31] L. Susskind, Phys. Rev. D16 (1977) 3031.
[32] C.B. Lang and H. Nicolai, Nucl. Phys. B200 [FS 4](1982) 135;
A. Hasenfratz and P. Hasenfratz, Phys. Lett. 104B (1981) 489.
[33] T. Matthews and A. Salam, Nuovo Cimento 12 (1954) 563; 2 (1955) 120.
[34] D. Weingarten, Monte Carlo Evaluation of Hadron Masses in Lattice Gauge Theories with Fermions, Indiana Univ. Preprint, IUHET-69, October 1981.
[35] F. Karsch, private communication.
[36] A. Hasenfratz, P. Hasenfratz, Z. Kunszt and C.B. Lang, Hopping Parameter Expansion for the Meson Spectrum in SU(3) Lattice QCD, CERN Preprint, Ref. TH.3220-CERN, December 1981.
[37] N. Kawamoto, Nucl. Phys. B190 [FS 3] (1981) 617.
[38] Eq. (4.13) should only be used in the quenched approximation. For a discussion of this point see ref. [34].
[39] See e.g., W. Marciano and H. Pagels, Phys. Reports 36 (1978) 137.
[40] E.V. Shuryak, Phys. Lett. 107B (1981) 103;
R.D. Pisarski, Phys. Lett. 110B (1982) 155.
[41] H. Satz, Phys. Lett. 25B (1967) 27 and Phys. Lett. 25B (1967) 220;
H. Satz, Nuovo Cim. 37A (1977) 141.
[42] C.B. Lang and H. Nicolai, Nucl. Phys. B200 [FS 4] (1982) 135.
[43] G. Bhanot and C. Rebbi, loc. cit. [28].
[44] M. Creutz, loc. cit. [28].
[45] M. Creutz, Phys. Rev. Lett. 45 (1980) 313;
E. Pietarinen, Nucl. Phys. B190 [FS 3] (1981) 239.
[46] R. Anishetty, P. Koehler and L. McLerran, Phys. Rev. D22 (1980) 2793.
[47] T. Celik, F. Karsch and H. Satz, Phys. Lett. 97B (1980) 128.
[48] E.V. Shuryak, loc. cit. [40].
[49] R. Pisarski, loc. cit. [40].

PHYSICS REPORTS (Review Section of Physics Letters) 88, No. 5 (1982) 365–378. North-Holland Publishing Company

4. Heavy Ion Collisions in the Hydrodynamical Model

Joseph KAPUSTA*
CERN, Geneva, Switzerland

and

Los Alamos Scientific Laboratory, Los Alamos, New Mexico, U.S.A.

4.1. Introduction

Since 1973 there has been much theoretical and experimental interest in colliding heavy nuclei at high energy. Heavy nuclei means mass numbers greater than 40, and high energy means a beam energy greater than 200 MeV per nucleon, usually considerably greater. The hope is that we will be able to learn something about the properties of hadronic matter at high energy density occupying a large volume. The simplest scenario is that thermalization is achieved during central collisions of heavy nuclei, and therefore we ought to be able to extract some information on the equation of state of the produced matter. If thermalization is not achieved then one might still learn something about the properties of bulk matter at high energy density, but it will not be the equation of state. The aim of these studies then is orthogonal to e^+e^- annihilation physics where one likes to concentrate a large amount of energy in a small volume.

There has been considerable speculation on the types of exotic matter which may be formed in central heavy ion collisions. At high baryon density conjectures have centered on pion condensation [1], Lee–Wick nuclear matter [2], delta isomers [3] and quark matter [4]. At high temperature one might encounter a limiting temperature [5] or a transition to quark-gluon matter [6]. (Since the field is so large these and other references are meant to be illustrative but not exhaustive.)

Hydrodynamical models are well suited theoretically to the study of heavy ion collisions at high energy. This is because the only variable input for solving the hydrodynamic equations of motion for a given nucleus–nucleus collision is the hadronic matter equation of state. If heavy nuclei were collided at the highest energies attainable in current proton accelerators, the hydrodynamical model would predict energy densities so great that the resulting matter would be in the deconfined quark-gluon phase. However, caution must be used when comparing the results of hydrodynamic calculations with experiment, since real nuclei are not macroscopic objects in the classical sense of being composed of 10^{23} particles. It remains an open and intriguing question as to whether even uranium is large enough. If we were able to collide neutron stars, and some day mankind or his descendants may have that capability, there would be no controversy.

We can make some semi-quantitative estimates. The mean free path for a particle which belongs to an ensemble of particles which is in or near thermal equilibrium is $\lambda = 1/n\sigma\sqrt{2}$, where n is the particle number density and σ is the scattering cross-section. (If the particle in question does not belong to the ensemble but is shot into the gas at high velocity the $\sqrt{2}$ is taken away.) At normal nuclear density and

* Present address: Physics Department, University of Minnesota, Minneapolis, Minnesota, U.S.A.

nucleus	radius (fm)	diameter (fm)
p	0.8	1.6
^{12}C	2.7	5.4
^{40}Ar	4.1	8.2
^{238}U	7.4	14.8

with a cross-section of 40 mb we find that $\lambda = 1.2$ fm. Let L be a typical dimension of the nuclei which are colliding against each other. The radii and diameters of some typical nuclei are listed in the table. (Recall, however, that real nuclei have a diffuse surface of width 1 fm.) If $\lambda \gg L$ then we would expect a single nucleon knock-out model to be valid [7]. That is, one nucleon from each of the nuclei would scatter together once and then leave the collision zone and fly off toward the detectors. If $\lambda \gtrsim L$, then the individual nucleons would undergo several binary collisions with other nucleons and we would expect the validity of the more complicated intranuclear cascade models [8, 9]. If λ was to become too small compared with L, then we might begin to worry about the effects of the dense packing of nucleons, many-body forces, off-mass-shell propagation, etc., which are not contained in the intranuclear cascade models. If $\lambda \ll L$ then these and other effects might be incorporated more conveniently or correctly by using a realistic equation of state and by solving the equations of motion of hydrodynamics. This is equivalent to saying that local thermal equilibrium is achieved during the collision. If $\lambda \lesssim L$, then strict local equilibrium may not be valid and we should incorporate the effects of finite gradients of pressure, temperature, etc. We would then need to solve the equations of motion of imperfect fluid dynamics, which would require knowledge of the bulk and shear viscosity coefficients, the thermal conductivity coefficient, as well as the equation of state. The domain of overlap between intranuclear cascade and imperfect fluid dynamics is an interesting problem in non-equilibrium statistical mechanics. The effect of a finite mean free path on expanding fireballs will be investigated later in section 4.3.

4.2. Experimental evidence for non-trivial behaviour

The first question we should ask is whether or not there is any evidence at all for non-trivial behaviour in heavy ion collisions. By trivial behaviour it is meant that all such collisions could be described by the single nucleon knock-out model. In fig. 4.1 some data [10] for $\mathrm{Ar} + \mathrm{KCl} \to \mathrm{p} + \mathrm{X}$ at a beam energy of 800 MeV per nucleon is shown. The inclusive single particle invariant cross-section is plotted as a function of the angle in the CM and at fixed kinetic energy. The predictions of two models are shown for comparison. The single nucleon knock-out, or hard scattering, model [7] uses an elementary single particle momentum distribution for nucleons in the nucleus of the form $(p/p_0)/\sinh(p/p_0)$, $p_0 = 90$ MeV/c. This contrasts with the Fermi–Dirac distribution $\theta(p_F - p)$, where $p_F \approx 260$ MeV/c is the Fermi momentum. It was found that the former distribution, when used in this model, produced much better agreement with the data than the latter. However, the model still predicts much more angular asymmetry than is present in the data. Recall that at these energies elementary nucleon–nucleon collisions are forward-backward peaked. Thus the data would indicate some degree of multiple scattering, heading towards a more isotropic distribution. The predictions of a fireball model [11] calculation is also shown. For collisions between symmetric size nuclei the fireball is always formed at rest in the CM. Hence this model predicts complete isotropy. However, in its original version the fireball model does not conserve angular momentum. If the fireball was given the correct amount of

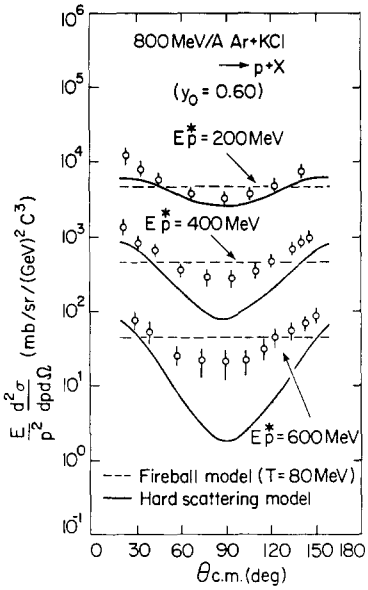

Fig. 4.1. The angular distribution of protons for fixed centre-of-mass kinetic energy, from the collisions of Ar with KCl. The data [10] are compared with two opposing models of the reactions.

spin it would produce a forward-backward asymmetry which might reproduce the data.

In fig. 4.2 some data [12] for Ne + U → charged particles + X at a beam energy of 250 MeV per nucleon is shown. The data refers to the summed-charge single particle differential cross-section, obtained by summing contributions from p, d, t, ^{3}He and α. For comparison, the predictions of three different models are also shown. There are two versions of fluid dynamics [13] and one version of

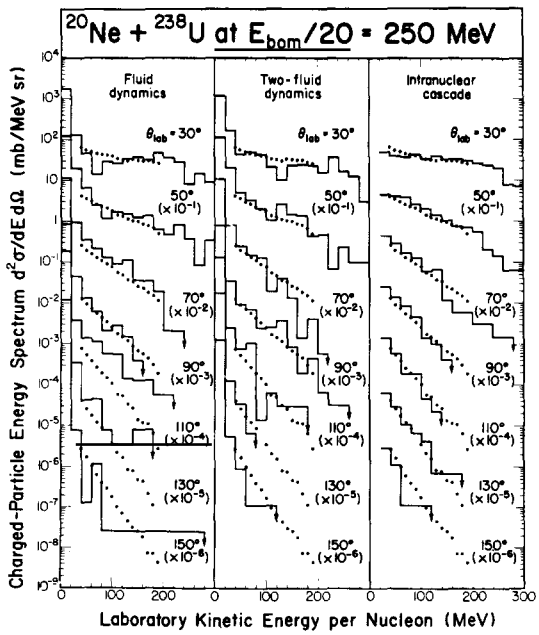

Fig. 4.2. The charged-particle energy spectrum, for fixed laboratory angle, from the collisions of Ne with U. The data [12] are compared with three model calculations.

intranuclear cascade [8]. Notice that there are no major qualitative differences among the model predictions and with the data. This is despite the fact that intranuclear cascade and fluid dynamics approach the reaction dynamics from opposite extremes. This could mean that λ really is small enough for these collisions to exhibit hydrodynamic behaviour even in the cascade approach. Or, it could mean that too much information is lost by summing over all charged particles and by summing over all impact parameters.

To help decide the issue the experiment [14] can also measure the multiplicity associated with the detection of a proton of given momentum. The result of such a measurement is shown in fig. 4.3. The reactions Ne + U → p + X at a beam energy of 393 MeV per nucleon are separated into low multiplicity (of X) events and high multiplicity events. Naively we expect higher multiplicity events to be associated with smaller impact parameters, since the overlap of the target and projectile would be greater. The shape of the proton differential cross-section is qualitatively different when one triggers on high multiplicity events as opposed to low multiplicity events. This rules out a single nucleon knock-out model description of these reactions since the shape of the proton spectrum in that model is predicted to be independent of multiplicity and impact parameter. It seems that intranuclear cascade models have only a very weak impact parameter dependence which is not able to reproduce this qualitative difference. This difference is, in contrast, predicted by hydrodynamic calculations [15].

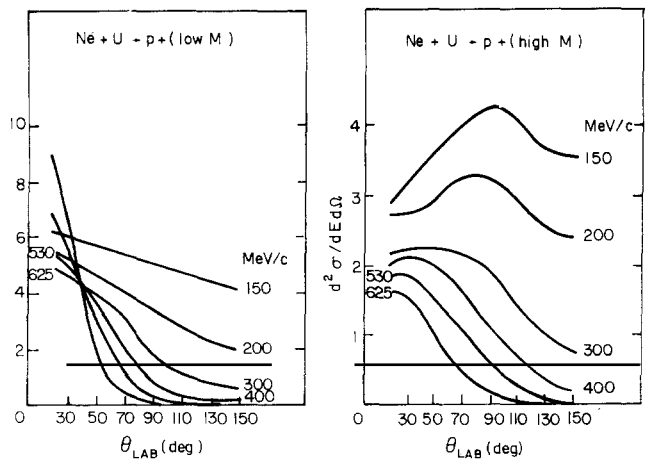

Fig. 4.3. The angular distribution of protons, for fixed laboratory momentum, from the collisions of Ne with U. The graph on the left is for low associated multiplicities while the graph on the right is for high associated multiplicities.

4.3. Fluid dynamics in the one GeV per nucleon domain

The equations of motion of relativistic hydrodynamics express the conservation of energy-momentum

$$\partial_\nu T^{\mu\nu} = 0\,, \tag{1}$$

and of baryon number

$$\partial_\nu N^\nu = 0\,. \tag{2}$$

The notation is as follows. The energy-momentum tensor

$$T^{\mu\nu} = Pg^{\mu\nu} + (P+\rho)U^{\mu}U^{\nu} \tag{3}$$

depends on the pressure P, the total energy density ρ as measured in the rest frame of the fluid, and the four-velocity U^{μ}. The latter has time component $U^0 = (1-\boldsymbol{v}^2)^{-1/2}$ and space components $\boldsymbol{U} = \boldsymbol{v}U_0$, where $\boldsymbol{v}$ is the local velocity of the fluid relative to a fixed computational frame. The baryon current is $N^{\mu} = nU^{\mu}$, where n is the local baryon density in the rest frame of the fluid. The thermodynamic quantities P, ρ and n are related by an equation of state which we may choose to write in the form $P = P(\rho, n)$. The independent quantities ρ, n and $\boldsymbol{v}$ then depend on position $\boldsymbol{x}$ and time t.

Numerical methods have been developed to solve these equations in three dimensions [13]. We have performed such calculations [16] for the collisions of equal-mass nuclei at various impact parameters at a beam energy of 800 MeV per nucleon (182 MeV per nucleon in the CM). In fig. 4.4 the time

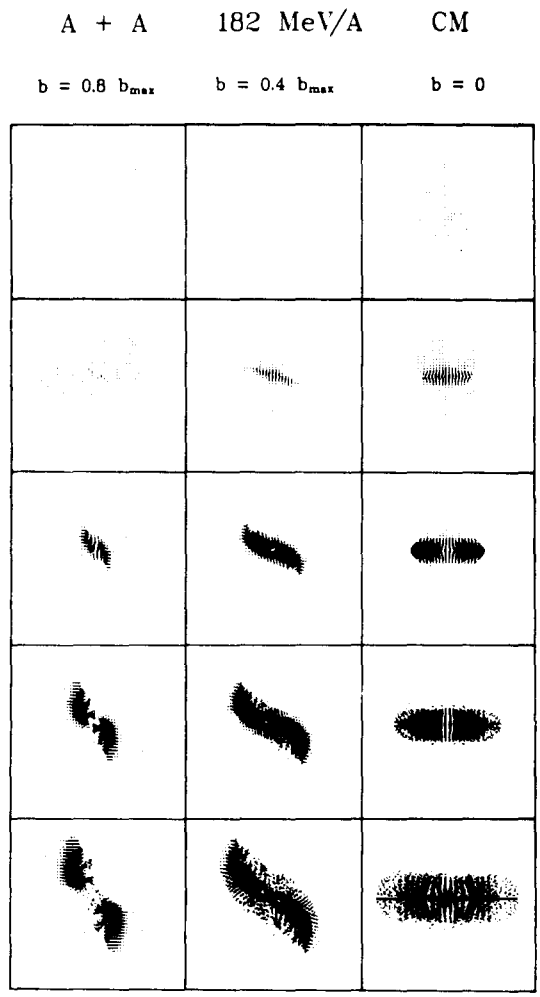

Fig. 4.4. The time development, in equal time steps, of the projected baryon density in the centre-of-mass at three different impact parameters obtained from a three-dimensional relativistic hydrodynamic model. The equivalent laboratory beam energy is 800 MeV per nucleon.

development of such collisions at three different impact parameters is shown. (We have also made a colour movie, for collisions at four impact parameters, entitled *Super Ion, The Movie.* Copies are on deposit with the American Association of Physics Teachers and the Los Alamos National Laboratory film libraries and are available for short term loan.) The results are scale invariant, that is, they are independent of the physical size of the nuclei. Notice in particular the qualitative difference between large and small impact parameters. At $b = 0.8b_{\max}$ there is only a small volume of overlap between the colliding nuclei. The large target and projectile fragments leave the collisions with essentially the same velocity with which they entered. At $b = 0$, however, all the matter participates directly in the collision. There is a flattening of the nuclei as they compress, with some of the matter bouncing backwards but with most of it splashing out to the side. The maximum compression of matter attained was about 3 to 4.

We wish to quantify these global aspects of the collisions by means of thrust,

$$T = \max_{\hat{n}} \sum_i |\boldsymbol{p}_i \cdot \hat{\boldsymbol{n}}| \Big/ \sum_i |\boldsymbol{p}_i| \,. \tag{4}$$

The sum is over all particles i with momentum $\boldsymbol{p}_i$ in the CM. The thrust is especially relevant for nucleus–nucleus collisions since it is relatively insensitive to such things as pion production and nuclear clustering in the final stages of the collision.

The result of a thrust analysis applied to these calculations is shown in fig. 4.5. It displays the expected behaviour. At $b = b_{\max}$ the nuclei just begin to interact. $T = 1$ and occurs at an angle of 0°

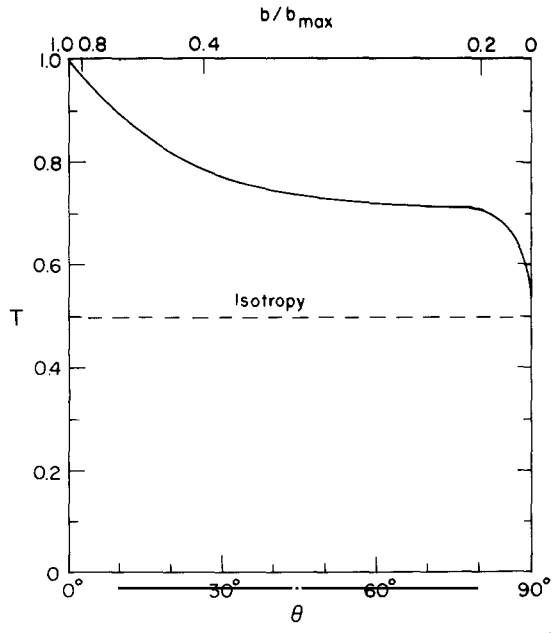

Fig. 4.5. Thrust as a function of impact parameter and angle relative to the beam axis. See also fig. 4.4.

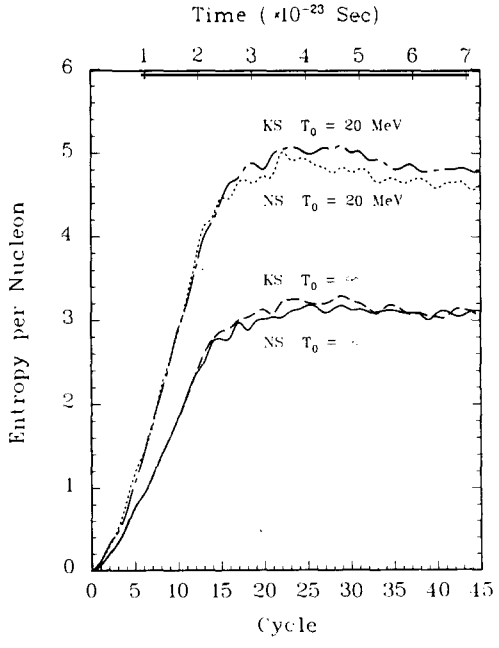

Fig. 4.6. The entropy per nucleon as a function of time and computational cycle for central collisions of mass 40 nuclei at 800 MeV per nucleon. See also fig. 4.4. The top two curves correspond to equations of state which are thermally much softer than those corresponding to the bottom two curves.

relative to the beam. As the impact parameter is reduced the nuclei interact more strongly. The nuclear matter is compressed and shoved out to finite angles. T decreases in magnitude because some of the initial collective momentum is distributed in a range of angles centered about θ and because some of it is converted, via shock heating, into randomized thermal energy. For a central collision the momentum comes out preferentially as a sidewards splash.

Since the hydrodynamic equations are scale invariant these results might represent collisions between alpha particles, between uranium nuclei or between neutron stars. Certainly hydrodynamics is not applicable to alpha particle collisions, but just as certainly they are applicable to neutron star collisions. The big question is whether or not they are applicable to uranium collisions. The necessary exclusive or semi-exclusive experiments will be done in the next year or two.

It is also possible to compute the spectra of π, p and d in this model [17]. Besides the thrust the entropy is a convenient global quantity to characterize the state of the system. Hydrodynamic flow is normally adiabatic, i.e., entropy conserving. However, when nuclei collide at velocities greater than the speed of sound, shock waves occur and heat the system to finite temperatures. The build-up of entropy as a function of time is shown in fig. 4.6 for central collisions of the type displayed in fig. 4.4. The nuclei begin in the ground state so their entropy is zero. After some time the shock heating ends and an adiabatic expansion phase begins. At various times the elementary fluid elements drop below normal nuclear density. When this happens the constituents fly apart on straight line trajectories with a thermal momentum distribution. Included in this thermal and chemical equilibrium breakup stage are π^+, π^0, π^-, p, n, d, d*, t and ^{3}He. This allows us to calculate the invariant differential cross-sections for protons, deuterons and pions as shown in figs. 4.7–4.9. These calculations are compared with some data for Ar + KCl collisions [10].

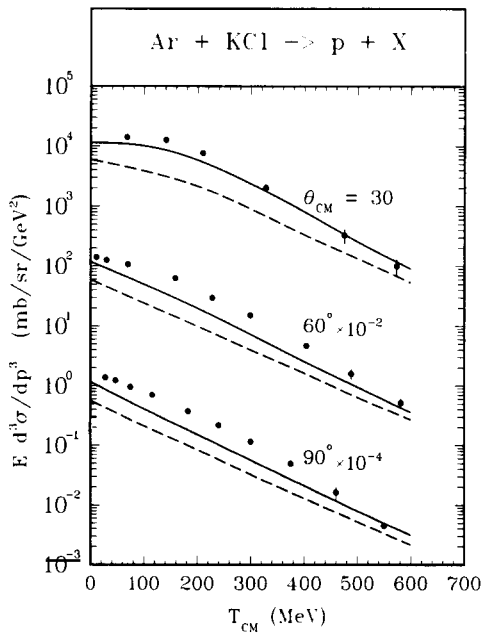

Fig. 4.7. The proton invariant cross-section, plotted in the centre-of-mass frame, at a beam energy of 800 MeV per nucleon. The solid line corresponds to KS $T_0 = 20$ MeV and the dashed line to NS $T_0 = \infty$. See fig. 4.6. The data are from ref. [10].

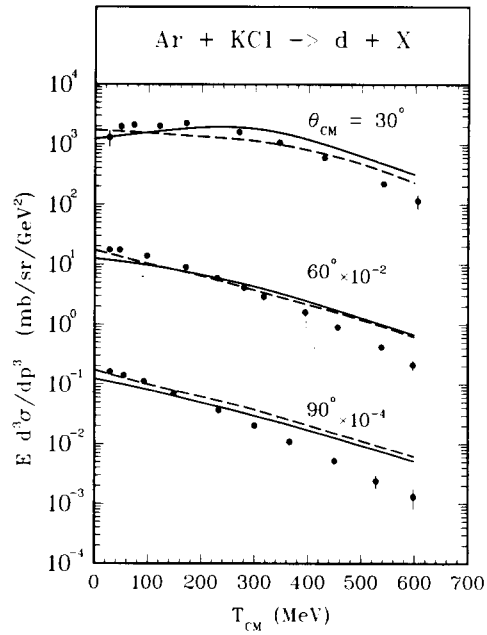

Fig. 4.8. The deuteron invariant cross-section. The labelling is the same as in fig. 4.7.

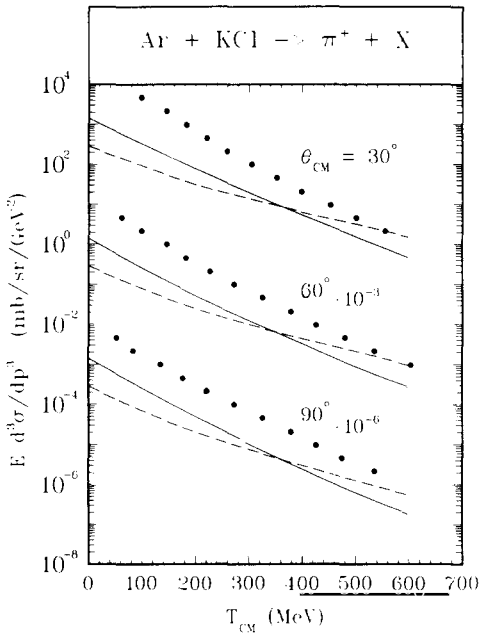

Fig. 4.9. The positive pion invariant cross-section. The labelling is the same as in fig. 4.7.

The important aspects of these four figures are the following. For an equation of state which is very soft more entropy is produced during the collision than for a stiffer equation of state. Entropy is equivalent to disorder. If, at the end of the collision, the entropy per baryon is high, then more of the baryon number will emerge in the form of free nucleons as opposed to nuclear clusters like d, t, ^{3}He, etc. Also more pions will be produced. Hence by varying the equation of state we can vary the final chemical composition of the measured fragments.

In comparison with the data notice that even with a very soft equation of state there are not enough free protons emitted. Notice also that there are far too few pions produced by these calculations which is in contrast to purely thermal models and intranuclear cascade models which predict too many. These observations tend to suggest that more energy is contained in collective flow than predicted by these other models, but less than that predicted by the pure hydrodynamical model, at least for Ar + KCl at 800 MeV per nucleon. From the point of view of fluid dynamics, perhaps viscosity and heat conduction (frictional forces) play a role in reducing the amount of energy contained in collective hydrodynamic flow and keeping it in the form of internal excitation energy and pions. One might also expect in principle that heat conduction and viscosity would have an effect on a system as light as Ar + KCl since the nucleon mean free path is not negligible compared to the size of the system. The partitioning of the available energy among temperature, collective flow and pion mass, seems to be rather crucial.

The effect of a finite mean free path on the expansion stage of central collisions between heavy nuclei at a beam energy of 800 MeV per nucleon has been studied in a non-relativistic imperfect fluid dynamic approach [18]. A gas of point nucleons with localized interactions was assumed for definiteness and for comparison with intranuclear cascade. Kinetic theory, going back to J.C. Maxwell in 1860, then provides the thermal conductivity and viscosity coefficients in terms of the nucleon–nucleon cross-section. The equations of motion were solved for a spherically expanding fireball which had an initial uniform density of twice normal density. The final breakup density was taken as 0.4 of normal density.

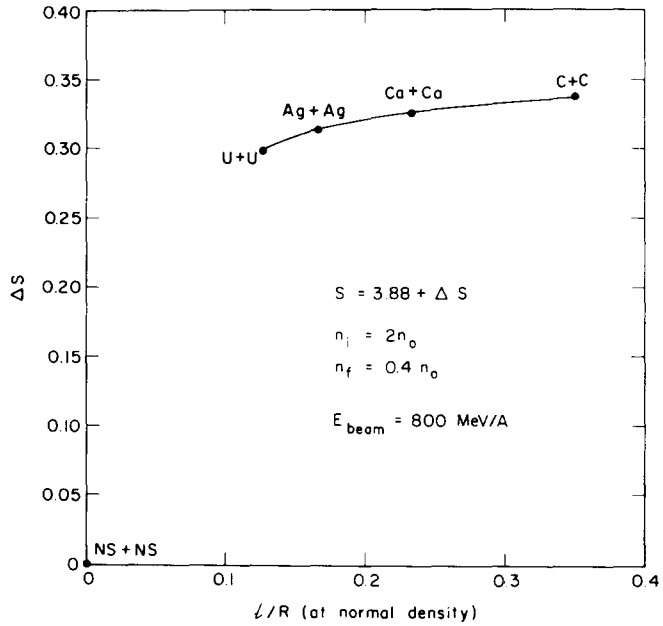

Fig. 4.10. The effect of a finite mean free path on the value of the entropy generated during the expansion stage of central collisions between carbon nuclei, calcium nuclei, silver nuclei, uranium nuclei and neutron stars. The mean free path divided by the radius of the combined system is evaluated at normal nuclear density and is proportional to $A^{-1/3}$.

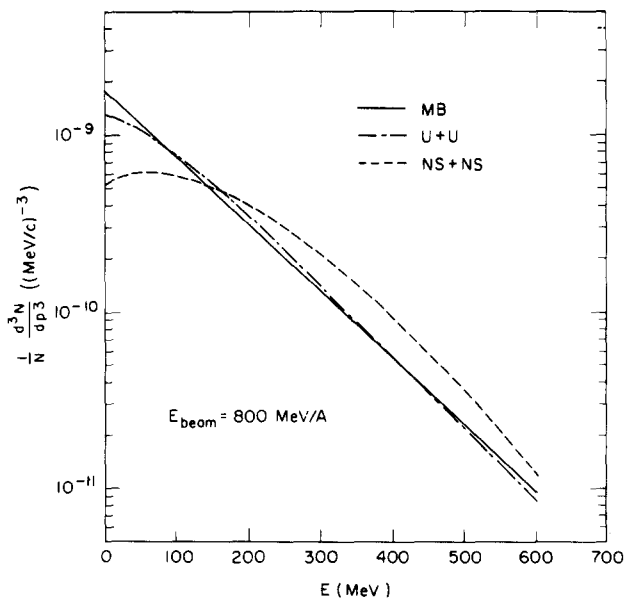

Fig. 4.11. The nucleon momentum distribution for a Maxwell–Boltzmann (straight line), for a viscous uranium plus uranium expansion, and for a pure hydrodynamical expansion represented by neutron star collisions.

There are two obvious ways of gauging the effect of a finite mean free path: entropy generation and the final nucleon momentum distribution. The additional entropy per nucleon generated during the expansion is plotted in fig. 4.10 as a function of the ratio of the mean free path divided by the radius of the system, evaluated at normal density. The calculations were done for C + C up to U + U. The additional entropy generated was less than 10% of the initial value of 3.9 units, which is a small effect. However, the ΔS for uranium collisions lies closer to the ΔS for carbon collisions than it does to the $\Delta S = 0$ of neutron star collisions. This somewhat surprising result is reinforced when we look at the momentum distributions in fig. 4.11. There we see that the viscous uranium plus uranium expansion looks more like a pure Maxwell–Boltzmann distribution than a pure hydrodynamic expansion as represented by neutron stars.

4.4. Fluid dynamics in the ultra-relativistic domain

We should not expect fluid dynamics to be generally applicable during the whole time evolution of a collision between nuclei at ultra-relativistic energies. This is because the basic nucleon–nucleon scatterings at very high energy are usually soft. In a typical collision the nucleons lose only a relatively small fraction of their total linear momentum so that more scatterings would be needed to stop them than can be provided by even a uranium nucleus. One might think that the pions created during the collision would provide an additional breaking mechanism. We know from proton-nucleus studies that this is not the case. Thanks to special relativity and a finite formation time pions are produced outside the target nucleus. Although Landau's hydrodynamical model and numerous variants of it are able to claim phenomenological successes, these are more likely to follow from the basic conservation equations and cylindrical phase space than from a detailed applicability of hydrodynamics. [For an interesting, heretical point view see ref. [19].]

However, from the point of view of the fluid dynamicist, there are three reasons for optimism. Firstly, neutron stars are such huge objects that they will behave hydrodynamically, as shown in fig. 4.4, even for the highest energy deemed necessary to form quark-gluon matter. Secondly, nucleus–nucleus collisions at ultra-relativistic energies will probably be characterized by large fluctuations, even at a fixed impact parameter. For example, consider a geometrically central collision. One possible outcome is that each of the nucleons undergoes diffractive interactions with the nucleons from the other nucleus. Thus the nuclei will pass through each other. An entirely different outcome would arise if each of the nucleons underwent hard collisions with the nucleons from the other nucleus. Then the nuclei would stop each other in a rather hydrodynamic fashion. The likelihood of such an event is probably much higher than one would naively estimate, since the hard scattering of a few nucleons on the front sides of the nuclei should serve as a catalyst for the hard scattering of nucleons on the back sides. It will be the task of the experiments to pick out these more interesting events from the background. An obvious criterion would be to look for events where most of the energy and baryon number came out near the CM rapidity. Thirdly, it may be that fluid dynamics is not adequate to describe the initial stage of the collision but, nevertheless, large globs of high energy density matter are formed. Fluid dynamics might then adequately model the subsequent expansion of this matter into the vacuum. It is to this last possibility that we now turn our attention.

For our phenomenological equation of state we will call on the MIT bag model [20]. This model incorporates both high energy perturbative behaviour and low energy confinement. The total pressure is the thermal pressure minus the bag constant,

$$P = P^* - B, \tag{5}$$

and the total energy density is the thermal energy density plus the bag constant,

$$\rho = \rho^* + B. \tag{6}$$

When the quarks are treated as massless and non-interacting this leads to the equation of state

$$P = \tfrac{1}{3}(\rho - 4B). \tag{7}$$

In this case P depends only on the energy density ρ and not on the baryon density n. The picture is one of free quarks and gluons moving in a perturbative vacuum which is surrounded by the true vacuum of lower energy density. It turns out in this model that all hadrons have the same energy density $4B$. Phenomenologically $B^{1/4} \approx 150$ MeV.

The model we have is very simple. Quark-gluon matter is formed at some high energy density $\rho(0)$. Being an unstable situation, the matter will expand hydrodynamically until it reaches the energy density $4B$, at which time it breaks up into hadrons. The aim is to find the time evolution of the volume-averaged thermodynamic quantities such as energy density. We will consider a spherical expansion for simplicity.

The total energy of the system is

$$E_{\text{total}} = \int \mathrm{d}V[\gamma^2(P + \rho) - P], \tag{8}$$

and the total entropy is

$$S_{\text{total}} = \int \mathrm{d}V \gamma s, \tag{9}$$

where $s = \partial P/\partial T$ is the local entropy density. Rather than solving the equations of motion numerically, which does not seem to be called for at this stage, we seek a volume-averaged description in the form

$$\begin{aligned} &\rho^*(t) = \rho^*(0)/\lambda^4(t), \qquad s(t) = s(0)/\lambda^3(t), \\ &V(t) = V(0)\, R^3(t), \qquad \gamma = \gamma(t). \end{aligned} \tag{10}$$

Here $\lambda(t)$ and $R(t)$ are scaling variables. We assume that the system begins to expand from rest at time $t = 0$ so that $\lambda(0) = 1$, $\dot{\lambda}(0) = 0$, $R(0) = 1$, $\dot{R}(0) = 0$, $\gamma(0) = 1$. Then eq. (8) gives

$$R^3(t) \cdot [\tfrac{1}{3}(X - 1)(4\gamma^2(t) - 1) + \lambda^4(t)] = X\lambda^4(t), \tag{11}$$

and eq. (9) gives

$$R^3(t)\, \gamma(t) = \lambda^3(t), \tag{12}$$

where $X \equiv \rho(0)/B$ is the input parameter.

We could solve for the full time development of eqs. (11) and (12), if we wanted, by identifying the flow velocity $v(t) = (1 - \gamma^{-2}(t))^{1/2}$ with dR/dt, where t is measured in units of the initial physical radius of the system, as is R. This is not necessary if all we are interested in is the state of the system at time t_f when the system breaks up into hadrons. Then $P(t_f) = 0$ and $\rho(t_f) = 4B$. We find that

$$\gamma(t_f) = \frac{X}{4}\left(\frac{3}{X-1}\right)^{3/4}, \qquad R^3(t_f) = \frac{4}{X}\left(\frac{X-1}{3}\right)^{3/2}. \tag{13}$$

Some rather simple but interesting results may be deduced from the above considerations. The fraction of the total energy which is converted to collective energy is $1 - \gamma^{-1}(t_f)$ and the fraction which remains in internal energy (mass and temperature) is $\gamma^{-1}(t_f)$. We can estimate the average transverse momentum of the emitted hadrons in the following way. Assume that the fluid elements give rise to a momentum distribution for particles in their rest frames of the usual form $\sim \exp(-p/T_0)$. Here T_0 is of the order of $B^{1/4}$. Then we sum over all fluid elements, taking into account the radial velocity of each [21], to obtain

$$\langle p_\perp \rangle = \frac{3\pi}{4} T_0 \gamma(t_f). \tag{14}$$

The average $p_\perp$ is increased by the radial expansion of the matter.

At present, of course, no experiments have been done for heavy nuclei at ultra-relativistic energies. Therefore, to show how the analysis of experiments might go, let us be highly speculative about interpreting the recent data taken at the CERN SPS $\bar{p}p$ collider [22]. It was reported that the average $p_\perp$ for these 540 GeV CM energy collisions is larger than the 350 MeV/c found for pp collisions at the ISR. It is a long-standing observation that, prior to the $\bar{p}p$ collider, the average $p_\perp$ seemed to have saturated well before the peak ISR energy of 63 GeV in the CM was reached. It seems reasonable to assume a cluster-type model for both. The average $p_\perp$ would saturate if the energy density at ISR energies saturated at $4B$, i.e., the clusters were produced at normal hadronic densities. Then $\langle p_\perp \rangle_{ISR} = 350$ MeV/c would imply that $T_0 = 150$ MeV.

If, in going to the $\bar{p}p$ collider energy, a threshold was passed for attaining greater energy densities which lead to the production of quark-gluon matter then, taking $\langle p_\perp \rangle_{\bar{p}p} = 500$ MeV/c, one obtains $\gamma(t_f) = 10/7$. From eq. (13) we would infer that the quark-gluon matter was formed at 9 times the energy density in a proton!

From the MIT bag model one obtains an energy density in the proton of about 0.3 GeV/fm^3, whereas an estimate based on a radius of 0.8 fm gives 0.45 GeV/fm^3. Compression by a factor of 9 gives values in the range 2.7 to 4.0 GeV/fm^3. This compares with a value of 0.15 GeV/fm^3 for cold nuclear matter at normal density. The three-dimensional hydrodynamic calculations, presented in part 4.3, produced maximum energy densities on the order of 0.5 GeV/fm^3. When considering that the CM beam energy has been increased from 0.2 GeV per nucleon for Ar + KCl to 270 GeV per nucleon for $\bar{p}$ + p this possible compression by a factor of 9 seems rather modest.

As applied to $\bar{p}p$ collisions this model is highly speculative. However, it does imply longer range correlations between produced particles and is consistent with azimuthal symmetry, both of which seem to be consistent with the data. Furthermore, we could calculate the number of dilepton pairs and real photons produced during the expansion [23] to check for consistency. It would be 238 times more interesting if the p and $\bar{p}$ could be replaced by uranium nuclei at the same beam energy!

4.5. Summary

It is of course impossible to adequately survey this field which goes back thirty years in such a short time and space. My discussion has naturally centered around those examples with which I am most familiar.

One should not be dogmatic in regarding the applicability of fluid dynamics to high energy heavy ion collisions. It may turn out to be an inadequate model to describe uranium collisions at 1 GeV per nucleon, yet at the same time it may have some usefulness for describing $\bar{p}p$ collisions at 270 GeV per beam, or vice versa. It is still an open question which can be answered only by a concerted effort by (i) theorists working in the fields of non-equilibrium statistical mechanics and quantum field theory, (ii) phenomenologists performing the calculations to compare with data and (iii) experimentalists to obtain the data.

The aim is to obtain information on the properties of hadronic matter at high temperature and density. Apart from possible terrestrial experiments with heavy ion beams there are two other alternatives. One might envisage colliding neutron stars, but that is far in the future. High temperatures and densities were almost surely obtained in the early Universe, but that was long ago, and the number and variety of relic observables pertaining to a quark-gluon→hadron phase transition seem to be severely limited (I know of none).

Perhaps even more important than the specific information being sought after are the benefits to be had from bringing together people from diverse subfields of physics to work on a common problem.

Acknowledgements

I would like to thank all those involved in the organization of this Rencontre de Moriond for providing such an interesting and stimulating atmosphere. This work was partially supported by a NATO-NSF Postdoctoral Fellowship.

References

[1] A.B. Migdal, Rev. Mod. Phys. 50 (1978) 107.
[2] T.D. Lee, Rev. Mod. Phys. 47 (1975) 267.
[3] J. Boguta, Phys. Lett. 109B (1982) 251.
[4] G. Baym and S.A. Chin, Phys. Lett. 62B (1976) 241.
[5] R. Hagedorn, in: Cargèse Lectures in Physics, Vol. 6, ed. E. Schatzmann (Gordon and Breach, New York, 1973).
[6] J.I. Kapusta, Nucl. Phys. B148 (1979) 461.
[7] R.L. Hatch and S.E. Koonin, Phys. Lett. 81B (1978) 1.
[8] Y. Yariv and Z. Fraenkel, Phys. Rev. C20 (1979) 2227.
[9] J. Cugnon, Phys. Rev. C22 (1980) 1885.
[10] S. Nagamiya et al., Phys. Rev. C24 (1981) 971.
[11] G.D. Westfall et al., Phys. Rev. Lett. 37 (1976) 1202.
[12] A. Sandoval et al., Phys. Rev. C21 (1980) 1321.
[13] J.R. Nix, Prog. Part. Nucl. Phys. 2 (1979) 237.
[14] R. Stock et al., Phys. Rev. Lett. 44 (1980) 1243.
[15] H. Stöcker et al., Phys. Rev. Lett. 47 (1981) 1807.
[16] J. Kapusta and D. Strottman, Phys. Lett. 106B (1981) 33.
[17] J.I. Kapusta and D. Strottman, Phys. Rev. C23 (1981) 1282.
[18] J. Kapusta, Phys. Rev. C24 (1981) 2545.

[19] P. Carruthers, Annals of the N.Y. Acad. Sciences 229 (1974) 91.
[20] A. Chodos, R.L. Jaffe, K. Johnson, C.B. Thorn and V.F. Weisskopf, Phys. Rev. D9 (1974) 3471.
[21] P.J. Siemens and J.O. Rasmussen, Phys. Rev. Lett. 42 (1979) 880.
[22] K. Alpgård et al., Phys. Lett. 107B (1981) 310.
[23] K. Kajantie and H.I. Miettinen, Z. Phys. C9 (1981) 341.

PHYSICS REPORTS (Review Section of Physics Letters) 88, No. 5 (1982) 379–391. North-Holland Publishing Company

5. Physical Conditions that might be Achieved in Ultra-Relativistic Heavy Ion Collisions

L. McLERRAN

Research Institute for Theoretical Physics, University of Helsinki, Helsinki, Finland

and

Physics Department, University of Washington, Seattle, Washington, U.S.A.

5.1. Introduction

The experimental study of ultra-relativistic nuclear collisions might provide unique information about novel, non-perturbative aspects of QCD, such as the disappearance of confinement and the restoration of chiral symmetry in matter at high energy density [1]. Dynamical mechanisms have been proposed which may explain confinement and chiral symmetry breaking in the vacuum, and the disappearance of these effects in high density matter may provide tests of these proposals. Monte-Carlo lattice gauge theory computations have shown the existence of a confinement-deconfinement phase transition [2], and a chiral symmetry restoration transition [2–3]. An experimental verification of these results provides a dramatic test of QCD.

The energy densities required to probe such novel, non-perturbative features of QCD are many times the energy density of nuclear matter. Are such energy densities achieved in ultra-relativistic nuclear collisions? If such energy densities are achieved, does the matter remain at high energy densities long enough to come into thermal equilibrium? In the absence of experimental information, answers to these questions must be found in theoretical space-time pictures [4–6].

These space-time pictures may be applied to head-on collisions between large nuclei of equal baryon number A at asymptotically large center-of-mass energies. We shall typically take uranium as an example, and consider center-of-mass per nucleon energies $E_{cm} > 30$ GeV. Head-on collisions will be taken as those collisions with an impact parameter less than the range of the nuclear force, $b < 1$ fm.

Head-on collisions are not extremely rare, since geometrical considerations show that $\frac{1}{2}\%$ of all uranium–uranium collisions are head-on. These collisions are not easily confused with peripheral collisions. Assuming the multiplicities in nuclear collisions grow as the nuclear baryon number, A, the multiplicity in a head-on collision between heavy nuclei at $E_{cm} > 30$ GeV is $n \sim 10^3$–10^4. Statistical fluctuations in peripheral collisions might only rarely simulate an event with so large a multiplicity. In addition, head-on collisions will be signaled by a violent, complete disintegration of projectile and target nuclei.

5.2. A space-time picture in the hydrodynamical model and in the quark-parton model

An elegant, simple space-time model of nuclear collisions is provided by Landau's hydrodynamical model. In the simplest version of this model, the collision of two nuclei is studied in the center-of-mass

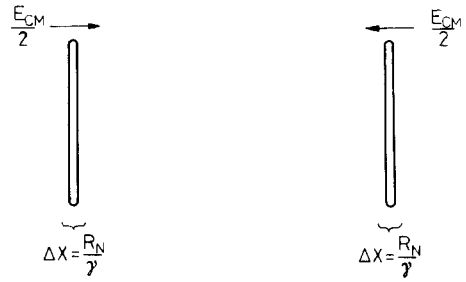

Fig. 5.1. Two nuclei of thickness $\Delta X \simeq RN/\gamma$ approaching one another in the center-of-mass frame. This thickness is appropriate for the simplest version of Landau's hydrodynamical model of the collision.

frame [4]. The two nuclei appear in this frame as two Lorentz contracted pancakes flying towards one another at near the velocity of light (fig. 5.1). The thickness of these two nuclei is

$$\Delta X = R_N/\gamma \tag{1}$$

where $\gamma = E_{cm}/2M$ is the energy per nucleon of each nucleus and R_N is the rest frame nuclear radius. When these two nuclei collide, they stick together and produce a distribution of hot hadronic matter with thickness $\Delta X_m = 2\Delta X$ (fig. 5.2). This matter then undergoes hydrodynamic expansion according to Landau's equations (fig. 5.3). The outward flow of matter is primarily along the axis of the beam of nuclei, and most of the particle production takes place during the initial collision when two nuclei stick together. This collision and subsequent expansion may be represented by the light cone diagram of fig. 5.4.

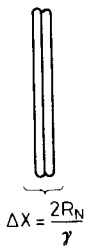

Fig. 5.2. The two nuclei sticking together immediately after a collision in the simplest version of Landau's hydrodynamical model.

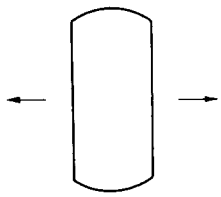

Fig. 5.3. The expansion of the hot hadronic matter according to Landau. The arrows indicate the outward flow of matter.

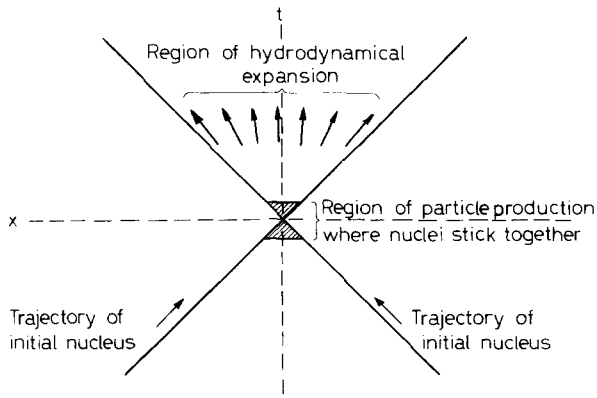

Fig. 5.4. A light cone diagram of a nuclear collision in the simplest version of Landau's model.

The energy density achieved in such a model is

$$\varepsilon \simeq \gamma \varepsilon_{\mathrm{NM}} \tag{2}$$

where $\varepsilon_{\mathrm{NM}}$ is the energy density of nuclear matter. The achieved energy density grows linearly with center-of-mass energy. For $E_{\mathrm{cm}} > 30$ GeV, $\varepsilon > 15\varepsilon_{\mathrm{NM}}$. Since the density of matter inside a proton,

$$\pi_{\mathrm{p}} \simeq \frac{1}{\frac{4}{3}\pi r_{\mathrm{p}}^3} \sim 450\ \mathrm{MeV/fm^3} \tag{3}$$

where r_{p} is the r.m.s. proton radius, is only a few times the energy density of nuclear matter, a quark-gluon plasma might form. Since ε rises linearly with center-of-mass energy, tremendously high energy densities arise at Isabelle energies, and in this simple version of the Landau model the formation of a quark-gluon plasma would seem certain.

This conceptually simple and attractive version of the Landau hydrodynamical model has difficulty, however, explaining many features of conventional hadronic interactions. The leading particle effect in hadron–hadron interactions suggests that two hadrons would very rarely stick together and then bounce off one another in high energy interactions. In most collisions, the hadrons apparently pass through one another. This transparency is most dramatic in high energy hadron–nucleus interactions. The projectile hadron must pass through many mean free paths of the target nucleus. The distribution of the scattered projectile and inelastically produced particles with momenta close to that of the projectile is nevertheless very similar to that of hadron–hadron interactions. The hadron projectile behaves almost as if it passed through the target nucleus and only scattered once. Another problem for simple hydrodynamical models of hadronic interactions is approximate scaling. Approximate scaling gives the total multiplicity as some power of the logarithm of the center-of-mass energy. Simple hydrodynamical models typically have the multiplicity proportional to a power of the center-of-mass energy. Such a proportionality appears to be at odds with SPS data on $\bar{\mathrm{p}}\mathrm{p}$ collisions [8]. Finally, the observed jet structure in $\mathrm{e^+e^-}$ collisions is not simply explained by a hydrodynamical model.

The quark-parton model provides an alternative description of hadronic interactions which incorporates the leading particle effect, transparency in hadron nucleus interactions, approximate scaling, and jets in $\mathrm{e^+e^-}$ collisions. The successful application of this model to hadron–nucleus interactions provides a guide for a corresponding application to nucleus–nucleus collisions [5, 9–10].

The qualitative features of the quark-parton model of nucleus–nucleus collisions which distinguish it from the Landau hydrodynamical model are simply understood. The dynamics of the central region is best understood when a nucleus–nucleus collision is analyzed in the center-of-mass frame. In this frame, the target and projectile nucleus are Lorentz contracted pancakes with a limiting thickness $\Delta X \sim 1$ fm which approach one another at near the velocity of light (fig. 5.5) [8]. This limiting thickness is a consequence of the Heisenberg uncertainty principle. The low longitudinal momentum component of the nuclear wavefunction must have a spatial extent $X \sim 1/p_{\|}$. The low momentum, wee parton component of the nuclear wavefunction is composed of gluons and quark–antiquark pairs, or, in a different base of states, virtual pions. These degrees of freedom have momentum $p_{\|} \sim 200$ MeV corresponding to $\Delta X \sim 1$ fm. The higher momentum components of the nuclear wavefunction have smaller spatial extent. The valence quark, or alternatively, nucleon component of the nuclear wavefunction has a spatial extent of $\Delta X \sim R/\gamma$, as was the case for the Landau hydrodynamical model.

When these two nuclei pass through one another, the low momentum component of the nuclear

Fig. 5.5. Two nuclei of thickness $\Delta X \simeq 1$ fm which approach one another in the center-of-mass frame. This thickness is appropriate for the quark-parton model of nucleus–nucleus collisions.

wavefunction interacts strongly and comes to rest in the center-of-mass frame. The higher momentum components interact less strongly and pass through one another (fig. 5.6). This low momentum component which has been scraped off from the two nuclei may now begin a hydrodynamic expansion. Since the low momentum component of the nuclear wavefunction (or, for that matter, of a nucleons wavefunction) is approximately independent of the center-of-mass energy, and since the low energy interactions which are primarily responsible for stopping this component are also independent of $E_{\rm cm}$, the energy density of matter scraped from the nuclei into this space-time region is approximately energy independent.

After the low momentum component of the nuclear wavefunctions have interacted, the nuclei continue to inelastically produce matter. The low momentum matter which has been scraped away from the nuclei interacts with higher longitudinal momentum components of the nuclear wavefunctions. This interaction is strong so long as the relative momenta of the scraped away matter and the components of the nuclear wavefunction are small. These higher momentum components are formed in a time $\tau \sim R_0$, where $R_0 \sim 1$ fm, in their own rest frame. This formation time is dilated in the center-of-mass frame, $\tau \sim p_\parallel R_0$, since these components have longitudinal momenta $p_\parallel$. These components arise from a region of spatial extent $\Delta X \sim R_{\rm N}/p_\parallel$ in the Lorentz contracted nuclei. The matter forms in an inside-outside cascade (fig. 5.7).

The inside-outside cascade may be represented by a light cone diagram (fig. 5.8). Matter is produced at the edges of the forward light cone and propagates forwards in time. Matter was formed primarily at the apex of the light cone in the Landau hydrodynamical model. After formation the matter may undergo hydrodynamical expansion [11].

The energy density of the matter forming at the edge of the light cone may be measured in a frame

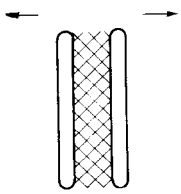

Fig. 5.6. The two nuclei after passing through one another. The shaded area represents heat formed in the central region.

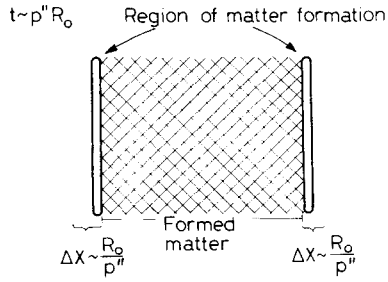

Fig. 5.7. The two nuclei forming an inside-outside cascade at time $\tau \sim p_\parallel R_0$.

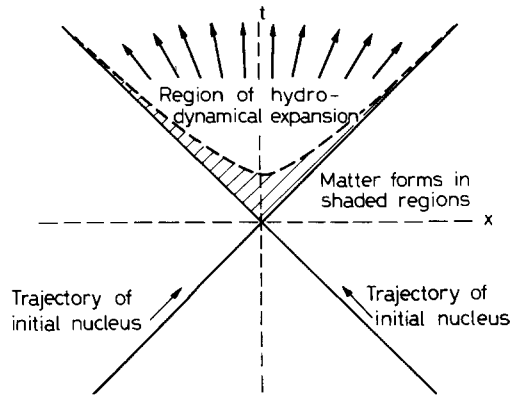

Fig. 5.8. A light cone diagram for the inside-outside cascade.

co-moving with this matter. In the simplest parton model, this energy density is taken to be independent of its position on the light cone. If the total multiplicity of centrally produced particles in nucleus–nucleus collisions is proportional to $A^{2/3+\alpha}$, the energy density at the edge of the light cone will be proportional to A^{α}.

After a time $\tau \sim \frac{1}{2}E_{\mathrm{cm}}R_0$, the valence quark, or nucleon, component of the nuclear wavefunction begins to materialize. The formation of this matter is most simply described in the rest frame of one of the nuclei. The target nucleus sees a Lorentz contracted projectile nucleus with a limiting thickness $\Delta X \sim R_0$ in this frame (fig. 5.9). The target is, of course, not moving and not Lorentz contracted.

As the projectile nucleus passes through the target, the low momentum components of its wavefunction interact strongly with the target. This component heats the target. The amount of heat should be approximately energy independent at asymptotic projectile energies. The projectile nucleus also compresses the target. This target probably forms a "fireball" which moves off in the direction of the

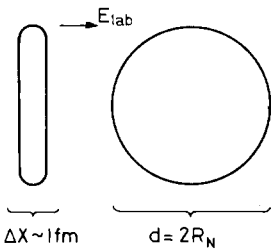

Fig. 5.9. The projectile nucleus with limiting thickness $\Delta X \sim 1$ fm approaches the target nucleus.

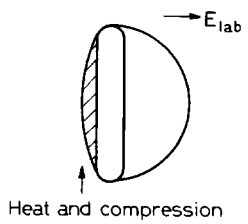

Fig. 5.10. The projectile nucleus begins to pass through the target.

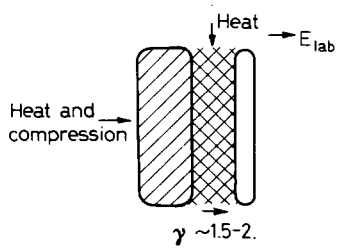

Fig. 5.11. The compressed, hot target nucleus begins to move down the beampipe. Matter begins forming in the central region.

projectile. The nucleons in this "fireball" may acquire longitudinal momenta typical of hadron–nucleus interactions. The Lorentz factor of the "fireball" is, therefore, $\gamma \sim 1.5$–2.0 (figs. 5.10, 5.11). After the projectile passes through the target, heat begins to materialize in the central region. This materialization was described in the previous paragraphs.

5.3. Expected energy densities in heavy ion collisions

In the next few paragraphs, I shall present the results of a semi-quantitative analysis of ultra-relativistic nuclear collisions [6]. I shall later describe the derivation of these results. Possible techniques for refining these computations are the subject of the closing paragraphs.

The analysis of nucleus–nucleus collisions simplifies in rapidity variables,

$$y = \ln \frac{E + p_{\parallel}}{m}, \tag{4}$$

where E is a particle's energy, $p_{\parallel}$ is its longitudinal momentum, and m is its transverse mass. The fragmentation regions of the nuclei are identified by particles with rapidities close to that of the target and projectile nuclei. For heavy nuclei, such as uranium, the width of the nucleus fragmentation region is $\Delta y \sim 3$–4. For nuclei with baryon number A,

$$\Delta y \simeq \ln A^{1/3} + \text{constant}. \tag{5}$$

The region of rapidity not included in the fragmentation region is the central region. Heavy nuclei, such as uranium, must have $E_{\text{cm}} > 30$ GeV before a central region is kinematically allowed.

If the multiplicity in the central region grows as the nuclear baryon number, A, and if the multiplicity continues to rise with energy as it does at ISR energies, the energy density of hot, dense matter in the central region may be as high as 2 GeV/fm^3 at ISR energies and 4 GeV/fm^3 at Isabelle energies.* If the multiplicity grows as $A^{2/3}$, the energy density is probably too small, $\varepsilon \sim 300$–600 MeV/fm^3 to produce a plasma, unless the coefficient of the $A^{2/3}$ term is anomalously large. Some data from hadron–nucleus collision indicate that if the multiplicity grows as $A^{2/3}$, the coefficient is indeed anomalously large, and even for uranium–uranium collisions the difference between an A and $A^{2/3}$ multiplicity growth is only a factor of two [12]. The energy density in the central region might be $\varepsilon \sim 1$–2 GeV/fm^3 in this case.

Hot, dense baryon-rich "fireballs" of hadronic matter may form in the fragmentation regions. The energy density of this matter may be $\varepsilon \sim 2$ GeV/fm^3, assuming the multiplicity grows as the baryon number A in the fragmentation region. This growth is consistent with hadron–nucleus collision data.

The dependence of the energy densities on baryon number of the nuclei is $A^{1/3}$ if multiplicities grow as A and constant if they grow as $A^{2/3}$. There is recent cosmic ray data on nucleus–nucleus collisions which are consistent with a multiplicity growth proportional to A [13]. In fig. 5.12, a pseudo-rapidity plot for the interaction of a 10 TeV/nucleon calcium nucleus with, presumably, a carbon nucleus is shown. About 600 charged particles are produced. The density of particles in the central region is consistent with a $\log^2 s$ multiplicity growth and growth proportional to A, but is inconsistent with $A^{2/3}$ and $\log^2 s$ (if the coefficient of $A^{2/3}$ is one). There is also preliminary data on a high energy

*For proton–proton interaction ISR and Isabelle energies correspond typically to 60 GeV and 800 GeV in the center-of-mass systems.

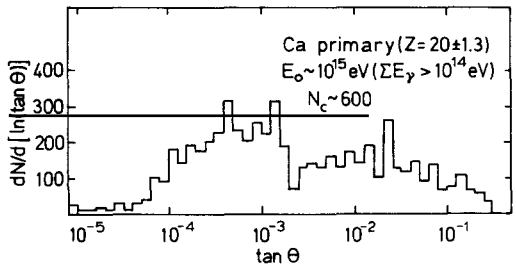

Fig. 5.12. A pseudo-rapidity distribution for a 10^3 TeV calcium nucleus-emulsion event.

silicon-emulsion nucleus interaction [13]. This event appears to have anomously high multiplicity, producing a situation in which a formation of a quark-gluon plasma is even more likely.

A distinction between matter produced in the fragmentation regions and the central region is found in the baryon number density. This density is the difference between the number of baryons and antibaryons per unit volume. There should be only a small baryon number density in the central region. If a quark-gluon plasma forms in both the central and fragmentation region, the study of the transition region between the fragmentation region and central region would allow a study of the dependence of characteristics of the quark-gluon plasma on baryon number density.

A hypothetical rapidity distribution for baryon number (baryons minus antibaryons) for a head-on collision between nuclei of baryon number A is shown in fig. 5.13a. The baryon number is concentrated in a nucleus fragmentation region of width $\Delta y \sim 2$–3. The heights of these fragmentation regions are porportional to A.

A hypothetical rapidity distribution for mesons in this collision is shown in fig. 5.13b. If the height of the central region was proportional to $A^{2/3}$, it would be clearly separated from the fragmentation region at Isabelle energies. The width of the fragmentation region for pions is $\Delta y \sim 3$–4.

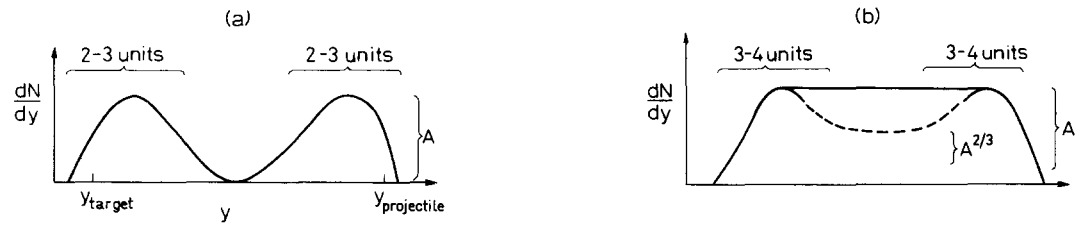

Fig. 5.13. Rapidity distributions for head-on nucleus–nucleus collisions: (a) The baryon number (nucleons minus antinucleons), (b) The meson distribution assuming heights in the central region proportional to A (——) and $A^{2/3}$ (----).

A feature of nucleus–nucleus collisions which distinguishes them from hadron–hadron and hadron–nucleus collisions is the extremely large number of particles which are produced in the collision. If enough particles are produced in the primeval distribution of hot, hadronic matter, and if the matter stays hot and dense long enough, the constituents of the matter will come into thermal equilibrium. The characteristic time scales for matter in the central region is $\tau \sim 2$ fm and is independent of baryon number. This is the characteristic time for the matter to decrease its energy density by a factor of two. The characteristic time scale in the fragmentation region is $2\,\text{fm} < \tau < A^{1/3}$ fm. This time depends on whether the dominant cooling mechanism is expansion generated from momentum gradients present in the initial formation of matter as the nuclei collide, or by radiation from an expanding "fireball" present in the fragmentation region.

Estimates which employ the parton model indicate that kinetic equilibrium is established in the fragmentation region [6]. The establishment of kinetic equilibrium requires that the momentum space distribution of particles is thermal in the region of momentum space most occupied by particles. The conclusion that kinetic equilibrium is attained is also verified by perturbative QCD computations [14]. These perturbative calculations also suggest that chemical equilibrium may also be achieved [15]. Chemical equilibrium requires that the relative population densities of different particle flavors is thermal. The matter in the central region also probably achieves kinetic equilibrium if the energy density is $\varepsilon > 1$–$2\ \mathrm{GeV/fm}^3$.

The parton model picture of hadronic interactions leads to the results of the preceding paragraphs [5, 9–10]. An important feature of this picture is the inside-outside development of cascades in hadronic interactions. This cascade development explains transparency in hadron–nucleus interactions, and is a consequence of time dilation and an intrinsic formation time for hadronic matter.

The inside-outside cascade may be understood by studying the hadronic interaction shown in fig. 5.14. A massless fragment is inelastically produced in the interaction between a projectile and target hadron. After a time t, the projectile and fragment have separated distances

$$\Delta r_\perp \sim (p_\perp/p_\parallel)\tau \tag{6}$$

and

$$\Delta r_\parallel \sim (p_\perp/p_\parallel)^2\tau\,. \tag{7}$$

In a frame co-moving with the fragment, that is, a local zero longitudinal momentum frame, the distances are

$$\Delta r_\parallel \sim \Delta r_\perp \sim (p_\perp/p_\parallel)\tau\,. \tag{8}$$

A Lorentz invariant generalization of this result for massive particles follows from the replacement $p_\perp \to \sqrt{p_\perp^2 + m^2}$.

The fragment may be properly included as part of the projectile hadron's wavefunction if the separation between fragment and projectile is $\Delta r_\perp$, $\Delta r_\parallel < 1$ fm in a frame co-moving with the fragment. This is the intrinsic formation time for hadronic matter. This time is dilated in the laboratory frame. The time for a fragment to materialize in a cascade in this frame is $\tau \sim p_\parallel$, so that the slow fragments materialize before the fast fragments.

This cascade development may be elegantly re-cast in terms of rapidity variables [16]. The Lorentz γ factor and velocity of a particle with rapidity y is

$$\gamma = \frac{\sqrt{p^2 + m^2}}{m} \cosh y \tag{9}$$

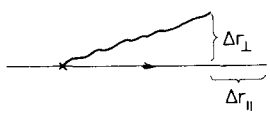

Fig. 5.14. Inelastic particle production.

$$v = \tanh y . \tag{10}$$

The time it takes for a particle to form in its rest frame is $R_0 \sim 1$ fm. The time in an arbitrary frame is obtained by Lorentz boosting and using eqs. (9)–(10). The density of particles when they first materialize is easily found from eqs. (9)–(10). Consider a pion which has just been inelastically produced in a hadron–hadron collision (fig. 5.15). We shall consider the rest frame of this pion. A nearest neighbor

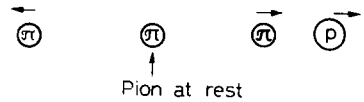

Fig. 5.15. Materialization of pions in hadron–hadron collisions. The arrows represent the direction of particle momenta.

pion materializes at the space-time coordinates $X \sim t \sim (\gamma + \sqrt{\gamma^2 - 1})R_0 = R_0 e^y$. The spatial separation between these pions is

$$\Delta X \sim R_0 e^y . \tag{11}$$

Since the rapidity density of pions in the central region is $dN/dy \sim 2$ for pp interactions at ISR energies,

$$\Delta X \sim \tfrac{1}{2} \text{fm} . \tag{12}$$

At Isabelle energies

$$\Delta X \sim \tfrac{1}{4} \text{fm} . \tag{13}$$

There is a large momentum difference $\Delta p_\parallel$, between these pions since

$$p_\parallel = m_\pi \sinh y \tag{14}$$

which is numerically

$$dp_\parallel/dX = 200 \text{ MeV/fm-pion} . \tag{15}$$

These simple pictures demonstrate the difficulty of forming a thermalized distribution of hadronic matter in ordinary hadronic interactions. The pions materialize at a distance of $\Delta X \sim \frac{1}{2}$ fm from one another. As they materialize, they are flying away from one another at near the velocity of light. It would be very difficult for these pions to interact sufficiently to produce a thermal distribution. In high multiplicity events, this situation is somewhat less difficult.

The production of matter in a nucleus–nucleus collision is similar to that in hadron–hadron collisions. An essential difference is that the multiplicities are much higher. Many "strings" of matter are produced by the large number of nucleon–nucleon interactions [10]. Each "string" is surrounded by many other "strings", and the matter from different "strings" may thermalize (fig. 5.16).

In the central region of nucleus–nucleus collisions, matter is composed on inelastically produced particles. The cross-sectional area of the matter in the central region is $S \sim \pi R^2 \sim 4A^{2/3}$. Assuming the height of the central region in nucleus–nucleus collision is proportional to A, the number density of

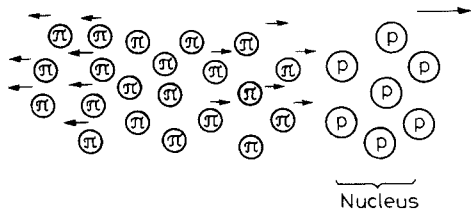

Fig. 5.16. The matter produced from many nucleon–nucleon interactions. Thermalization arises from the interaction of matter produced by many different nucleons.

pions is

$$n \sim \tfrac{1}{2}A^{1/3}\,\text{pions/fm}^3 \tag{16}$$

at ISR energies and

$$n \sim A^{1/3}\,\text{pions/fm}^3 \tag{17}$$

at Isabelle energies. If each pion has an average energy $E \sim 600$ MeV in a local $p_\parallel = 0$ frame, the energy densities are $\varepsilon \sim 2\,\text{GeV/fm}^3$ at ISR energies and $\varepsilon \sim 4\,\text{GeV/fm}^3$ at Isabelle energies. These energies are smaller, and A independent if the total multiplicity in the central region $n \sim A^{2/3}$.

The characteristic time scale for the expansion of matter in the central region follows from the momentum gradiant of eq. (15), or eq. (10) for the velocity. The time it takes for pions to increase their separation by a factor of two is $\tau \sim 2$ fm.

The energy densities achieved in the fragmentation region in nucleus–nucleus collisions arise from inelastic production of matter which becomes trapped with the nucleons, and by compression of the nucleons. The low momentum particles, which will be thought of as pions, may be produced and trapped in the nuclei. These low momentum pions have longitudinal momentum $p_\parallel < (R_N/R_0)p_\perp$. Estimates of the number of pions trapped in the nucleus fragmentation region give about 3–4 pions/nucleon for uranium–uranium collisions at ISR energies. At Isabelle energies, this number would be increased by perhaps a factor of two arising from scaling violations. The number of pions should be proportional ln $A^{1/3}$ since linearly increasing $A^{1/3}$ linearly increases the rapidity interval in which pions may become trapped. A hypothetical distribution of the regions in rapidity space from which pions are trapped is shown in fig. 5.17 for various reasonable assumptions on the cut-off in $p_\perp/p_\parallel$.

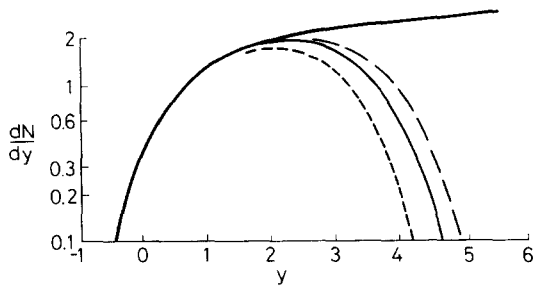

Fig. 5.17. The regions of phase-space from which pions are trapped in the nucleus fragmentation region using various trapping criteria. A plot of dN/dy for pp collisions is shown with the heavy line.

The energy trapped per nucleon is $E/N \sim 3$–4 GeV at ISR energies. This energy might be a factor of two higher at Isabelle energies. Uncertainties in the evaluation of this energy are about a factor of two. This number follows from assuming the energy per trapped pion is $E \sim 600$ MeV and per nucleon $E \sim 1$ GeV.

After the target nucleons are struck, they acquire longitudinal momentum. This longitudinal momentum is approximatley that of a pp collision, corresponding to a $\gamma \sim 2$. The nucleons and trapped pions may form a baryon-rich fireball which moves down the beampipe with a $\gamma \sim 2$.

As the projectile nucleus traverses the target, imparting longitudinal momentum to the target nucleons, the target is compressed. As shown in fig. 5.18, this compression results from the sequential encounters of the projectile nucleus with the target nucleons. After the left-most target nucleon is encountered, this nucleon acquires a velocity v. It travels a distance vR before the second nucleon is struck. In the lab frame, the apparent compression is $1/(1-v)$. In the rest frame of the struck nucleus, the compression is

$$C = \frac{1}{\gamma(1-v)} \simeq 2\gamma . \tag{18}$$

The energy density in the fragmentation region is estimated from the compression C, the trapped energy per baryon, E/N, and the energy density of nuclear matter as

$$\varepsilon \sim \rho_0 C^E/N \sim 2\,\mathrm{GeV/fm^3} . \tag{19}$$

This energy density might be as much as a factor of two higher at Isabelle energies.

The characteristic time scale for expansion in the fragmentation region may be larger than that of the central region. In the central region, the matter expands with characteristic time scale $\tau \sim 2$ fm. In the fragmentation region, expanding heat runs into nucleonic matter which is almost locally at rest in the rest frame of the "fireball' formed in the fragmentation region. If the nucleons could absorb the momenta gradients in the heat, the "fireball" would not be initially expanding. In this case, the fireball

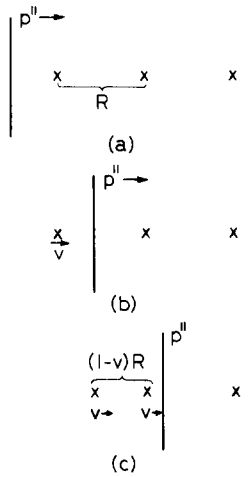

Fig. 5.18. Compression of the target nucleus: (a) Before encountering the first nucleon, (b) After encountering the first nucleon, (c) After encountering the second nucleon.

would cool by thermal emission from its surface. The characteristic time scale for this expansion is the time it takes a sound wave to cross a compressed nuclear diameter. For $v_s^2 \sim \frac{1}{3}$, this time is $\tau \sim A^{1/3}$ fm. The characteristic time scale for expansion may therefore be in the range $2\,\text{fm} < \tau < A^{1/3}$ fm.

5.4. Towards a more accurate picture

The description of nucleus–nucleus collisions advocated in the previous paragraphs is phenomenological. A proper theoretical treatment of the collision should address at least two issues: the approach to equilibrium from a non-equilibrium distribution of matter in the colliding nuclei, and the subsequent hydrodynamic expansion of the matter after it has achieved equilibrium. The approach to equilibrium might be studied using transport theory [17]. Perhaps the collisions which are most responsible for the approach to equilibrium are energetic enough that perturbative QCD, or at least weak coupling QCD, might be appropriate. Applying QCD to transport theory is, however, extremely difficult since infrared divergences arise from the masslessness of the gluons [17]. The proper application of QCD to the approach to equilibrium will be a major project, and will take considerable hard work to carry through.

The primary effect of the pre-equilibrium processes is to generate a distribution of matter which is locally in thermal equilibrium with energy density ε_0 after some time τ_0. This distribution provides initial conditions for hydrodynamic equations,

$$\partial_\mu T^{\mu\nu} = 0\,, \tag{20}$$

where $T^{\mu\nu}$ is the stress-energy tensor [4, 11]. The relationship between energy density and pressure are needed to compute $T^{\mu\nu}$. This relationship may be evaluated using Monte-Carlo techniques [2]. The hadronic matter distribution might therefore be computable, with currently available theoretical methods, from the time equilibrium is achieved until the time hadronic matter decouples! This time corresponds to an energy density of nuclear matter. This situation may be unique in the study of hadronic collisions.

Acknowledgements

I have benefitted from conversations with many people during the development of the ideas discussed in this paper, and I especially benefitted from conversations with R. Anishetty, J. Bjorken, J. Gunion, M. Guyallassey, L. Van Hove, M. Jacob, K. Kajantie, J. Kapusta, P. Koehler, H. Miettinen, H. Satz and W. Willis.

References

[1] For reviews, see
E.V. Shuryak, Phys. Reports 61 (1980) 71;
D.J. Gross, R.D. Pisarski and L.G. Yaffe, Rev. Mod. Phys. 53 (1981) 43.
[2] For a review, see
H. Satz, section 3.
[3] J. Kogut, S. Shenker, J. Shigemitsu, D. Sinclair, M. Stone and H. Wyld, University of Illinois Preprint, I 11-Th-82-5 (1982).

[4] L. Landau, Proc. Academy of Sciences, USSR, Physical Series, Vol. 17 (1953) p. 51.
[5] J. Bjorken, Lectures at DESY Summer Institute (1975), Proceeding edited by J.G. Kärnes, G. Kramer and D. Schildnecht (Springer Verlag, 1976).
[6] R. Anishetty, P. Koehler and L. McLerran, Phys. Rev. D22 (1980) 2793;
L. McLerran, Proc. 5th High Energy Heavy Ion Study, May 18–22 (1981), Lawrence Berkeley Laboratory, Berkeley, California.
[7] E.V. Shuryak, Phys. Lett. 78B (1978) 150.
[8] UA5-collaboration CERN, Phys. Lett. 107B (1981) 310, 315;
UA1-collaboration CERN, Phys. Lett. 107B (1981) 320.
[9] K. Gottfried, Proc. Fifth Intern. Conf. on High Energy Physics and Nuclear Structure, Uppsala (1975).
[10] A. Bialas, Proc. First Workshop on Ultra-relativistic Nuclear Collisions (1979).
[11] This picture of nucleus–nucleus collisions was first described to the author by J. Bjorken, private communication.
[12] A. Mueller, Proc. 1981 Summer Workshop, High Energy Heavy Ion Physics, BNL 51443, Vol. 2 (1981) pp. 618–653.
[13] T. Burnett et al., Proc. AIP Conf. Proc. pp Collider Physics, Madison, Wisconsin (1981).
[14] K. Kajantie and H. Miettinen, Z. Physik C 341 (1981).
[15] T. Biro and J. Zimanyi, Budapest preprint KFK I-1981-69 (1981).
[16] K. Kajantie, private communication.
[17] Sai-ping Li and L. McLerran, University of Washington Preprint 40048-82-PT 9 (1982).

PHYSICS REPORTS (Review Section of Physics Letters) 88, No. 5 (1982) 393–400. North-Holland Publishing Company

6. Experiments on High Energy Density States

W. WILLIS
CERN, Geneva, Switzerland

6.1. Physics goals

The motivations of experiments of the sort described here have been discussed in the previous sections, but it will be convenient to recapitulate them here in a form adapted to this section.

It is assumed that the principal goal is to study the confinement of quarks and gluons. We suppose that these are normally confined within hadrons by the colour confining properties of the physical vacuum. We accept, as a hypothesis, that this effect is due to a spontaneous breaking of the symmetry of the physical vacuum. In this case, it is rather likely that the symmetry is restored by the local presence of a sufficiently high energy density. This can be achieved by compression of cold matter or by sufficient heating. The transition from a system of hadrons to a deconfined plasma of quarks and gluons should take place somewhere between 0.5 and 1.5 GeV/fm^3, that is, three to ten times normal nuclear density. It is believed that such states can be created in suitable high energy collisions. Our first task must be to select such collisions and to measure the volume and the energy density. We must also utilize measures of the equilibration of the energy, to establish that the energetic state exists long enough for the effects of deconfinement to manifest themselves, as described in section 6.2.

If the desired conditions are demonstrated to be established, we may look for the characteristic signals of deconfinement. These are of several kinds. The most characteristic are critical phenomena near phase transition. Perhaps easier to observe are the gross properties of the extended quark-gluon plasma. More speculative experiments search for exotic states of matter created from the quark-gluon plasma or phenomena related to its existence. These will be discussed in section 6.3.

6.2. Creation and identification of extended energetic states

The goal of high energy density has been emphasized, but of course energy density is not the sole requirement. The energy density in the first stage of a high energy e^+e^- annihilation is very high indeed, but that system is not useful for our purposes. Confinement is a long range effect, as we know quarks and gluons act as if they were free over short distances. To see the effects of confinement, we must study distances >1 fm. The overall size of the system must be larger than that, so at least several fm. Nuclei naturally suggest themselves, but the energy density in a static nucleus is sufficiently far below the critical value that it seems that one can describe nuclei in terms of hadrons without recognizing any obvious effects due to colour confinement. Rather large amounts of energy have to be introduced into the nucleus to bring the energy density up to the desired range. For example, the volume of a lead nucleus is about 1500 $(fm)^3$, so to provide 1 $GeV/(fm)^3$ requires an addition of about 1300 GeV of excitation energy. The cheapest way, in principle, to obtain that energy is by collision with another

0 370-1573/82/0000–0000/$2.00

similar nucleus with 1100 GeV of centre-of-mass kinetic energy, or about 5 GeV kinetic energy per nucleon in the centre-of-mass. This is in the unrealistic case when every bit of available energy is converted into excitation thermalized in the nucleus. On the other hand, no benefit is assumed from volume reduction by compression or Lorentz contraction. The realistic calculations described in the previous sections show that substantially higher incident energies are probably required. It then seems that we are speaking of SPS, ISR or higher energy machines.

If we speak of SPS beams with about 200 GeV per nucleon energy in the lab, and projectile mass A' equal to target mass A, about one quarter of the CMS energy needs to be converted to excitation to reach the desired energy density. It is clear that this will happen in only a small fraction of events. First, most collisions are peripheral, and there is certainly no chance of absorbing their energy efficiently. About five per cent of the collisions will be nearly central, on geometrical grounds. They can easily be recognized by observing the spectator fragments of the projectile which have not interacted. They will retain the velocity of the projectile, and remain with small transverse momenta, so that they occupy a very small region of phase space and can easily be distinguished from other particles. A forward calorimeter is convenient for this purpose. The central collisions are those which have very few such fragments.

Once the central collisions have been selected, the distribution of energy deposited can be determined quickly by measuring the transverse energy, $E_T = \Sigma_i E_i \sin\theta_i$. In particular, one would measure $dE_T/d\eta$ as a function of η, the pseudo-rapidity, in a large solid angle segmented calorimeter. In the case of fixed target experiments at SPS energies, where one may be limited to fairly light projectiles, such as $A' = 12$–40, it is presumably advantageous to use targets considerably larger than the projectile. Then the most favourable case is that in which a substantial amount of the energy is stopped in the target nucleus. The result is a system moving rather slowly in the lab., typically with $\gamma < 2$, and emitting particles at rather large angles. A large peak of dE_T/dy in the target rapidity region, $0 < \eta < 2$ in the laboratory, presumably signals the high deposit of energy in the target nucleus that we desire, as shown in fig. 6.1. We have no information at present on the fluctuation from event to event under these circumstances. We may assume that the interactions are a superposition of individual nucleon interactions, in which case statistical averaging reduces the fluctuations. With the calorimeter triggers just described, we may search for rare events, and the tail of the energy deposit distribution is even harder

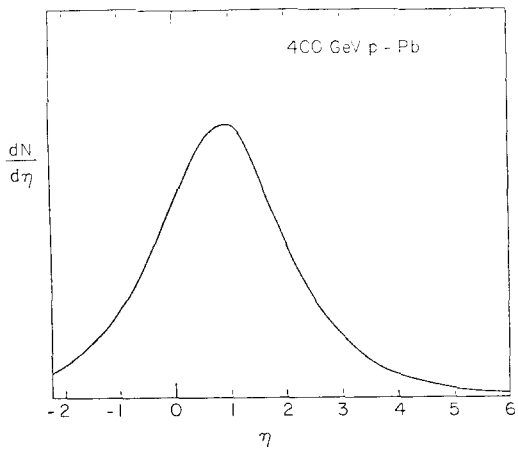

Fig. 6.1. The pseudorapidity distribution for 400 GeV p–Pb collisions where all of the energy is deposited in the lead.

to estimate. All our experience indicates that most such distributions do in fact have a long tail, and selecting rare events with high energy deposit may be a very effective way of reaching higher energy densities, given a fixed maximum beam energy.

This strategy for selecting rare collisions with high energy deposit is quite reminiscent of experiments on high p_T phenomena in p–p collisions, where one selects very rare events indeed, as rare as one in 10^{10}. This suggests that events of interest might be obtained in very rare collisions of protons with heavy nuclei. For example, in 400 GeV proton–lead collisions, kinematics would allow 250 GeV to be deposited in the nucleus, though we know that typical events deposit only a few GeV. In this case, we know that the fluctuations are large, but it is still not clear how far we can go out on this tail. It is interesting to ask if the state achieved by depositing 100 or 200 GeV this way is the same for our purposes as that produced by depositing the same energy by a nuclear projectile. Let us assume for the moment that the deposited energy is successfully thermalized in each case. I believe that the cases will still be different when we come to look for our signals of deconfinement, because our observables are always integrated over the thermal history of the source. A proton initiated event with a large energy deposit probably starts with a very violent collision between the proton and a cluster of quarks in the target, generating a high E_T. This amounts to the creation of a very hot spot, which then spreads in some way. This will radiate photons and lepton pairs vigorously, perhaps obscuring the radiation from the large equilibrium system which we wish to observe. The "pre-equilibrium" phenomena are clearly minimized by the use of the collisions with the largest possible A', the gentlest collisions which give the desired energy density. We can see how the projectile A' dependence can be used to separate the equilibrium signals from pre-equilibrium phenomena, which have their own intrinsic interest. The extreme case in this regard would be high E_T p–p collisions in the colliders, where comparable E_T can be reached.

Once states which are candidates for high energy density have been selected on the basis of absence of beam fragments, and large peak dE_T/dy, they can be tested for thermal equilibrium conditions. The energy flow should certainly display azimuthal symmetry. The longitudinal distribution would display the spherical symmetry characteristic of a completely thermalized system or in the extreme case where all of the incident energy flow has been stopped in the target. More realistically, one expects to see fragments of the target which have not participated in the thermalization, and have very small energies, and beam fragments which have punched through the target nucleus before hadronizing to particles with large rapidities. The high E_T trigger will minimize these components, but they will always be visible, and must be taken into account in evaluating the degree of thermalization in the system of interest, that corresponding to the selected peak in dE_T/dy.

After we have studied the energy flow and identified a structure in $dE_T/d\eta$ which seems to be a candidate of interest, the individual particle spectra can be inspected. These must have several components: the thermalized system of interest (as we hope); the pre-equilibrium emission from the high E_T system; and the target and projectile remnants not involved in the high E_T system. The last component can largely be separated in rapidity as mentioned above, and the low energy target fragments are probably not a very serious background, but the pre-equilibrium radiations must be unfolded, with the aid of incident energy, A' and A dependences. The result will be a determination of the parameters of the thermalized system. There will be some internal checks in this procedure, from spectral shapes and comparison of different particles, but further checks are surely desirable. One such could be the check on the energy radiated from the measured volume of the thermalized system at the temperature measured. The volume can be determined by measurements of identical particle interference. This technique is well known when applied to like sign pions, but some particularly impressive

results were recently obtained using two-proton interference, fig. 6.2 (the correlation in orthogonal planes containing two protons from p–Pb collisions). This allows a measurement of the dimensions of the source in the beam direction, and the transverse direction, which turn out to be quite different in this case. With this battery of measurements, the events should be characterized rather well, and the search for confinement effects may proceed.

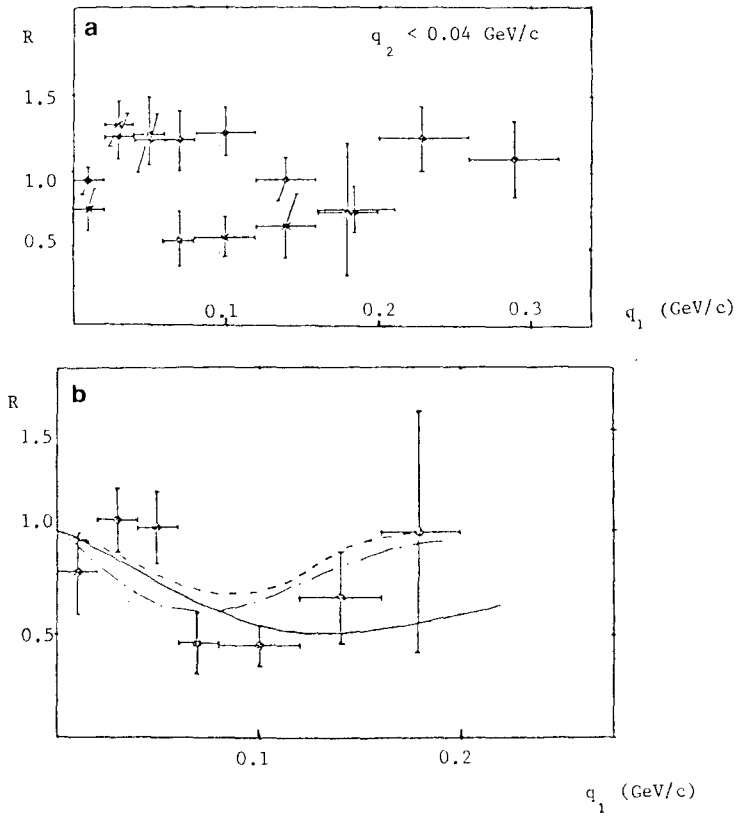

Fig. 6.2. (a) The correlation functions of two protons from p–Pb collisions. The dots are pairs in a plane perpendicular to the beam, the crosses are pairs in a plane containing the beam. (b) The data of the crosses of (a) with theoretical fits.

6.3. Observable signals of deconfinement

We wish to observe differences between two phases, one a hot gas of hadrons, and the other a plasma containing quarks and gluons (*and* perhaps certain hadrons as we will mention later when we discuss chiral symmetry). We know that short range phenomena should look the same in the two systems because of asymptotic freedom. Long range phenomena, on the other hand, risk to be dominated by effects at the surface of the interaction volume, such as hadronization and final state scattering, perhaps rendering many observables rather insensitive to the state of affairs in the interior. Little theoretical study of these difficult matters has been made. The task for the experimentalist seems to be to devise as many relevant measurements as possible, so that a convincing picture can be built up, despite doubts about individual items. One may seek signals of two types: those which have to do with

the transition between phases and those which reveal some property of the quark gluon phase by which it can be distinguished from the hadron gas phase. We deal first with the former, which would be particularly clear and informative, though they may turn out to be difficult.

The simplest suggestion is to observe effects in inclusive spectra as the deconfinement transition is crossed. The transition can be crossed by changing the energy density, or perhaps by increasing the fraction of particles which are baryons. The latter possibility may be convenient at high energies with $A' \simeq A$ where the control and fragmentation regions can be distinguished. In that case, the fraction of baryons can be changed, at more or less constant energy density, by varying the rapidity. For varying the energy density itself we have available the incident energies, A' and A, and the impact parameter.

A change in the pion spectrum or multiplicity across transition would be an easy signal to see, but it has not been shown that the pions are not dominated by surface and final state effects. Another suggestion is that the fraction of strange particles should be higher in the deconfined phase, due to SU(3) symmetry restoration, and this effect may be less influenced by the surface. The ideal way to avoid these problems is to use weakly interacting probes, photons and leptons and perhaps charmed particles. Since these may originate anywhere inside the interaction volume and still escape, while pions and nucleons originate, or scatter last, near the surface, ratio of these weakly interacting particles to ordinary hadrons depends on the volume to surface ratio. For large interaction volumes, the real and virtual photons etc. may be considerably enhanced over the values observed in p–p collisions.

Experience in studying phase transitions in other areas of many-body physics suggests that correlations may be much more informative than inclusive spectra. We have mentioned in part 6.2 the use of the correlations between identical particles in order to measure the size and shape of the interaction volume. Two or three particle correlations are also sensitive to the degree of phase coherence at the points where the particles are emitted. For example, some observations of two pion correlations are consistent with a chaotic phase, while others imply some degree of phase coherence. Near a phase transition, especially near a critical point, we may expect some amount of long range order. If we consider the correlation function $R(\Delta q)$ for $\Delta q \simeq 0$, as a function of the energy density of the system, we know that for two pion correlations $R_{\pi\pi}(0) \simeq 2$ for energy densities well below the deconfinement transition. If we may assume that the effects of long range order extend to the surface, we might expect $R_{\pi\pi}(0)$ to decrease as the transition is approached. Above transition $R_{\pi\pi}(\Delta q)$ may display several types of behaviour depending on the nature of the transition, the presence of domain structure, and so on. Ideally, one would measure correlations of two photons in order to avoid surface effects. This might even be possible if photon emission is sufficiently enhanced for large interaction volumes.

Another kind of two particle correlations is the measurement of the production of two electrons or muons through virtual photons. This experiment has been much discussed in the literature, because it seems particularly clean. The virtual photon provides us with a weakly interacting probe while its finite mass eliminates most meson-decay background. The lepton pair spectrum observed in p–p collisions is shown in fig. 6.3. One sees peaks corresponding to the decays of the vector mesons $\rho/\omega, \phi, \ldots$, superimposed on a continuum which rises at low masses. If we could observe an interaction volume at sufficiently high energy density so that only quarks and gluons are present and sufficiently large so that surface effects could be neglected, we would not expect to see any decays of vector mesons since these would have "melted". The continuum would be present at a high level due to thermal radiation from the quark gluon plasma, as shown in fig. 6.4. We learn two things from such a spectrum. The continuum gives us a measurement of the temperature of the plasma and the peaks reveal the presence of vector mesons.

Recent studies have indicated that the above picture is probably over-simplified. The formation of

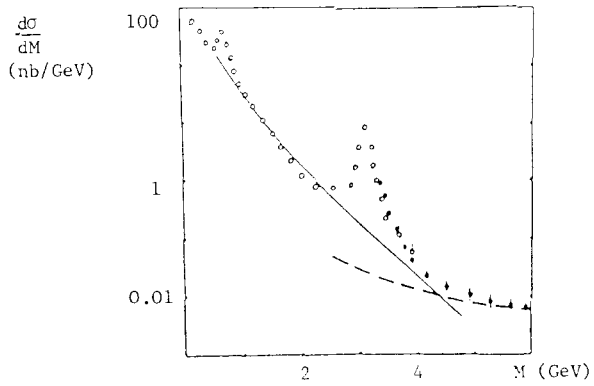

Fig. 6.3. Data from Chicago Princeton II on the muon pair mass distribution showing a continuum well above the Drell–Yan prediction for masses below 3 GeV.

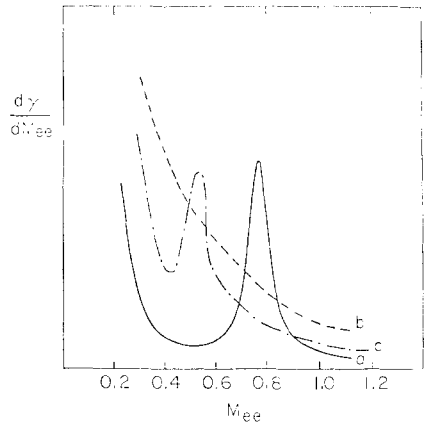

Fig. 6.4. Predictions for the electron pair mass distribution: (a) the data from pp collisions during the ρ dominance and some direct continuum; (b) the prediction of a strong continuum and no resonances, at very high temperature; (c) the prediction of a shifted ρ by Pisarski, in the deconfined phase below the chiral symmetry restoration transition.

the pion from a pair of quarks is governed by the breaking of chiral symmetry which will also be restored by high energy density but probably at considerably higher densities. There are, thus, three phases: the hadron gas; an intermediate phase with quarks and gluons and also pions and their resonances; and the high temperature quark gluon phase. It has been predicted that in the intermediate phase, the mass value of the ρ will be shifted substantially downward by the effect of the mean field of the quark gluon plasma, while retaining a narrow width. This situation is illustrated by the curve (c) in fig. 6.4. The observation of this effect would be a striking confirmation of the theory of symmetry restoration. The ϕ meson is presumably less affected by chiral symmetry because of the large mass of the strange quarks and we might suppose that it will disappear already at the deconfinement transition. Correction for vector mesons emitted from the surface will always be necessary.

Another interesting suggestion is to search for the disappearance of the "blast wave" at deconfinement transition. The blast wave is the radial expansion of hadrons thought to be observed in nucleus–nucleus collisions. It is detected by a shift in the inclusive spectra of pions and protons. As the energy density is raised, more energy is available for the blast wave, and its observation should become clearer. Shuryak has predicted that when the quarks and gluons are deconfined and occupy one large "bag", the blast wave will disappear. This is an attractive experiment, because it involves only the comparison of inclusive spectra.

Among the properties of the quark gluon plasma which might give rise to gross effects in the event structure, we might single out the extended colour fields. This makes the quark gluon plasma a bit like ordinary plasmas with their coupling to electrical and magnetic fields. By analogy, it is easy to imagine collective motions generated in this plasma, particularly in events where the impact parameter is different from zero and a large angular momentum is present. These motions could manifest themselves by chunks of material being ejected with large total transverse momentum. Given the large amount of energy present, it is easy to obtain what we might call "super-jets". These would have more transverse momentum than would be possible for the ordinary jets from hard scattering of hadron constitutents. Consequently, their observation would be very easy, and a sure sign of collective effects, though it would be hard to identify the details of its origin.

6.4. Detector ideas

The previous sections have ignored the practical problems of measuring the desired quantities. Some of these problems are unusual in terms of normal high energy physics experiments, and may require novel solutions. In other cases, the peculiarities of the reactions considered here allow opportunities for new experimental techniques not normally feasible.

The most striking feature of the events with very high energy density is the large multiplicity expected. The emulsion event in fig. 6.1 has a peak value of about 200 charged particles per unit of rapidity. With suitable triggering and high luminosity, this number may double or even triple. This is certainly a most obvious problem with conventional techniques, but also presents several new opportunities. Most of section 6.2 dealt with measurements of energy flow, and both the large amounts of energy being discussed and the very high multiplicities are great advantages for the measurement of energy by the calorimetric technique. The energy resolution of a well-made calorimeter improves as $E^{-1/2}$, and the imperfections which exist in all real devices are substantially ameliorated by having the energy spread over many particles rather than a few. This advantage becomes particularly striking when the energy is to be subdivided in various ways. In fact, once we want a map of the energy flow over all solid angles, the large amount of energy and high multiplicity become vital in getting a good result. For example, take a 200 GeV/A ^{16}O beam, with 3200 GeV. A reasonable 4π solid angle calorimeter set up might have 1000 cells to map the energy, separately for the approximately equal electromagnetic and hadronic component sections of the calorimeter, or an average of 1.6 GeV/cell. A very good calorimeter will then give an energy resolution in the *average* cell of ±20%, with much better resolution in the cells with high energy. The result would be a map of energy flow separately for hadron and electromagnetic components, a measurement which is not even considered for normal multiplicity events, but is particularly appropriate for these reactions, where we have reason to suspect a substantial direct photon component.

Much of the work on individual particle spectra described in sections 6.2 and 6.3 can be done with photons where we assume that most photons come from $\pi \to \gamma\gamma$. These are very convenient to measure in high multiplicity events, because the measurement may be done calorimetrically in two dimensional arrays with read out in the form of tiny towers. This is possible because of the small transverse extent of the showers in sodium iodide or bismuth germanate. The use of these materials also allows a very good energy resolution (<10%) to be maintained at the low energies characteristic of target fragments and high multiplicity events. It is quite practical to provide such towers with an angular size corresponding to 10^5 units over 4π. It is not suggested that 10^5 units actually be used, since the statistical nature of the events allows valid conclusions to be drawn by *sampling* a portion of the solid angle. The representative character of the area sample can be determined by the information from the calorimeter which does cover 4π. Alternatively, the calorimeter can be used to trigger on events which are oriented so as to place some characteristic feature in the solid angle covered by the fine grained detectors.

After all the above has been said, we must admit that we will want to know about the individual charged particles, in order to identify pions, protons and kaons, to measure two and three particle correlations, and so on. Even to use the fine-grained photon detectors, it is desirable to know whether the particle entering a given tower was charged or neutral. For the last purpose, we immediately see that we would like a charged particle detector with two dimensional planar read-outs corresponding to the towers of the fine-grained detector. It would be possible to do this by means of a proportional chamber with cathode pad read-out.

This kind of geometry is so well suited to our problem that we are tempted to go further and attempt

to measure track angles and ionization density in this geometry, perhaps only for a fairly short length of tracks. For tracks of relatively low momentum, this angle would suffice to determine the sign and momentum, and combined with the fine-grained tower signal, would allow us to identify slow π, K and p.

We have noted briefly the possible importance of charmed particle probes. The very small transverse dimension of the possible targets and beams in fixed target experiments allow us to consider very powerful vertex detectors, particularly when looking at target fragments, which may make possible some unusual experiments on short-lived particles.

Editorial note

The Bielefeld workshop on "quark matter formation and heavy ion collisions" held in May 1982 was the occasion to discuss experimental possibilities, in particular at the CERN-SPS. The reader is referred to its proceedings for a description of the promising set-ups which were considered (WSPC, Singapore; eds. M. Jacob and H. Satz). Detailed discussions of specific experimental techniques followed different lines, namely Light ion physics, Photon and leptons, Few particle correlations, Peripheral interactions, Inclusive spectra and particle identification, Visual and imaging detectors, and Large solid angle calorimeters.

PHYSICS REPORTS (Review Section of Physics Letters) 88, No. 5 (1982) 401–413. North-Holland Publishing Company

7. Review on $\alpha\alpha$ and αp interactions in the CERN-ISR

M.A. FAESSLER
CERN, Geneva, Switzerland

7.1. Introduction

In 1980 a special run with α particles took place in the CERN Intersecting Storage Rings (ISR). It lasted only one week, but a large amount of data was collected by five experimental teams working at different intersection regions. This report reviews some of the results and some of the theoretical efforts relating to them. Naturally, the topics studied in the beginning were mainly inclusive distributions and the like. Whilst even at this level more work has to be done, the data recorded by the large solid-angle detectors call for more sophisticated types of analysis.

To start, I will briefly sketch the parameters of the run and give a survey of the experiments. The α beams were accelerated to the maximum momentum 31.5 GeV/c per charge (15.7 GeV/c per nucleon). The week of data-taking was divided into two halves. One half was with α particles in both rings. The c.m. energy was $\sqrt{s}$ = 125 GeV or, per average nucleon–nucleon collision, $\sqrt{s_{\mathrm{NN}}}$ = 31.5 GeV. The other half was with α's in one ring and with 31.5 GeV protons in the other ring (c.m. energy $\sqrt{s}$ = 88 GeV or $\sqrt{s_{\mathrm{NN}}}$ = 44 GeV). The luminosities were $3\times10^{28}\,\mathrm{cm^{-2}\,s^{-1}}$ for $\alpha\alpha$ collisions and $8\times10^{29}\,\mathrm{cm^{-2}\,s^{-1}}$ for αp collisions.

The following experiments took data using various triggers:
Experiment R110 measured π^0 production at very large transverse momenta p_{T} with a superconducting solenoid magnet and lead-glass and lead/scintillator sandwich shower counters.
Experiment R210 measured small-angle elastic scattering with plastic scintillator and drift tube hodoscopes.
Experiment R418 measured elastic scattering at larger angles, inelastic interactions, and large-p_{T} hadron production with the Split-Field Magnet (SFM) detector, which covers a solid angle close to 4π using multiwire proportional chambers (MWPCs).
Experiment R806 measured π^0 production at large p_{T} with two liquid-argon/lead-plate calorimeters.
Experiment R807 measured the production of hadrons with large p_{T} and inelastic interactions with the Axial-Field Magnet (AFM) detector and two forward calorimeters.

A general remark is in order explaining why one finds it interesting to operate with high-energy light ions, thus adding further complexity to the already complex nucleon–nucleon (NN) interaction. The answer derives from the fact that one introduces a controllable number of rescatterings or multiple interactions. Their essential feature is that they occur within the small volume of a nucleus, i.e. on space and time scales of the order of 1 fm or 1 fm/c. Thus, highly excited or very short-lived states of hadrons may re-interact. It is this possibility of probing hadrons *in statu nascendi* which has been generating interest in high-energy nuclear interactions since many years. The specific case for light ions is given if an exact knowledge of the internal nuclear structure is required, and if one aims for a complete expansion in multiple scattering terms.

0 370-1573/82/0000–0000/$3.25

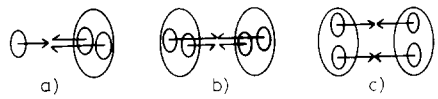

Fig. 7.1. Multiple scattering in nucleus–nucleus collisions: (a) hadron–nucleus type, (b) parallel interaction, (c) high-energy density interaction.

Let us consider the possibilities for multiple interactions in αp and $\alpha\alpha$ interactions. In the first case the incoming proton can interact, elastically or inelastically, with one to four nucleons. For $\alpha\alpha$ interactions we can distinguish between three basic cases (fig. 7.1):

(a) One nucleon out of one α interacts with one to four nucleons out of the other α. Since this is the same as in pα, we call it the "proton–nucleus type" of interaction.

(b) Two to four nucleon pairs (with partners from different nuclei) can interact in parallel. If these parallel interactions are independent they are trivial, and the result can be predicted by convoluting the corresponding number of NN interactions.

(c) Two or more pairs could interact in the same space-time volume. Thus, high energy and matter densities are reached. It is this sort of collision on which hopes are built that in heavy ion collisions new phases of matter may be created.

In order to be able to calculate the probability for the different multiple scattering terms, a good knowledge of the nuclear wave function is needed. Our basic philosophy is: We assume or hope that the nuclear structure is well known, and we want to use nuclei as a laboratory for studying high-energy hadron interactions.

The results will be presented in the following order: elastic scattering; normal inelastic interactions; and, finally, hard interactions leading to particles with large p_T. The first topic, elastic scattering, indeed provides an excellent illustration for the general remark on the use of light nuclei.

7.2. Multiple elastic scattering and inelastic intermediate states

For the elastic scattering of light ions we are provided with a very successful model: Glauber's multiple scattering model [1]. In short, the model takes the NN scattering amplitude and the nuclear structure as input, and predicts the amplitude for scattering from a nucleus as being a superposition of different multiple scattering terms.

Several people have predicted that at high energy, say SPS or ISR energies, the Glauber model needs a correction because of the occurrence of intermediate inelastic states (IIS) [2]. What IIS means is shown in fig. 7.2c for the case of double scattering. After the first collision the projectile turns into an excited state of mass M, and after the second or last collision it returns to the ground state. The intermediate excitation has to fulfil the coherence condition

$$q = (M^2 - m^2)/p_{\text{inc}} < \hbar/D,$$

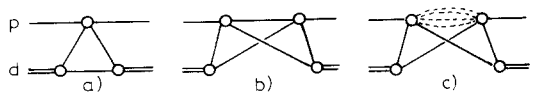

Fig. 7.2. Proton–deuteron elastic scattering terms: (a) single scattering, (b) double scattering, (c) rescattering with IIS.

i.e. the momentum transfer q has to be smaller than the inverse distance D between the two scatterings so as not to destroy the nucleus or the coherence of the outgoing waves. The condition implies that with increasing incoming momentum p_{inc}, higher masses M can be reached. Therefore the described mechanism for IIS should introduce an energy dependence in the elastic scattering amplitude, on top of the one of the "elementary" NN amplitude.

The elastic scattering cross-sections $d\sigma/dt$ as a function of the squared momentum transfer t measured by R210 [3] and R418 [4] are shown in fig. 7.3a,b. The t range covered by the two experiments is complementary. In the case of αp scattering (fig. 7.3a), the diffraction cone below the first diffraction minimum was measured by R210, and the data above the minimum up to $|t| = 0.8$ $(\text{GeV}/c)^2$ were measured by R418. There is considerable disagreement between the experiments in the small overlap region near the minimum. The broken line is a pure Glauber model calculation, whilst the solid line includes the IIS. The calculations were made by Proriol et al. [5]. In the region above the first dip, where the double scattering dominates, the correction is of the order of 20%. But the precision of the data is not sufficient to distinguish between the pure Glauber model and the one with IIS.

The next picture (fig. 7.3b) shows αα elastic scattering. In the overlap region there is again a considerable disagreement between the two data sets, which should be resolved in a further run. The two curves are calculations by Alberi et al. [6], one without and the other with IIS (broken and solid lines, respectively). Here the effect of the IIS correction is quite strong, so that we should in principle be able to fix the amount of IIS correction after the next measurement.

Meanwhile, let us return to theory. The above-mentioned story of the IIS seems, at a first glance, like an example of unnecessary complications arising from the use of nuclear targets. Taking a second look, we learn that this complication is necessary: the nucleus reveals the complicated structure of the projectile.

The intermediate states are quantum fluctuations of the incoming hadron. They are precisely the

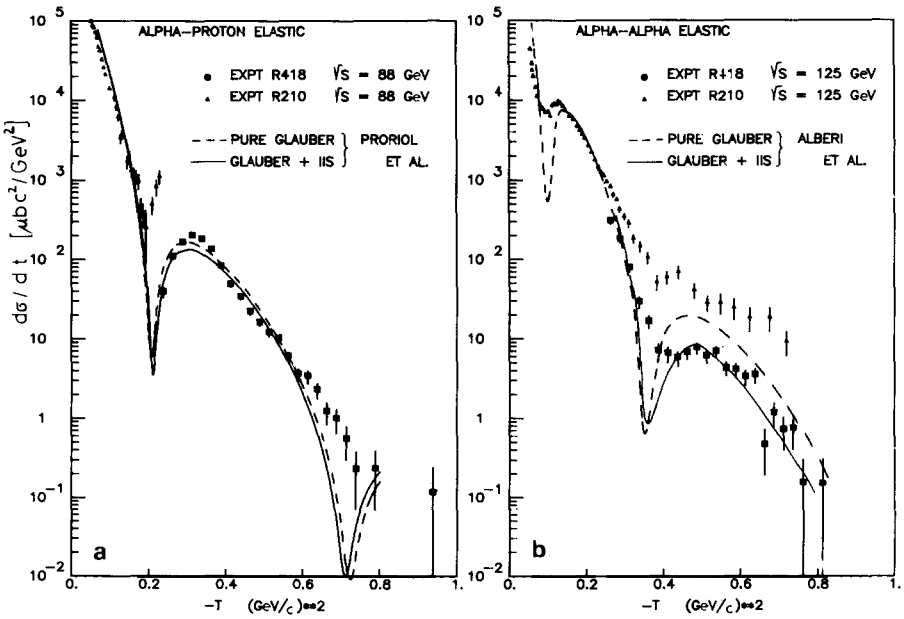

Fig. 7.3. Differential elastic cross-section $d\sigma/dt$ for: (a) αp and (b) αα scattering.

ones which one identifies as the diffractive dissociations of the hadron. Here, as IIS, they become intermediately real as long as the nucleus provides the necessary momentum transfer q to raise them on the mass shell. Also, they are prepared in quite a specific way. Thus one has an independent test for models of the diffractive dissociation.

The experimental situation concerning the IIS is not clear. Experiments at the CERN ISR [pd and dd [7]] and at FNAL [pα [8]] claim to have found evidence for the IIS. More recent experiments disagree, at least on the size of the effect [9, 10]. So it is necessary to aim for more precise data and for a measurement of the energy dependence of the elastic cross-sections over the ISR energy range.

7.3. Multiple inelastic interactions

In fig. 7.4a,b a preliminary multiplicity distribution P_{N^-} of negative tracks in $\alpha\alpha$ collisions is shown and compared with the one in pp collisions at the same $\sqrt{s_{NN}}$ [R418 [11]]. Only negative tracks are counted, because for these the detector acceptance is more homogeneous and better understood, and, by charge conservation ($N^{ch} = 2N^- + Z_1 + Z_2$), P_{N^-} is equivalent to $P_{N^{ch}}$. Figure 7.4 also shows a recent calculation by Chao and Pirner [12]. In their model, which is similar to the "Dual Fragmentation" model of Capella and Tran Than Van or the "Two Sheet" model of Chao et al. [13, 14], two colour-flux tubes or "chains" are formed at the first inelastic NN interaction. In the second and following interactions, only one additional chain is formed each time. The hadronization of these chains follows simple stochastic laws. The three free parameters of the model are adjusted to reproduce the pp multiplicity distribution as a function of the energy. The distribution of multiple collisions is calculated in a geometrical probabilistic model.

The curves labelled (a), (b), and (c) in fig. 7.4 indicate the contributions from the different classes of multiple interactions as shown in fig. 7.1; namely: (a) hadron–nucleus, (b) parallel, and (c) high-density interactions. It is interesting to note that, adding up all these contributions, one still gets a distribution which obeys KNO scaling remarkably well, despite the fact that the individual contributions – such as contribution (b) – do not obey KNO scaling. At high multiplicity the calculation is lower than the data, which were preliminarily corrected for acceptance, but the agreement is better with our later results.

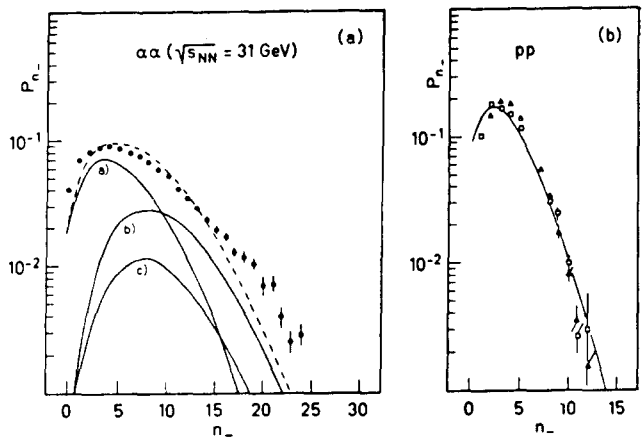

Fig. 7.4. Multiplicity distribution of negative tracks for: (a) $\alpha\alpha$ and (b) pp inelastic interactions. The curves are calculations by Chao and Pirner [12] (see text).

One can see in fig. 7.4 that, according to the calculation, high multiplicities are mainly due to multiple parallel interactions. This has been also shown experimentally by R807 [15]. In order to understand this measurement one has to see a sketch of the set-up. The apparatus (fig. 7.5) consists of a central scintillator hodoscope and of two calorimeters surrounding the beam tubes, one on each side of the intersection. This is only a small part of the AFM detector, but for the particular measurement described here it was the only equipment used. The barrel hodoscope measures the charged particle multiplicity in the central region (rapidity $|y| < 1.7$), and the forward calorimeters measure the energy deposit of particles deflected from the beam by more than 22 mrad and less than 111 mrad. The idea is that non-interacting nucleons go down the beam pipe, whilst interacting nucleons, together with some energetic secondaries, interact in the calorimeter.

The correlation between energy deposit in the calorimeter and the multiplicity observed in the counter hodoscope is displayed in fig. 7.6. The correlation function in itself can be qualitatively understood as follows. As the multiplicity increases, the energy deposit first rises, because more nucleons participate in the interaction; then it decreases, because more energy goes into the central region to angles larger than the calorimeter accepts. The picture also shows what can be obtained by convoluting two, three, or four independent pp multiplicity distributions. One observes the same dependence of energy deposit on multiplicity for $\alpha\alpha$ interactions as for four parallel pp interactions, at very high multiplicity. Hence it can be concluded that, in high multiplicity events, all four nucleons of each α particle participate in the interaction. Moreover, the authors [15] conclude that the four nucleon pairs interact independently, but I am not sure whether the correlation is sensitive to the (in)dependence of these interactions. We should, and will, make a more detailed examination of these high multiplicity events which correspond to central collisions, and study particle correlations, flavour ratios, and the like. The question is, what signal should one look for in order to (dis)prove that the parallel interactions are independent. This problem is indeed quite similar, or even related, to the one of finding a signal for the phase transition to quark matter in high-energy, heavy-ion collisions.

The feature of inelastic hadron–nucleus and nucleus–nucleus interactions which has probably received most of the theoretical and experimental attention, is the inclusive distribution $\rho(y)$ of produced particles in longitudinal phase space (e.g. rapidity y), or rather the change of this distribution

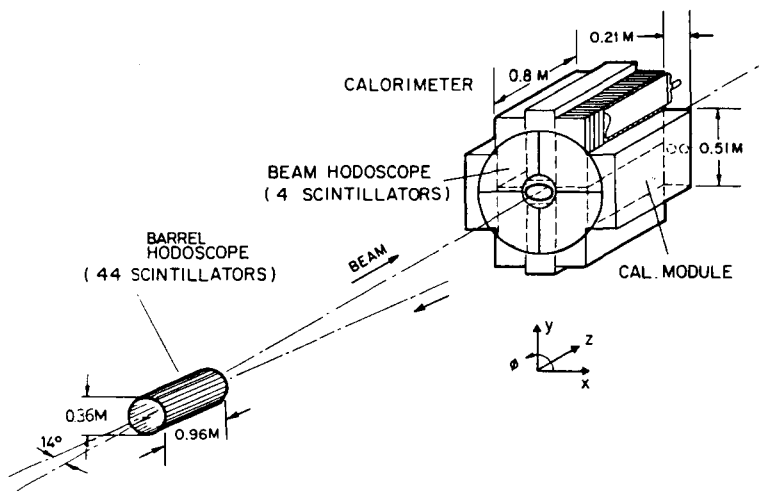

Fig. 7.5. Set-up used by R807 for the energy deposit versus multiplicity correlation shown in the next figure.

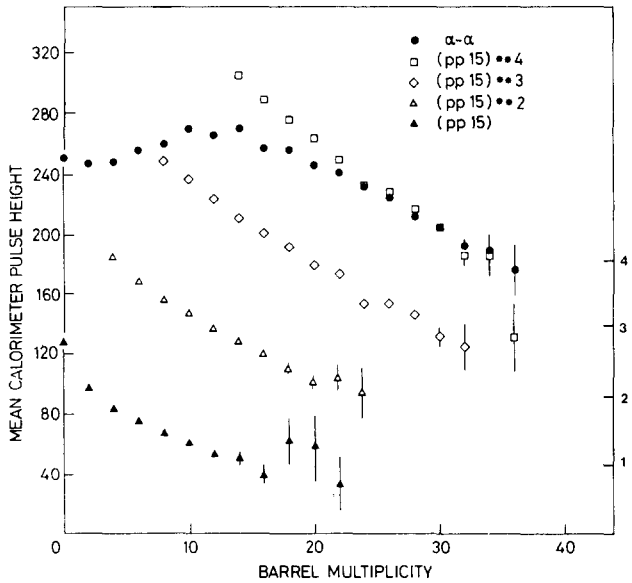

Fig. 7.6. Energy deposit versus central multiplicity for $\alpha\alpha$ and for one to four convoluted pp interactions.

when one goes from pp to pA or AA collisions. A region of particular interest is the central region (small y in the c.m. system). The central particles are mostly produced by non-diffractive processes. Thus a measurement of the ratio

$$R_y(\alpha\mathrm{p/pp}) = \rho(y)_{\mathrm{p}\alpha}/\rho(y)_{\mathrm{pp}} \qquad \text{and} \qquad R_y(\alpha\alpha/\mathrm{pp}) = \rho(y)_{\alpha\alpha}/\rho(y)_{\mathrm{pp}}$$

at $y = 0$ represents an important test for models of non-diffractive interactions. The ratio can be fairly precisely determined experimentally. It was found [R418 [16, 17]] that

$$R_y(\alpha\mathrm{p/pp}) = 1.18 + 0.07 \qquad \text{and} \qquad R_y(\alpha\alpha/\mathrm{pp}) = 1.74 + 0.09\,.$$

The fact that the central ratio is larger than 1 for αp collisions is in my opinion the most direct indication for the presence of hadron constituents in soft interactions. (More generally this would hold for any hadron–nucleus collision, provided the energy is so high that the two fragmentation regions are well separated and the central region has developed.)

The values of the central ratio have been well reproduced or predicted by three theoretical groups [13, 18, 19]. Their models have one common feature: they assume multiple, parallel constituent-interactions. For the rest they are quite different, so perhaps the real test for them is how well they explain the ratio R_y at other rapidities. However, I will not discuss the results for R_y now, since there are still some experimental difficulties with R_y outside the central region – for instance, one should rather use the particle density $\rho(y)_{\mathrm{NN}}$ (where N is 50% proton and 50% neutron) in the denominator of $R_y(\alpha\alpha/\mathrm{NN})$. Strong effects due to the different isospin or quark composition of α's and p's overshadow the effects of multiple scattering which one wants to study at large rapidities. There are two ways of overcoming this problem. One is to use existing information on charge flow in pp interactions (fraction of π^+ to π^- and of p to π^+). The other is to measure pd and dd interactions in the ISR. We intend to go both ways.

7.4. Hard inelastic interactions

It was not such a very long time ago that some people could assume the A-dependence of the particle production cross-section at large p_T to be the same as that of the total cross-section, namely approximately proportional to $A^{2/3}$. A systematic measurement of the A-dependence of the cross-section as a function of p_T, carried out by the Chicago–Princeton Collaboration at FNAL [20, 21], therefore led to a surprise: when the A-dependence of the cross-section was parametrized as

$$d\sigma/dp_T = A^{\alpha(p_T)},$$

the power $\alpha(p_T)$ was found to increase with p_T from about 0.8 to 1.1–1.3, depending on the species of the trigger particle. This behaviour was later confirmed in other experiments [22].

In the framework of parton models, the rise of $\alpha(p_T)$ to a value of 1 has been readily anticipated [23]. The basic subprocess leading to large-p_T particle production is supposed to be large-angle elastic scattering of point-like partons. Since the cross-section is very small, there should not be any shadowing and hence the cross-section should be proportional to A^1 and not to $A^{2/3}$.

The rise of $\alpha(p_T)$ above 1 for p_T larger than 2 GeV/c is harder to explain. This "anomalous nuclear enhancement" (ANE), as it was called, stimulated considerable theoretical activity. Many mechanisms have been discussed, such as the formation of several nucleons into big bags, the influence of Fermi motion or other collective effects [24], and last but not least, multiple scattering of partons [25]. Since for several theoretical and experimental reasons (e.g. Drell–Yan pair production from nuclear targets) the other explanations have been almost ruled out, suspicion has focused on the multiple scattering – more specifically, multiple hard scattering – of partons.

One of the motivations for the experiment with α particles in the ISR was that the (so far, only inclusive) measurements with nuclear targets could be implemented by a complete study of the structure of the final state after a hard interaction.

We shall nevertheless first have a look at the inclusive distribution obtained by the ISR experiments with α particles. All experiments applied old-fashioned, single-particle, large-p_T triggers, where the trigger jet has a small but well-understood "trigger bias", but the events are "jetty". In fig. 7.7 the invariant cross-section for negative tracks, which are mostly (70%) pions measured by R418 [26], is shown together with the π^0 cross-section measured by R806 [27] for αp and $\alpha\alpha$ interactions. Also shown for comparison are the cross-sections for pp interactions at the same $\sqrt{s_{NN}}$ [28].

The ratios $R_{p_T^-}$ and $R_{p_T^0}$ to the pp cross-section where, for instance,

$$R_{p_T^-}\left(\frac{\alpha p}{pp}\right) = \frac{(1/\sigma)\, d^2\sigma/dy\, dp_T^2(\alpha p)}{(1/\sigma)\, d^2\sigma/dy\, dp_T^2(pp)},$$

are shown in fig. 7.8. The different experiments [26, 27, 29] agree on a ratio $R_{p_T}(\alpha p/pp) = 4 \pm 1$ for $p_T > 1$ GeV/c (see fig. 7.10a). The ratio one expects to find by using $\alpha(p_T)$ from the FNAL experiment [21] is indicated in fig. 7.8a (solid curve). Whilst at $p_T < 4$ GeV/c the experimental points can be said to be consistent with this curve as well (as with a factor of 4), at higher p_T the π^0 are significantly lower. One reason for this could be that the comparison of the $\alpha p \to \pi^0$ data ($\langle y \rangle = 0.35$) with the $pp \to \pi^0$ data ($\langle y \rangle = 0.0$) was not made at the same rapidity.

The ratio $R_{p_T}(\alpha\alpha)$ for $\alpha\alpha$ interactions is shown in fig. 7.8b. It rises above 16 with increasing p_T. Sukhatme and Wilk [30] have derived a relation between the ANE in pA and in AA collisions from the

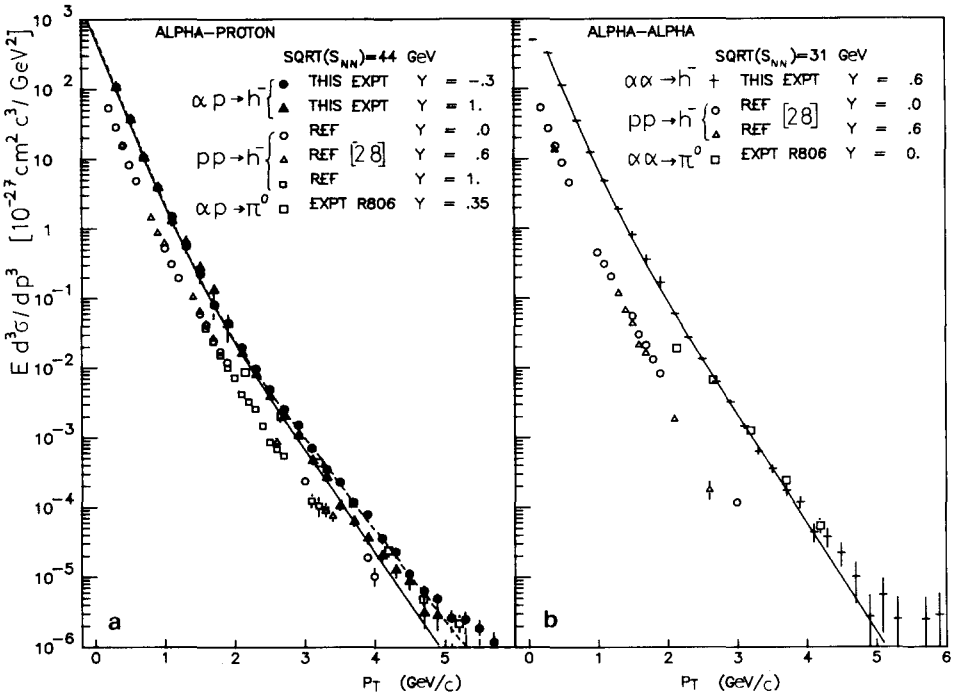

Fig. 7.7. Inclusive cross-sections $d\sigma/\pi\, dy\, dp_T^2$ for negative tracks (h^-) (R418) and π^0 (R806) for (a) αp and (b) $\alpha\alpha$ interactions compared with pp data at the same $\sqrt{s_{NN}}$. The curves are exponential fits to the data.

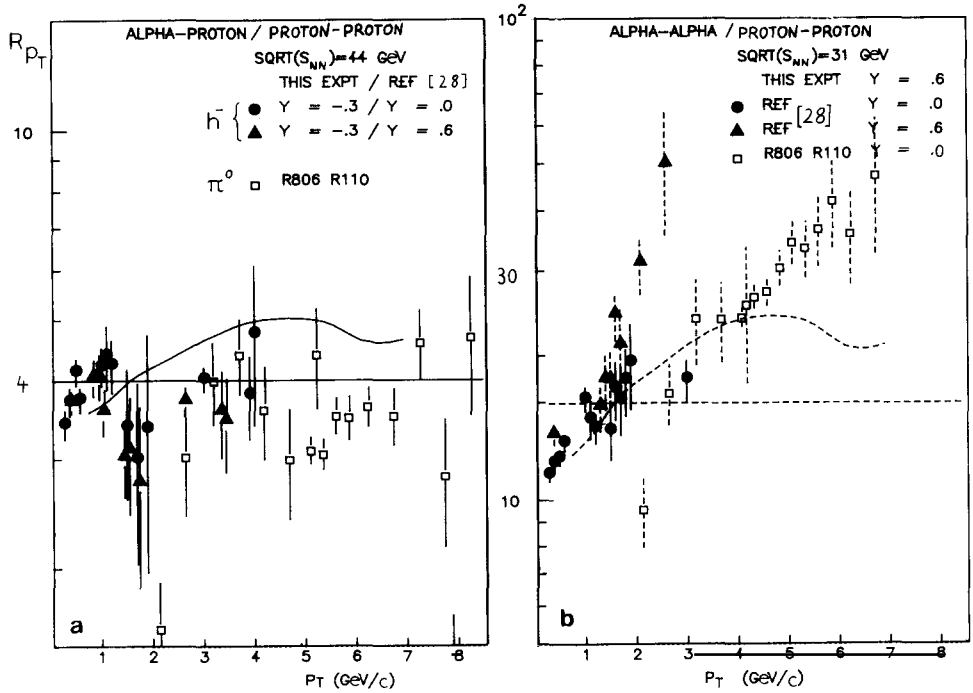

Fig. 7.8. Ratios of cross-sections as a function of p_T: (a) $R_{p_T}(\alpha p/pp)$; the curve corresponds to the function $4^{\alpha(p_T)}$ with $\alpha(p_T)$ from ref. [21]. (b) $R_{p_T}(\alpha\alpha/pp)$; the curve is a prediction (ref. [30]).

assumption that the mechanism causing the ANE is multiple scattering. The curve in fig. 7.8b is their prediction for $\alpha\alpha$. The experimental points show some significant deviations from this prediction. Firstly, at lower p_T the solid triangles [ratio of R418 $\alpha\alpha$ data at $y = 0.6$ to pp data at $y = 0.6$ [28]] rise much faster with p_T. This could be a fault of the pp data, as new measurements of the AFM Collaboration [31] indicate that the cross-sections at $y = 0.6$ (from ref. [28]) are too low. Secondly, at high p_T the data of R110 [29] increase beyond the theoretical prediction. If this trend is confirmed, it could eventually signify that something very interesting is going on in nucleus–nucleus collisions.

I will show only two examples of the work done on the structure of the final state. One is the x_e distribution of particles in the central region, where x_e is defined as

$$x_e = -\boldsymbol{p}_T \cdot \boldsymbol{p}_T(\text{trigger})/|p_T(\text{trigger})|^2 ,$$

i.e. $-x_e$ is the p_T of a track in the direction and in units of the trigger p_T. The second example is the momentum flow of particles for varying trigger conditions.

The x_e distributions should test whether parton rescattering plays any important role in large-p_T particle production from nuclear targets. One expects, in this case, that the p_T of the trigger particle (or rather trigger jet) is balanced by two or more medium-hard away jets instead of one hard jet in a single parton scattering event (fig. 7.9). Consequently, the x_e distribution should get steeper at large x_e on the away side. The x_e distributions for αp and $\alpha\alpha$ interactions are shown in fig. 7.10a,b for events with a trigger p_T larger than 3 GeV/c. Negative x_e correspond to tracks on the trigger side, positive x_e to tracks on the away side. The broken lines indicate the x_e distribution in pp interactions ($\sqrt{s} = 63$ GeV, data taken by the Annecy (LAPP)–CERN–Dortmund–Heidelberg–Paris (Collège de France)–Warsaw (ACDHPW) Collaboration but analysed with the same programs as those for the αp and $\alpha\alpha$ distributions). Superimposed on the figures are the "x_e distributions" in minimum bias events, where x_e was calculated with respect to a fictitious trigger particle with the same p_T and ϕ distribution as the large-p_T trigger track in large-p_T events. All distributions scale quite well and there is no statistically significant sign for a steepening at high x_e. (There is, however, a steepening at low x_e in $\alpha\alpha$ interactions, which can be explained by the general rise of the particle density at low p_T.) What sensitivity have we reached? To give a rather crude estimate: the background of particles not belonging to the away jet is supposedly low at $x_e \geq 0.5$. (Consider as a measure for this background the x_e distribution in minimum bias events.) Owing to the steep fall of the x_e distribution, one or two jets with half the momentum of the trigger jet would yield virtually no particles at $x_e \geq 0.5$. Therefore the decrease at $x_e \geq 0.5$ should be roughly proportional to the admixture of multiple scattering; that is, if we look at the ratio $R_{x_e}(\alpha\text{p/pp})$ or $R_{x_e}(\alpha\alpha/\text{pp})$ (see fig. 7.10c,d), the decrease below 1 at high x_e should be proportional to the amount of multiple parton scattering. We can see from the graphs that this amount is around 20 + 20% for αp and

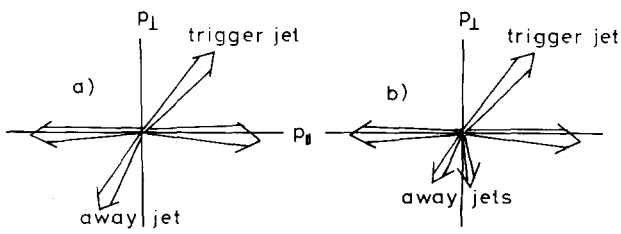

Fig. 7.9. Presumed jet structure of the final state for (a) single and (b) double hard-parton scattering in p_T versus p_y plane.

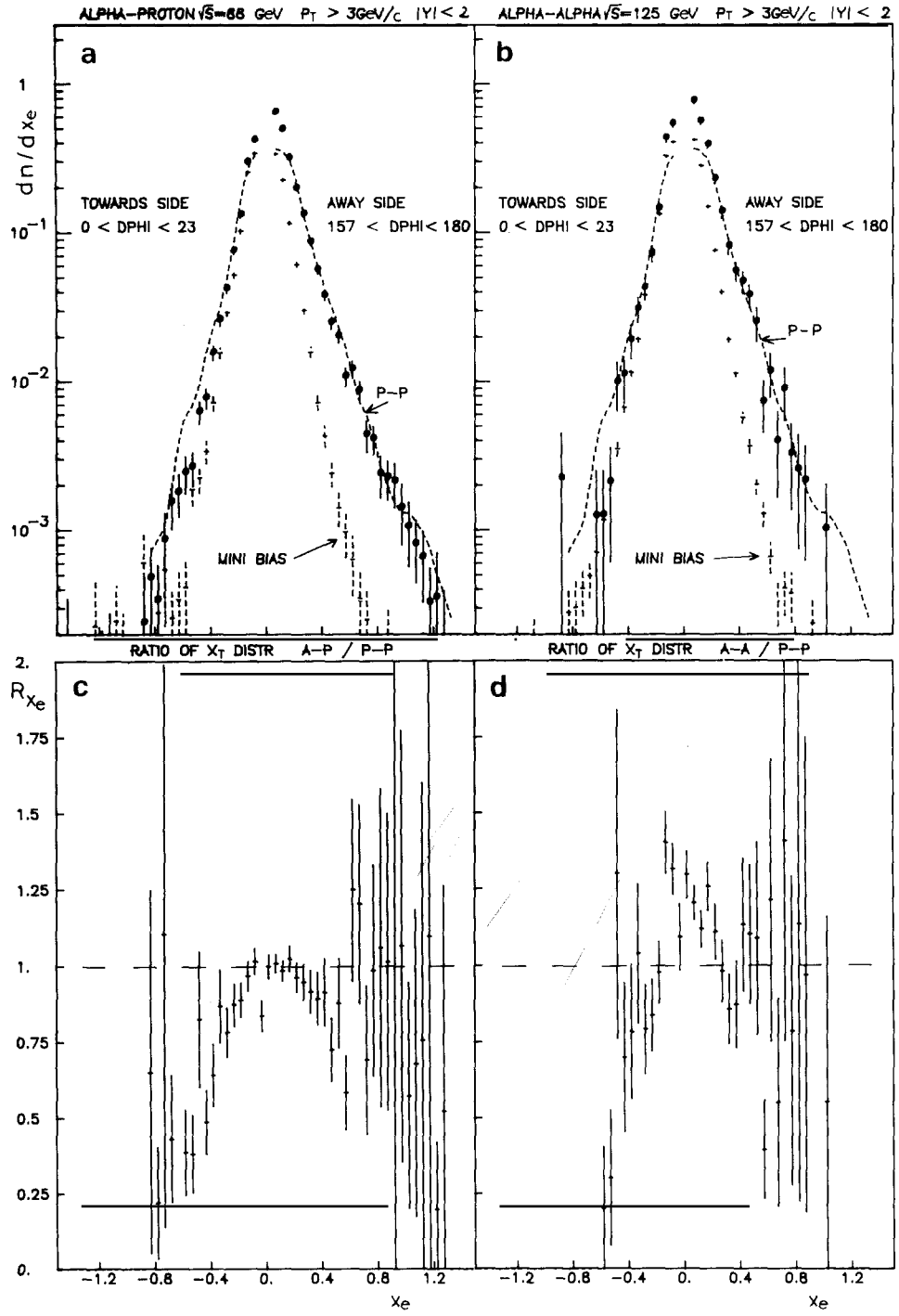

Fig. 7.10. Distribution in x_e of charged tracks in the central region for (a) αp and (b) $\alpha\alpha$ large-p_T interactions compared with the x_e distribution for pp interactions ($\sqrt{s_{pp}} = 63$ GeV, $p_T > 3$ GeV/c) and for αp and $\alpha\alpha$ minimum bias interactions. (c) Ratio $R_{x_e}(\alpha p/pp)$ and (d) $R_{x_e}(\alpha\alpha/pp)$ of the x_e distributions. (Trigger track is not contained in the plots.)

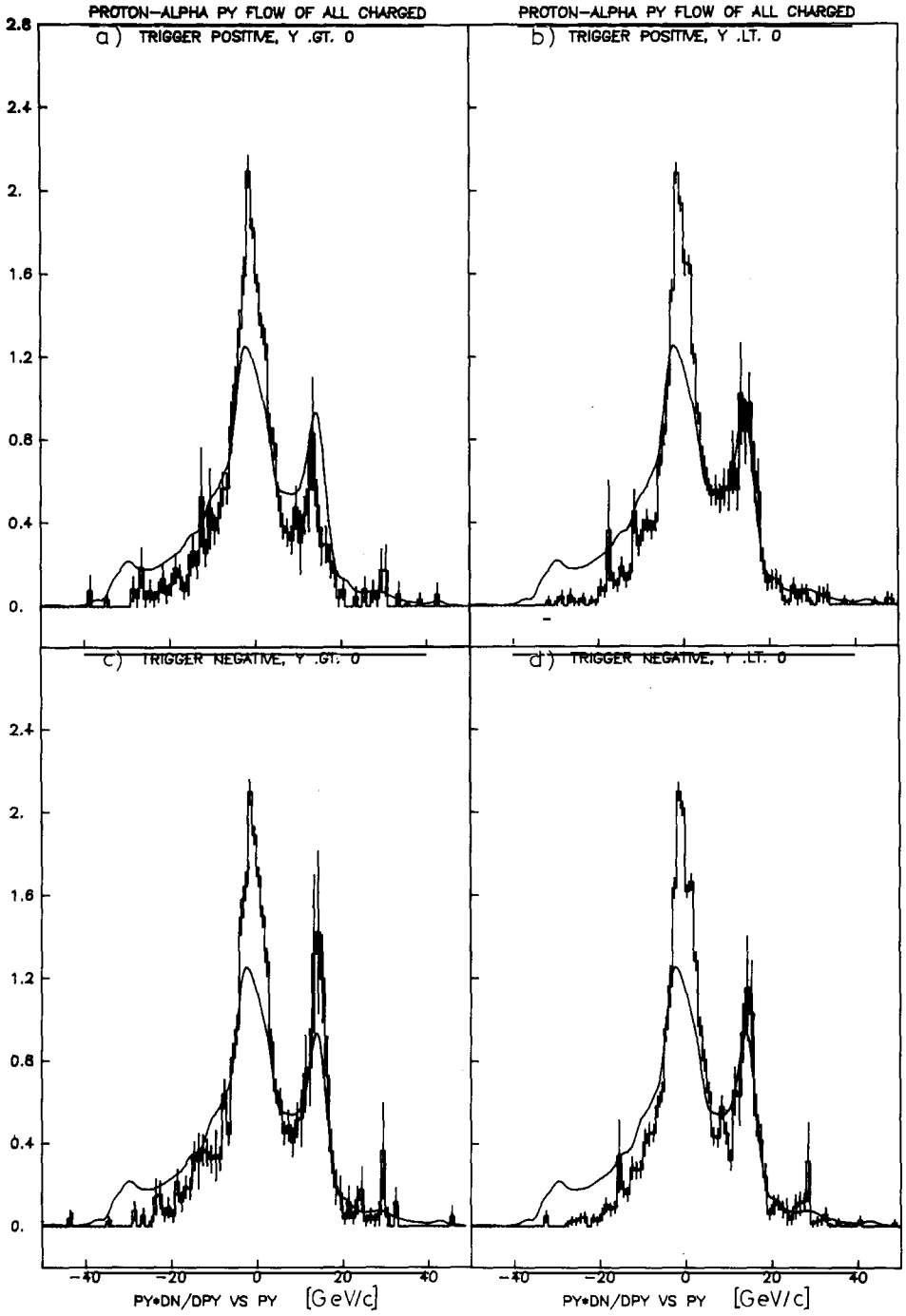

Fig. 7.11. Momentum flow in αp interactions: (a) positive trigger track, $y > 0$; (b) positive trigger track, $y < 0$; (c) negative trigger track, $y > 0$; (d) negative trigger track, $y < 0$. The trigger track is not contained in these plots. The curve corresponds to the momentum flow in αp minimum bias events.

50 + 50% for $\alpha\alpha$ events. But in our comparison we have neglected the different "trigger biases" of our event samples. As the c.m. energy $\sqrt{s_{NN}}$ decreases from pp (63 GeV) to αp (44 GeV) to $\alpha\alpha$ (31.5 GeV), the trigger bias increases, i.e. the fraction of the trigger jet momentum carried by the trigger track increases. Taking the trigger bias properly into account, the ratio will presumably tend to be closer to 1. A noticeable steepening occurs at the trigger side (negative x_e); this can also be attributed to the increasing trigger bias going from pp to αp and $\alpha\alpha$, and it actually provides a qualitative proof that the effective $\sqrt{s_{NN}}$ decreases. (In some models invoking collective nucleon interactions or Fermi motion, the effective $\sqrt{s_{NN}}$ for large-p_T particle production would be higher than the average $\sqrt{s_{NN}}$.)

The last pictures (fig. 7.11) show a comparison of the momentum flow, $(1/\sigma)p_y\, d\sigma/dp_y$ versus p_y, in αp events for four different trigger conditions (p_y = the longitudinal momentum along the beam axis). Is there any correlation between the spectator protons out of the α and the large-p_T trigger? The peak of the spectator protons can be very clearly recognized on the positive p_y side at 15 GeV/c. We observe a shrinkage of this peak in the case of a positive trigger on the α side, and an increase for a negative trigger on the α side, compared with the contents of the spectator peak in minimum bias events. One should properly subtract the steep shoulder below the spectator peak. This significant correlation between trigger particle and proton spectators suggests a direct involvement of valence quarks. Presumably, if the trigger particle was positive and on the α side, the interacting nucleon was more likely a proton, for a negative trigger more likely a neutron.

7.5. Summary and outlook

This survey on results from the αp and $\alpha\alpha$ survey runs in the ISR is, naturally, incomplete. Some of the results have been omitted because they have already been reported elsewhere [11, 16, 17, 32, 33]; other results, because they are too preliminary. So I have not discussed some interesting topics such as the double Pomeron interaction in $\alpha\alpha$ collisions, the search for multibaryon resonances in the α fragmentation, the study of two-particle correlations, or the analysis of K^0 and Λ production.

Although it is astonishing how much data could be obtained from two 60-hour runs and how much more physics can be extracted from these data, we have already encountered the need for more data at several instances, We hope to have another run with light ions in the ISR in the near future. Some important goals of this next run will be: measurements of pd and dd interactions, which will provide us with an ideal comparison for pα and $\alpha\alpha$ minimum bias interactions (see end of section 7.3), as for large-p_T interactions; a measurement of the elastic differential αp and $\alpha\alpha$ cross-sections at lower energy; increased statistics for large-p_T $\alpha\alpha$ interactions. In view of the new measurements, we are about to improve the forward telescopes at the Split-Field Magnet detector by adding more chamber planes for charged particle detection and two hadron calorimeters for the tagging of neutron spectators.

References

[1] R.J. Glauber, Lectures in Theoretical Physics, Vol. 1, eds. W.C. Brittin and L.G. Dunham (Interscience Publ., NY, 1959) p. 315;
V. Franco and R.J. Glauber, Phys. Rev. 142 (1966) 1195;
R.J. Glauber, Proc. 2nd Int. Conf. on High-Energy Physics and Nuclear Structure, Rehovoth, 1967, ed. G. Alexander (North-Holland Publ. Company, Amsterdam, 1967) p. 311.

[2] E.S. Abers et al., Nuovo Cimento 42A (1966) 365;
V.N. Gribov, Sov. Phys. JETP 29 (1969) 483;

J. Pumplin and M. Ross, Phys. Rev. Lett. 21 (1968) 1778;
G. Alberi and L. Bertocchi, Nuovo Cimento 61A (1969) 201;
D.R. Harrington, Phys. Rev. D1 (1970) 260;
C. Quigg and L.L. Wang, Phys. Lett. 42B (1973) 314.
[3] M. Ambrosio et al., preprint CERN-EP/81-117 (1981), submitted to Phys. Lett. B.
[4] W. Bell et al. (CERN–Heidelberg–Lund Collaboration), to be submitted to Phys. Lett. B.
[5] J. Proriol, S. Maury and B. Jargeaix, Phys. Lett. 110B (1982) 95;
J. Proriol et al., Univ. de Clermont II preprint PCCF RI 82/01 (1982).
[6] G. Alberi, private communication.
[7] G. Goggi et al., Phys. Lett. 77B (1978) 428;
G. Goggi et al., Phys. Lett. 77B (1978) 433;
G. Goggi et al., Nucl. Phys. B149 (1979) 381.
[8] A. Bujak et al., Phys. Rev. D23 (1981) 1895.
[9] J.P. Burq et al., Nucl. Phys. B187 (1981) 205.
[10] G. Warren et al., Imperial College (London) preprint IC/HENP 81-5 (1981).
[11] M.G. Albrow and M. Jacob (eds.), Physics with α particles, Discussion Meetings between Experimentalists and Theorists on ISR and Collider Physics (CERN, Geneva) Series 2, Nos. 2 and 3 (1981).
[12] W.Q. Chao and H.J. Pirner, Univ. Heidelberg preprint UNI.HD.81.4 (1981).
[13] A. Capella et al., Phys. Lett. 108B (1982) 347.
[14] W.Q. Chao et al., Phys. Rev. Lett. 44 (1980) 518.
[15] T. Åkesson et al. (Axial Field Spectrometer Collaboration), Phys. Lett. 110B (1982) 344.
[16] W. Bell et al. (CERN–Heidelberg–Lund Collaboration), Proc. 5th High-Energy Heavy Ion Study, Berkeley, 1981, LBL-12652 UC-34, CONF-8105104 (1981) p. 540.
[17] M.A. Faessler, Proc. 9th Int. Conf. on High-Energy Physics and Nuclear Structure, Versailles [Nucl. Phys. A374 (1982) 461c].
[18] S.J. Brodsky et al., Phys. Rev. Lett. 39 (1977) 1120.
[19] A. Białas et al., Cracow reports INP-1141/PH and TPJU-10/81 (1981).
[20] J.W. Cronin et al., Phys. Rev. Lett. 31 (1973) 1426.
[21] J.W. Cronin et al., Phys. Rev. D11 (1975) 3105;
L. Kluberg et al., Phys. Rev. Lett. 38 (1977) 670;
D. Antreasyan et al., Phys. Rev. D19 (1979) 764.
[22] U. Becker et al., Phys. Rev. Lett. 37 (1976) 1731;
D.A. Garbutt et al., Phys. Lett. 67B (1977) 355;
R.L. MacCarthy et al., Phys. Rev. Lett. 40 (1978) 213;
C. Bromberg et al., Phys. Rev. Lett. 42 (1979) 1202.
[23] G. Farrar, Phys. Lett. 56B (1975) 185.
[24] P.M. Fishbane and J.S. Trefil, Phys. Rev. D12 (1976) 2113;
G. Berlad et al., Phys. Rev. D13 (1976) 161;
S. Fredriksson, Nucl. Phys. B111 (1976) 167;
A. Krzywicki, Phys. Rev. D14 (1976) 152.
[25] J. Pumplin and E. Yen, Phys. Rev. D11 (1975) 1812;
P.V. Landshoff et al., Phys. Rev. D12 (1975) 3738;
J.H. Kuehn, Phys. Rev. D13 (1976) 2948;
P.M. Fishbane et al., Phys. Lett. 85B (1979) 407;
V.V. Zmushko, Sov. J. Nucl. Phys. 32 (1980) 127 and 231;
D. Treleani and G. Wilk, Nuovo Cimento 60A (1980) 201.
[26] W. Bell et al. (CERN–Heidelberg–Lund Collaboration), CERN-EP/82-25 (1982), submitted to Phys. Lett. B.
[27] A. Karabarbounis et al., Phys. Lett. 104B (1981) 75.
[28] B. Alper et al., Nucl. Phys. B100 (1975) 237.
[29] A.L.S. Angelis et al., High p_T π^0 production with $\alpha\alpha$ and αp beams at the CERN-ISR, submitted to the 20th Int. Conf. on High-Energy Physics, Lisbon, 1981.
[30] U.P. Sukhatme and G. Wilk, SLAC-PUB-2844 (1981), submitted to Phys. Rev. D.
[31] Axial Field Spectrometer Collaboration at CERN, private communication.
[32] M. Jacob, Proc. 5th High-Energy Heavy Ion Study, Berkeley, 1981, LBL-12652, UC-34, CONF-8105104 (1981) p. 581.
[33] M.A. Faessler, Proc. Int. Conf. on Physics in Collision: High-Energy e^+e^-, ep, pp Interactions, Blacksburg, 1981, eds. P. Trower and G. Bellini (Plenum Press, Inc., NY, 1982) in press. [See preprint CERN-EP/81-109 (1981).]